Multipath Arrival Tracking for Marine Vehicles Utilizing Pattern Recognition

by

Jordan William Fouquette

B.S., Systems Engineering
United States Naval Academy, 2010

Submitted to the Department of Mechanical Engineering
in partial fulfillment of the requirements for the degrees of

Naval Engineer

and

Master of Science in Mechanical Engineering

at the

MASSACHUSETTS INSTITUTE OF TECHNOLOGY

June 2018

Author .....
Department of Mechanical Engineering
May 11, 2018

Certified by .....
Henrik Schmidt
Professor of Mechanical and Ocean Engineering
Thesis Supervisor

Accepted by .....
Rohan Abeyaratne
Chairman, Department Committee on Graduate Students

Multipath Arrival Tracking for Marine Vehicles Utilizing Pattern Recognition

by

Jordan William Fouquette

Submitted to the Department of Mechanical Engineering
on May 11, 2018, in partial fulfillment of the
requirements for the degrees of
Naval Engineer
and
Master of Science in Mechanical Engineering

Abstract

In recent years, interest in the Arctic Region has been steadily growing as it has become more accessible due to continued ice recession. This increased accessibility opens up the possibility for nations to take advantage of the region's abundant resources and trade routes thereby increasing military, political, and commercial interest. The extreme temperatures and significant ice cover in this region have created a unique and challenging acoustic environment. At increased distances, individual acoustic ray path data becomes inconsistent due to improper ray path identification and fading. Marine vehicles have the ability to overcome these challenges and increase contact tracking capabilities by taking advantage of the patterns associated with these multipath arrivals.

Through the use of pattern recognition, a multipath arrival tracking algorithm was developed to utilize the unique characteristics associated with each individual ray path for long range tracking purposes. This tracking algorithm analyzes the amplitude and arrival time patterns amongst all individual ray paths in order to accurately identify each ray path as scattering and fading occurs, thereby increasing range-tracking capabilities. This becomes especially useful in the Arctic Region as contacts of interest can be tracked regardless of their position above, below, or within the Beaufort Duct- a newly discovered sound duct from 100 to 200 meters depth. Simulations covering the numerous depth combinations of sources and receivers with respect to the Beaufort Duct illustrate the difficulty in contact tracking within this harsh environment and highlight the effectiveness that is presented by utilizing multipath arrival data. The developed algorithm takes advantage of these unique patterns in order to provide a unique tracking capability for marine vehicles to employ.

Thesis Supervisor: Henrik Schmidt
Title: Professor of Mechanical and Ocean Engineering

Acknowledgments

There are countless individuals and organizations I would like to thank for supporting me and making this achievement possible. Although I can't list every individual, I would like to thank those family members, mentors, peers, coaches, and teachers who inspired and motivated me to work hard and believe in myself.

First, I would like to thank the United States Navy for affording me this amazing opportunity to attend one of the most prestigious universities in the world. It has been an absolutely incredible experience that I will forever cherish.

Thank you to my thesis advisor, Professor Henrik Schmidt. I truly appreciate your countless hours of mentorship and guidance throughout the completion of this thesis. You made this a very rewarding experience for myself and I can never thank you enough for all of your patience, help, and support.

Thank you to my 2N classmates as you all provided me with invaluable support and friendships that made it possible to get through this very demanding program. I will forever cherish the memories we made during this incredible experience.

Last, but definitely not least, I would like to thank my beautiful wife, Amanda, and my two wonderful children, Alaina and Emilia (and even our wild and crazy family dog, Miika). Words can not do justice to how much your love and encouragement has meant to me. Your patience and sacrifices, not only during the long days and late nights spent during these past three years, but in support of my Naval career is never taken for granted. You provide me with a constant source of motivation that made this achievement possible. I can never thank you enough, but know that I appreciate all that you do for me. I love you all very much.

THIS PAGE INTENTIONALLY LEFT BLANK

Contents

List of Figures

List of Tables

THIS PAGE INTENTIONALLY LEFT BLANK

Chapter 1

Introduction

In recent years, the Arctic has become a highly contested region of the world due to its increased accessibility and wide variety of resources. Maintaining a strategic advantage in the underwater domain of this region is imperative for the United States to maintain a military advantage and protect these resources. The harsh climate in this region has created a difficult setting to track submerged contacts due to the high multipath acoustic environment. This thesis seeks to take advantage of this high multipath environment by utilizing powerful pattern recognition and classification techniques to perform accurate, long-range underwater contact tracking based on the region's very unique and distinct characteristics.

1.1 Arctic Environment

1.1.1 Motivation

The Arctic Region is a very unique environment with extraordinary resources and one of the harshest climates in the world. In recent years, ice recession has increased the interest in this region as its accessibility has continued to grow. Figure 1-1 illustrates this increased accessibility by comparing the 30-year sea ice minimum average with the historical minimum from 2012, which is contained within the red line.

Figure 1-1: Map of Arctic Region illustrating continued ice recession [6]

Along with accessibility, increases in oil and gas development, fishing, tourism, and mineral mining have increased the strategic importance of this region as multiple nations seek to make investments and take advantage of these resources [6]. For example, America's continental shelf in the region alone holds a great deal of value. Estimates state that the economic potential of hydrocarbon resources could exceed $1 trillion, and the Alaskan Arctic may hold the second largest oil and gas reserves in the region containing an estimated 29.9 billion barrels of oil, over 221 trillion cubic feet of natural gas, and 5.9 billion barrels of natural gas liquids [2] [6].

Due to the rising interest in this region and the increased involvement of both Arctic and non-Arctic nations seeking to exploit these resources, it is becoming ever important for the United States to maintain a strategic advantage in this environment. Acknowledging the importance of this region, the U.S. Navy regularly conducts Ice Exercises (ICEX), which are military and scientific exercises aimed at advancing submarine operations and scientific research in the Arctic environment. Oceanographic exploration and understanding of the underwater acoustic environment in this area is at the forefront of this strategic advantage.

The extreme temperatures and significant ice cover in the Arctic present a very unique acoustic environment. This environment lends itself to containing a high amount of multiple acoustic ray paths (multipath). This means that the acoustic signal traveled from a source to a receiver has many different paths it can travel along as illustrated in Figure 1-2. Multipath environments tend to interfere with and disrupt contact tracking capabilities by making it difficult to properly determine the paths traveled by specific sound signals received. This makes it virtually impossible to retrace the received acoustic signals traveled path and calculate its distance traveled, or in other words, range to the contact being tracked.

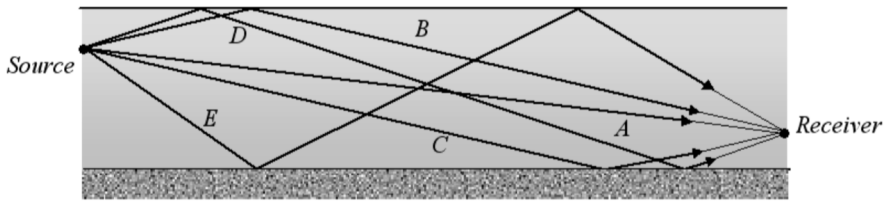

Figure 1-2: Multipath Illustration [9]

1.1.2 Multipath Environment Challenges

The two major difficulties that need to be overcome in order to perform accurate multipath arrival tracking are fading and improper ray path identification.

1. **Fading**

   When a beacon emits several active sound signals, the autonomous underwater vehicle (AUV), or receiver, expects to receive them in a particular order. Fading occurs when the AUV fails to receive certain sound signals at expected times. As seen from the example illustrated in Figure 1-3a, the beacon has sent two sound signals and the AUV expects to receive path 1 prior to path 2. If something unexpectedly blocks one of the signals, such as a seamount as seen in Figure 1-3b, the AUV will mistakenly identify path 2 as path 1, therefore

providing inaccurate and unreliable range information.

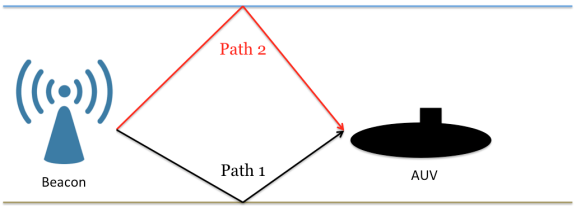

(a) AUV expects to receive Path 1 prior to Path 2

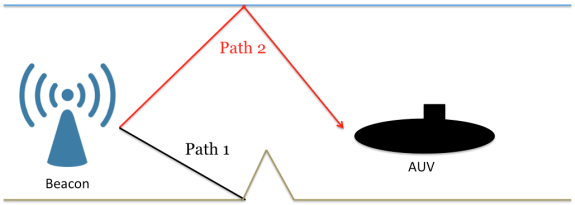

(b) AUV mistakenly identifies Path 2 as Path 1

Figure 1-3: Fading Illustration

2. **Improper Ray Path Identification**

Similar to fading, improper ray path identification is a major obstacle that must be overcome in order to properly perform multipath arrival tracking. At increased distances, individual ray path data becomes inconsistent. As various ray paths converge, they become difficult to separate and identify with their proper paths. Shown in Figure 1-4, an AUV is receiving multiple acoustic ray paths. If the AUV identifies the ray paths incorrectly, the range information will be inaccurate and unreliable as each ray path travels a different distance with different travel times. For example, the distances traveled by the yellow and green ray paths are drastically different. If the AUV mistakenly identifies the green ray as the yellow ray, the AUV's predicted range will be much greater than it actually is since the yellow ray travels a greater distance than the green ray. These types of errors can greatly diminish the accuracy of a system's contact tracking abilities.

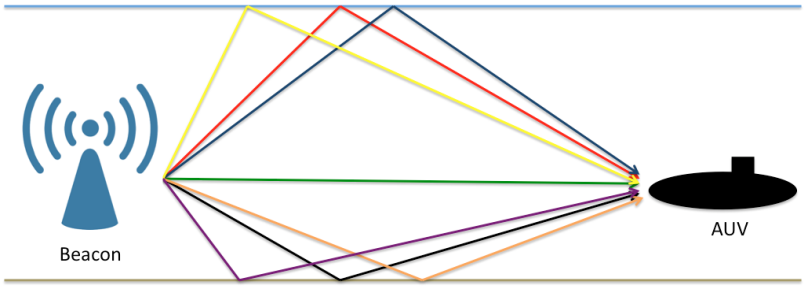

Figure 1-4: Improper Ray Path Identification Illustration

The challenge associated with fading is self evident when examining an arrival time plot for the Arctic. Figure 1-5 highlights these difficulties for an example of a source and receiver both located at 30 meters depth.

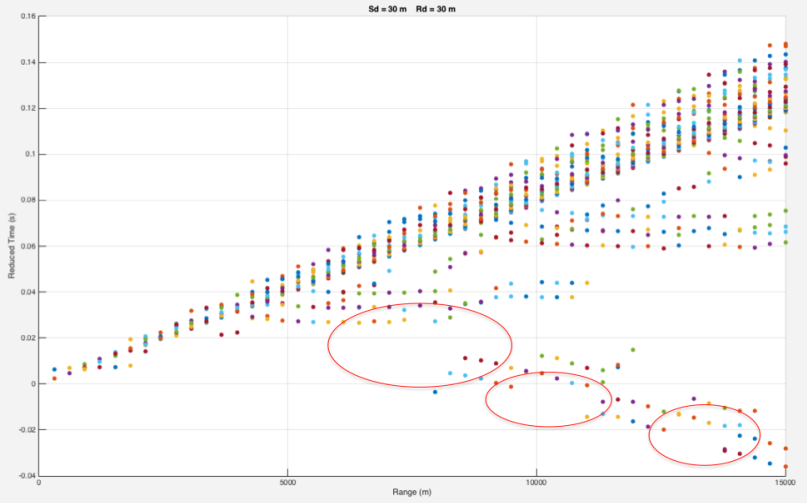

Figure 1-5: Arrival Time Fading Example for Sd=30m, Rd=30m

In Figure 1-5, arrival time is expressed in terms of "reduced time." Using reduced time is simply a means of showing all arrival times on a single graph by utilizing relative travel times rather than absolute travel times. The equation for reduced time is as follows:

$$Reduced\ Time = \frac{T - R}{1450} \tag{1.1}$$

where T is the signal's travel time, R is the signal's received range, and 1450 [m/s] is the assumed speed of sound in water. Within Figure 1-5, the red circles highlight several of the visible examples of fading. Each arrival possesses a noticeable pattern as they track along a trending line. Fading is visible when these trending lines begin to experience unexpected gaps. This thesis presents a method for overcoming these types of obstacles, specifically the presence of unexpected fading.

1.1.3 Introduction of the Beaufort Duct

A traditional Arctic sound speed profile (SSP) is characterized by an upward refracting profile over the entire water depth causing sound signals to undergo repeated surface reflections at the underside of the ice [7]. This SSP contains a surface sound duct between the surface and approximately 200 meters depth. The surface sound duct creates a high multipath environment as the sound signals from the source to receiver undergo repeated surface reflections, convergence zone propagation due to a spatially periodic refocusing phenomenon producing zones of high intensity near the surface, and direct path transmission [7]. This traditional Arctic SSP can be seen in Figure 1-6.

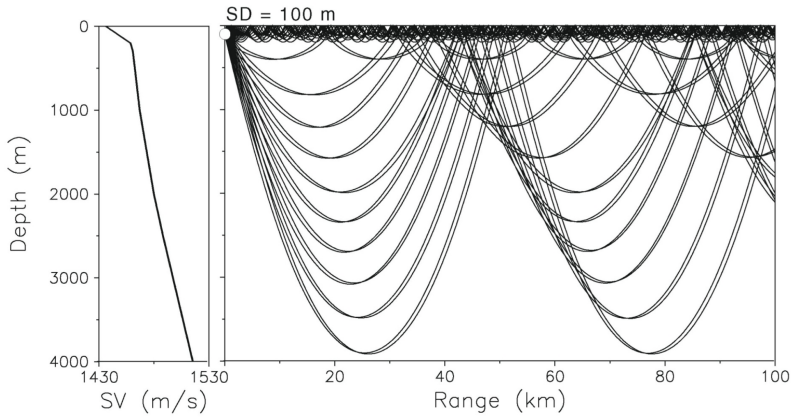

Figure 1-6: Traditional Arctic SSP [7]

A relatively new phenomenon in the Arctic called the "Beaufort Duct" was discovered in 2013 by the Woods Hole Oceanographic Institution through the Ice-Tethered Profiler (ITP) program [12] [13]. The Beaufort Lens is a layer of warm Pacific water

entering the Arctic through the Bering Strait, which is neutrally buoyant at approximately 70-80 meters depth in the Beaufort Sea [12].

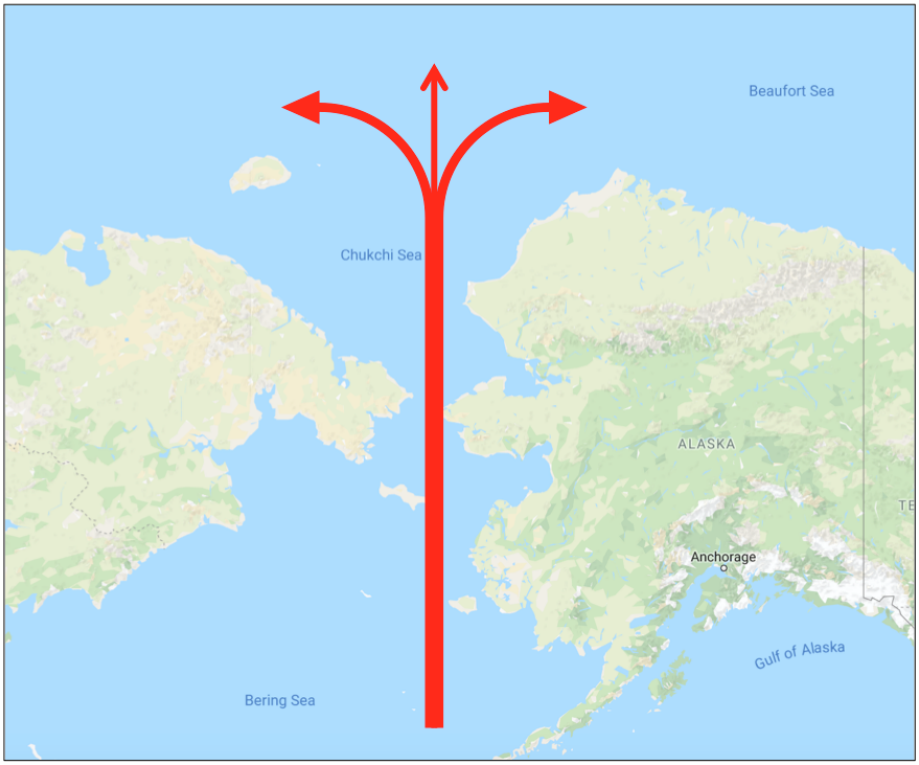

Figure 1-7: The Beaufort Lens

This lens has created a local maximum in the SSP, greatly altering the historically monotonic upward refracting SSP associated with the Arctic thereby creating a second sound duct between approximately 100 and 200 meters depth known as the Beaufort Duct [12]. A comparison of the traditional Arctic SSP with the new Arctic SSP containing the Beaufort Duct can be seen in Figure 1-8.

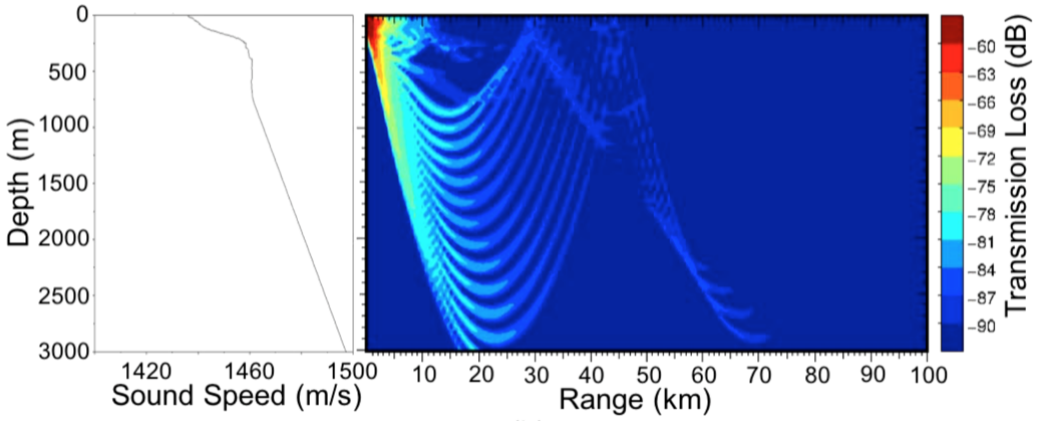

(a) Traditional Arctic SSP

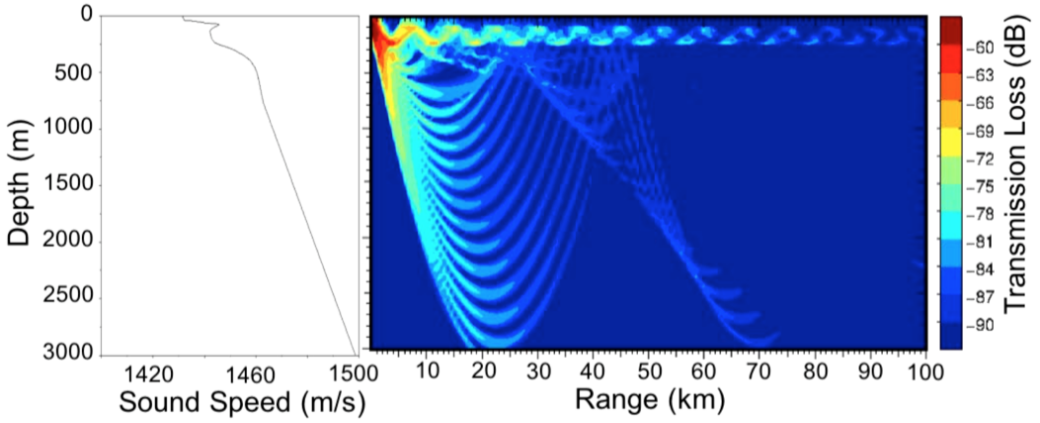

(b) New Arctic SSP with the "Beaufort Duct"

Figure 1-8: Beaufort Duct Effect within the Arctic SSP with corresponding Transmission Losses [12]

The introduction of this second sound duct has further complicated contact tracking capabilities in the Arctic as there now exists an increased multipath acoustic environment. Not only is the increased multipath environment causing tracking problems, but contacts now have the ability to essentially hide in completely different and very unique depth stratums with respect to the source. Contacts being tracked can hide above the Beaufort Duct (approximately 0-100 meters depth), within the Beaufort Duct (approximately 100-200 meters depth), or below the Beaufort Duct (below approximately 200 meters depth) making it difficult to track if the source is located in a different stratum. These difficulties highlight the environmental challenges that must be overcome in order to perform accurate, long-range underwater contact tracking in the Arctic.

1.2 Objective

Although the introduction of the Beaufort Duct and the increased multiple acoustic ray paths has complicated underwater contact tracking in the Arctic, the specific characteristics and patterns of the environment itself can be utilized for increased tracking capabilities. In his book, "Pattern Recognition and Machine Learning," author Christopher Bishop states:

"The field of pattern recognition is concerned with the automatic discovery of regularities in data through the use of computer algorithms and with the use of these regularities to take actions such as classifying the data into different categories [1]."

This thesis aims to utilize the tools presented in the field of pattern recognition and classification to overcome the challenges presented by the high multipath, complex acoustic environment that exists in the Arctic.

The Beaufort Duct undoubtedly creates a more challenging underwater contact tracking environment. Its presence has resulted in the creation of three different, unique depth stratums (above, within, and below the Beaufort Duct) with each possessing their own distinct patterns and characteristics. With these three depth stratums, there exist nine possible combinations for the locations of the sources (beacons) and receivers (AUV) with respect to the Beaufort Duct as illustrated in Figure 1-9.

1. Source = Above Beaufort Duct; Receiver = Above Beaufort Duct
2. Source = Above Beaufort Duct; Receiver = Within Beaufort Duct
3. Source = Above Beaufort Duct; Receiver = Below Beaufort Duct
4. Source = Within Beaufort Duct; Receiver = Above Beaufort Duct
5. Source = Within Beaufort Duct; Receiver = Within Beaufort Duct

6. Source = Within Beaufort Duct; Receiver = Below Beaufort Duct

7. Source = Below Beaufort Duct; Receiver = Above Beaufort Duct

8. Source = Below Beaufort Duct; Receiver = Within Beaufort Duct

9. Source = Below Beaufort Duct; Receiver = Below Beaufort Duct

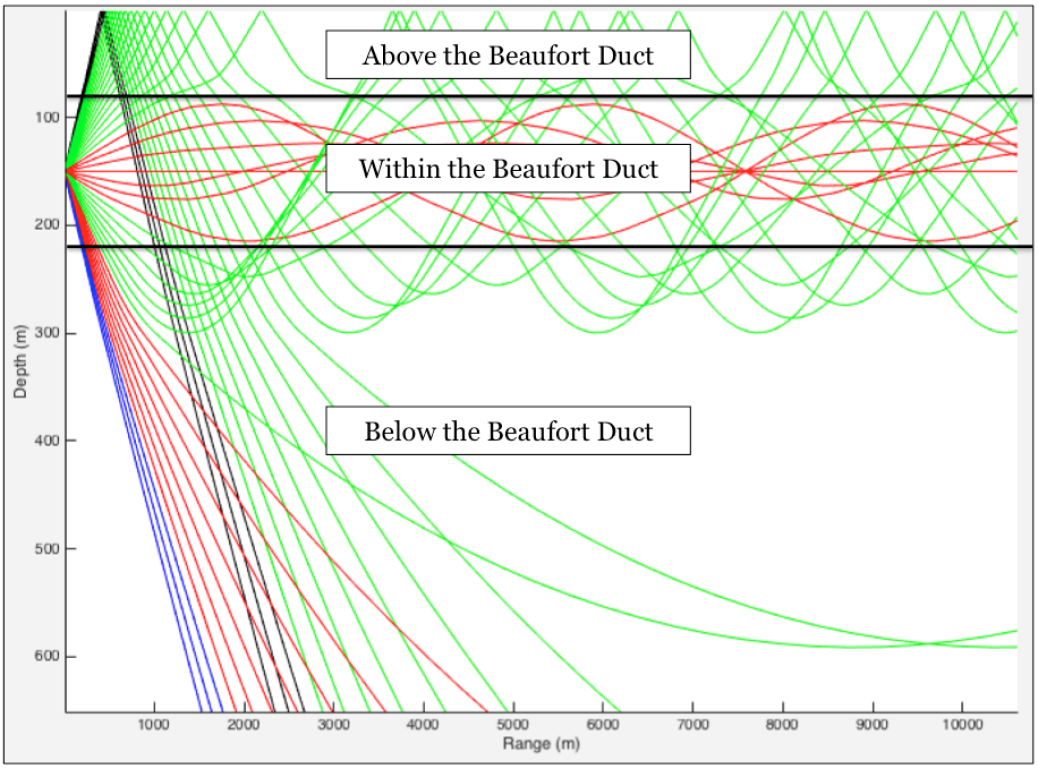

Figure 1-9: The Beaufort Duct

Every single range associated with each of these nine possible source/ receiver combinations possesses a very unique and distinct set of characteristics associated with the signal's received arrival time and the amplitude of this received signal. These arrival times and amplitudes can be thought of as "fingerprints." None are exactly the same, all are unique, and with the proper pattern recognition algorithm, these "finger prints" can be utilized for accurate underwater contact tracking purposes. Figure 1-10 shows a representative example of the signal arrival time patterns in the Arctic for a source and receiver at 30 meters depth.

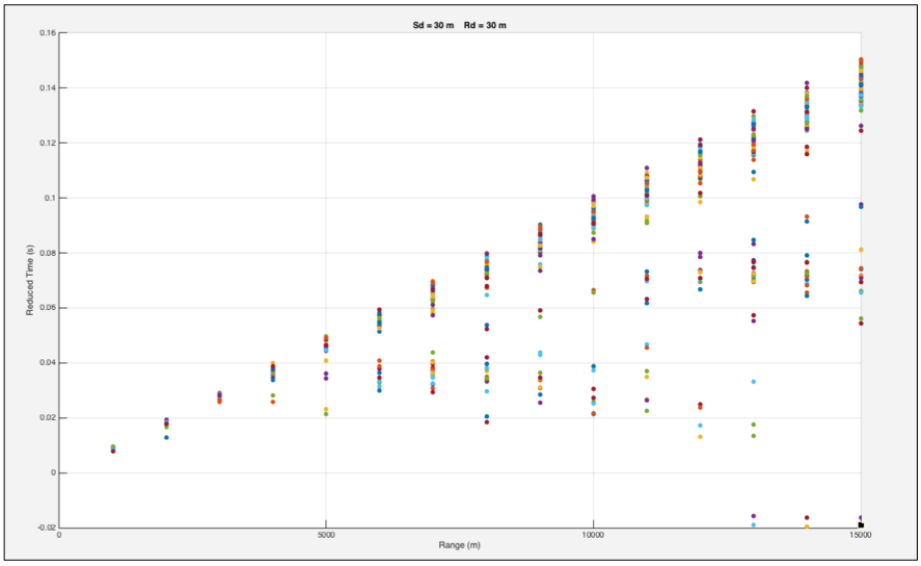

Figure 1-10: Arrival Time Example: Reduced Time vs Range for Sd=30m, Rd=30m

As can be seen in Figure 1-10, every incremental range of 1,000 meters possesses a unique arrival time pattern specific to its range associated with the depth combination of the source and receiver. These unique "fingerprints" are highlighted and illustrated in Figure 1-11.

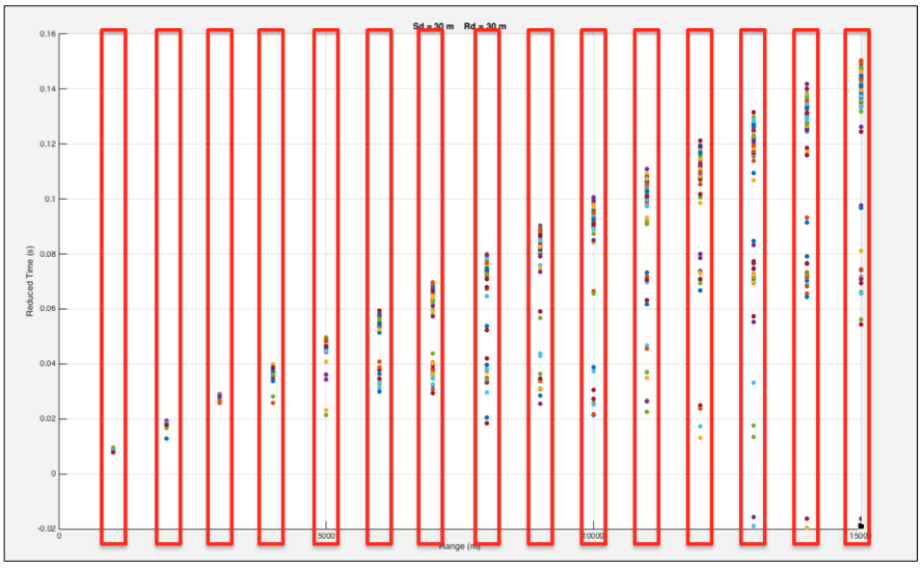

Figure 1-11: Arrival Time "Fingerprint" Illustration for Sd=30m, Rd=30m

Each range possesses its own unique set of patterns as shown in the following comparison of the arrival times seen at 1,000 meters and 15,000 meters, respectively, for the same example of a source and receiver at 30 meters depth.

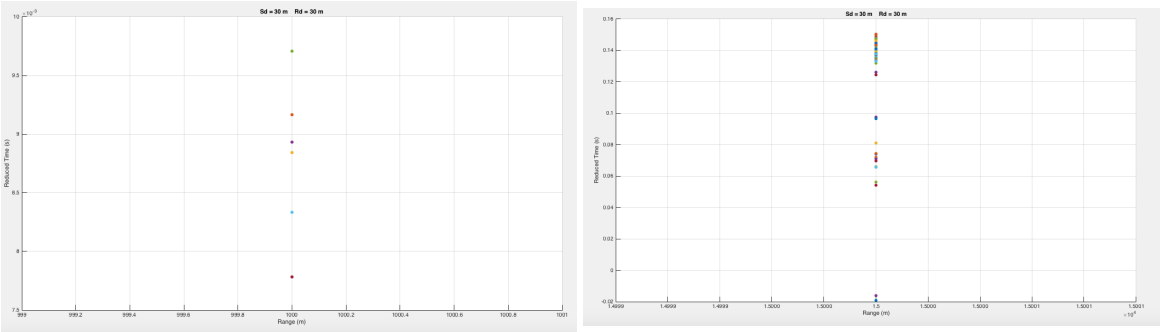

(a) Fingerprint at 1000m

(b) Fingerprint at 15000m

Figure 1-12: Arrival Time "Fingerprint" Comparison at 1000 and 15000 meters for Sd=30m, Rd=30m

All of these arrival times are accompanied by a specific signal strength, or amplitude. These signal amplitudes also provide a unique set of "fingerprints" which can be utilized to increase the fidelity of the pattern recognition analysis.

The overall objective for this thesis is to create a pattern recognition algorithm that utilizes the unique characteristics associated with the high multipath environment found within the Arctic to perform accurate, long-range underwater contact tracking. This will be accomplished by collecting known Arctic SSP data in order to obtain "fingerprint" data associated with signal arrival times and amplitudes within the environment along all ranges for all possible depth stratum combinations of sources and receivers. This arrival time and amplitude data, or "fingerprints," will then be used to construct regional databases. Received inputs of arrival times and amplitudes will then be analyzed against their associated regional data utilizing pattern recognition techniques to determine the desired contact's location, including range and depth.

1.3 Applications

1.3.1 Acoustic Navigation Systems

With the ultimate goal to perform accurate, long-range underwater contact tracking, the primary application for this thesis is the development of an AUV navigation system. The two most commonly used underwater navigation systems employed are long baseline and ultra-short baseline navigation systems.

1. **Long Baseline (LBL) Navigation System**

   A LBL system is comprised of multiple, fixed beacons at known locations. The navigation process begins as the AUV being tracked will actively emit a sound signal. When this emitted signal is received by the beacons, they will each transmit a sound signal at their own, unique frequency. The AUV is able to distinguish each received signal amongst all of the beacons based on their unique frequency signals. The AUV is able to determine the range to each beacon based on the two-way travel time (TWTT) it takes for the sound signal to be emitted by the AUV, and then received again as seen in Equation 1.2.

$$Range = C\frac{\Delta TWTT}{2} \tag{1.2}$$

   where C is the speed of sound underwater. Once the AUV has determined the range to all of the beacons, its location can be determined by triangulating the ranges from each beacon along their specific bearings to the AUV. This concept is illustrated in Figure 1-13.

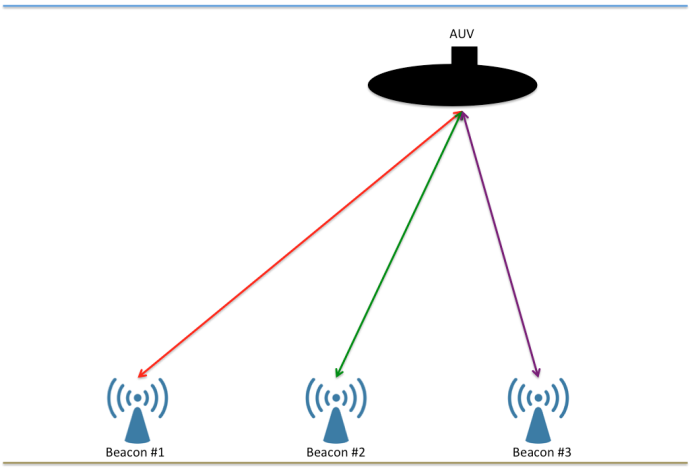

Figure 1-13: Long Baseline Navigation System

The disadvantages of this system are that its range tracking capabilities are limited to 5-10 kilometers due to the fixed locations of the beacons, and existing LBL systems are limited to the tracking of only one vehicle due to their utilization of a time divisive multiple access (TDMA) scheme [15].

2. **Ultra-Short Baseline (USBL) Navigation System**

An USBL system is comprised of a single, fixed transceiver beacon at a known location and an acoustic array on the AUV. Like a LBL system, the AUV will actively emit a sound signal. When this emitted signal is received by the beacon, the beacon will transmit a sound signal of its own. The AUV is able to determine range in the same manner as in the LBL system using the fundamentals of Equation 1.2 and the TWTT of the sound signals sent and received by the AUV. Bearing, and ultimately location, to the AUV is determined by measuring the changing bearings, or phase differencing, between individual elements on the AUV's acoustic array. This concept is illustrated in Figure 1-14.

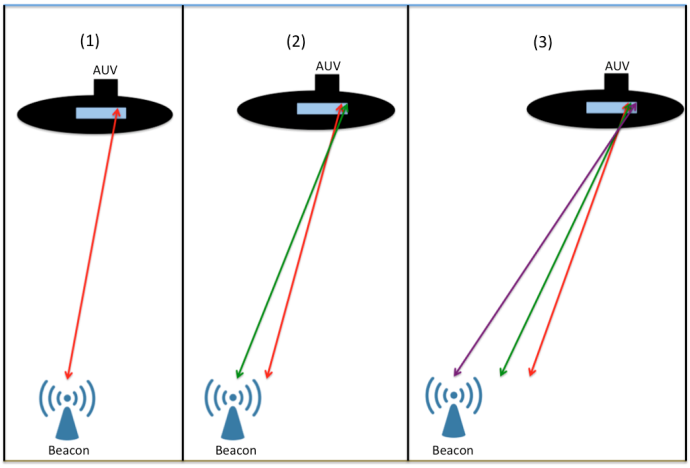

Figure 1-14: Ultra-Short Baseline Navigation System

The disadvantages of this system are that its accuracy is limited to short distances, and it is also limited to the tracking of only one vehicle when employing a TMDA scheme.

A major disadvantage of both LBL and USBL navigation systems are their dependency on TWTT for their range calculations as seen in Equation 1.2. These simple calculations may be accurate at short distances, but develop a great deal of error as the range becomes larger due to the basic limitations associated with an assumed constant underwater sound speed. Furthermore, the high multipath environment of the Arctic makes this range determination process difficult due to the previously discussed issues of fading and improper ray path identification. This is overcome by the use of the pattern recognition algorithms presented in this thesis, as well as one-way travel time (OWTT) acoustic navigation.

There have been a number of advancements made in recent years with regards to OWTT acoustic navigation. Work by Eustice et al. [15] successfully demonstrated the ability to implement the concept of OWTT for the purpose of underwater vehicle navigation through the creation of a synchronous-clock acoustic navigation system with the capability to conduct navigation for multiple underwater vehicles. This work successfully demonstrated the use of OWTT for underwater vehicle navigation through the implementation of a maximum-likelihood fusion framework which

combined OWTT range measurements with vehicle-odometry for bounded-error navigation [15].

Futhermore, work by Rypkema et al. [5] advanced the utilization of OWTT for underwater vehicle navigation through the development of a one-way travel-time inverted ultra-short baseline system (OWTT-iUSBL). This system is comprised of an acoustic beacon that is time-synchronized to a clock on the AUV, which is acoustically passive. This means that it does not output any acoustic signals therefore decreasing power and cost requirements, and allowing the possibility for tracking of multiple AUVs with no time or frequency sharing/ coordination required [5]. The beacon transmits a periodic signal which is received by the time-synchronized AUV using a tetrahedral hydrophone array. OWTT is used to determine range using a matched filter approach, while phased-array beamforming determines bearing to the beacon. This process is detailed in Figure 1-15.

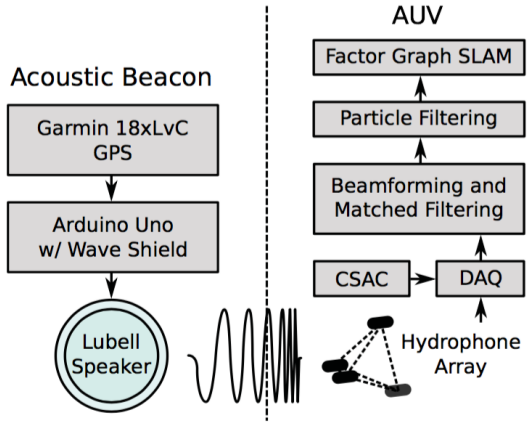

Figure 1-15: OWTT-iUSBL Approach [5]

Advancements in the field of OWTT acoustic navigation, including those by Eustice et al. [15] and Rypkema et al. [5] as previously discussed, have paved the way for its use in underwater vehicle navigation systems. These systems overcome the challenges associated with TWTT and the effects of fading and improper ray path identification found in a multipath environment. They have also opened up the possibilities for multi-vehicle navigation at increased distances. This thesis proposes a method for which such systems can accurately and precisely determine range to the

AUVs for implementation in the high multipath environment found within the Arctic region.

Applications for the work completed within this thesis can be further expanded due to the fact that the developed algorithm utilizes relative times associated with the determination of reduced time rather than the absolute travel time of received acoustic signals as previously discussed in reference to Equation 1.1. This means that the developed pattern recognition program can be applied to a scenario where no information in regards to the location of the source is known, such as tracking an unidentified submarine, AUV, or even a whale emitting sound signals, and detecting strong environmental activities including significant ice fractures in the Arctic. This is possible due to the fact that the pattern recognition program relies solely on "fingerprint" patterns for all range and depth combinations between the source and receiver, independently and non-related to the absolute travel time of the received acoustic signals. This broadens the application of the developed algorithm to a wide array of contact tracking scenarios, but can also be utilized to increase the fidelity associated with time-synchronized, OWTT tracking systems.

1.3.2 Geographical Implementation

The backbone of this thesis is the development of the "fingerprint data", or regional databases, which consist of known signal arrival times and amplitudes along all ranges for all source/ receiver depth combinations. This data was accumulated by utilizing known sound speed profiles at various locations in the Arctic and the ray tracing program, BELLHOP. While sound speed profiles in real-world environments maintain the same general shape and characteristics, they are constantly experiencing slight alterations due to changes in the weather, currents, and other various environmental factors. In order to combat the effects of continuously changing SSPs, the Arctic Region has been divided into smaller sections, in a grid-like manner as seen in Figure 1-16. Each grid square contains its own distinct SSP therefore resulting in the creation of its own unique regional database. The location of the source (beacon) will determine which specific grid square's regional database will be utilized for the

pattern recognition analysis and contact tracking.

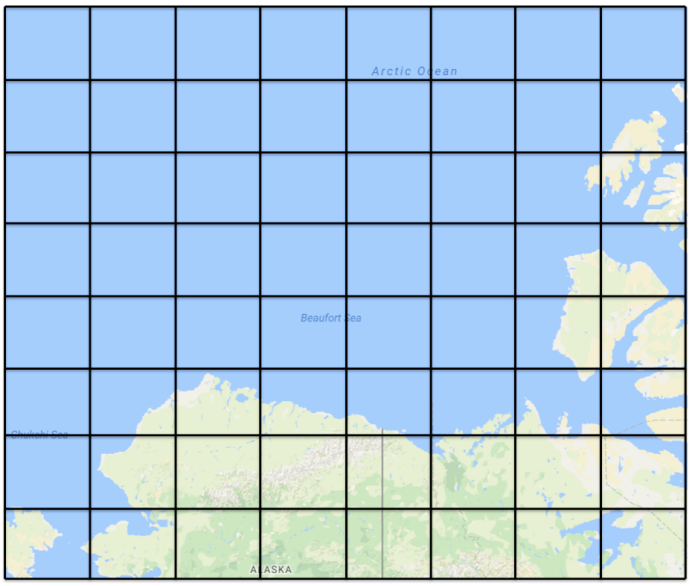

Figure 1-16: Arctic Map Grid Example

1.4 Related Work

In 1994, Max Deffenbaugh submitted a Master's thesis titled "A Matched Field Processing Approach to Long Range Acoustic Navigation [3]." His thesis presented the design and simulation of an acoustic listen-only navigation system for use in the time-varying multipath environment associated with the Arctic. The designed navigation system utilized a long baseline system comprised of beacons fixed at known locations that can transmit and receive acoustic signals therefore working in unison to triangulate a target's location. This was accomplished by utilizing all of the detectable arrivals of each beacon signal to invert for both target position and sound speed profile (SSP). The navigation system incorporated a matched field processing approach by examining an initial estimate of the position and SSP, and then generating a predicted received signal via a propagation model. The predicted signal is compared with the measured signal from the target vehicle thereby creating a prediction error. The prediction error is then inverted to provide updated estimates of the target's position and SSP [3].

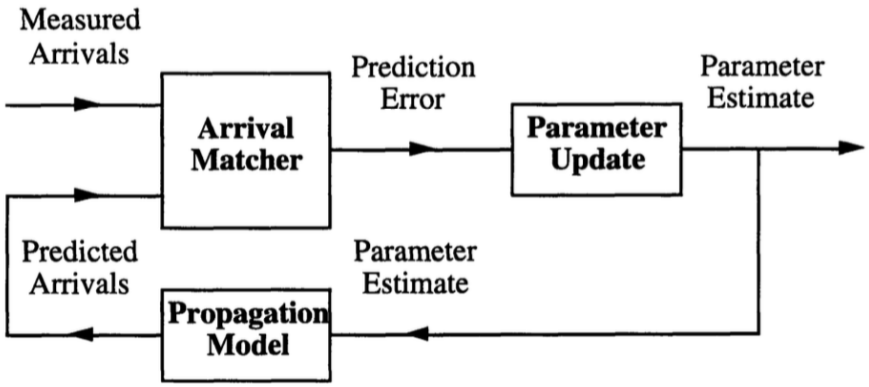

Figure 1-17: Block Diagram for "Matched Field Processing Approach to Long Range Acoustic Navigation" [3]

Mr. Deffenbaugh's thesis was successful in demonstrating that long range submerged contact tracking can be accomplished in a high multipath environment. The method employed evaluated the target's position and SSP in a time-varying environment based on prediction errors, and worked through feedback loops to continuously refine its accuracy.

1.5 Overview

Chapter 2 provides background theoretical information relevant to this thesis work. This includes the development of sound speed profiles, acoustic ray tracing, and an overview of BELLHOP, a ray tracing program which was heavily utilized in the analyses involved with this thesis.

Chapter 3 details the pattern recognition methods employed throughout this thesis. This includes a more detailed description of the signal amplitude and arrival time analyses.

Chapter 4 involves the evaluation and results portion of this thesis. This includes simulations using real-world sound speed profiles found in the Arctic.

Chapter 5 provides an overall conclusion and recommendations for future work to further grow the field of study introduced in this thesis.

Appendix A provides detailed results involved with the simulations conducted in Chapter 5.

Appendix B provides the "fingerprint" data used to construct the ITP84 and ITP85 regional databases.

Chapter 2

Theoretical Background

The purpose of this chapter is to lay the theoretical foundation for which all subsequent analyses completed in this thesis are derived from. These topics include the development of sound speed profiles, ray tracing, and an introduction to BELLHOP, a ray tracing program that was heavily used in the analyses covered within this thesis.

2.1 Sound Speed Profiles

A sound wave is generated from alternating compressions and rarefactions within its medium, which is water for underwater acoustic sound waves. The wave equation is a linear second-order partial differential equation used to describe the propagation of acoustic waves. The wave equation for pressure is derived from the principles of hydrodynamics and the adiabatic relation between pressure and density, specifically the conservation of mass, Euler's equation, and adiabatic equation of state [7]. It is defined as

$$\rho\nabla\cdot\left(\frac{1}{\rho}\nabla p\right)-\frac{1}{c^2}\frac{\partial^2 p}{\partial t^2}=0 \tag{2.1}$$

where ρ is density, ∇ is the gradient operator, p is pressure, c is sound speed, and t is time [7]. The wave equation is the backbone of many underwater acoustic analyses including ray tracing, normal modes, and parabolic equations, among others as illus-

trated in Figure 2-1.

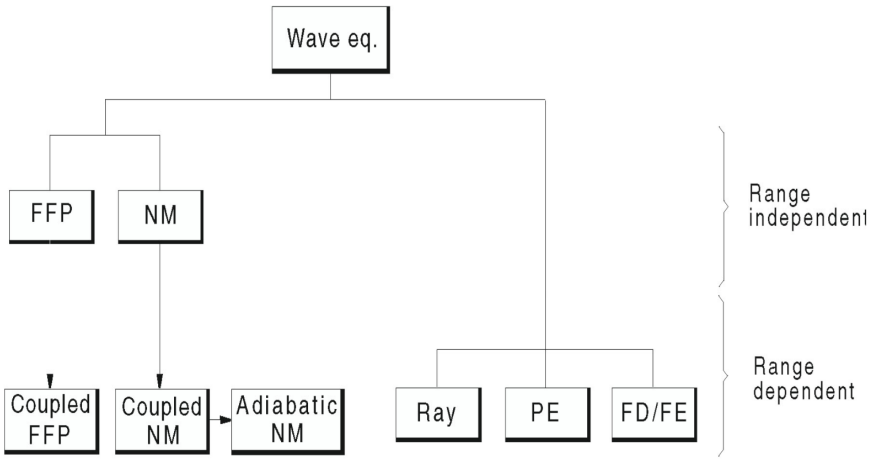

Figure 2-1: Wave Equation Implementation [16]

Another important aspect of many underwater acoustic analyses is the development of sound speed profiles. Sound speed profiles are comprised of an environment's sound speed in terms of depth as seen from the generic example provided in Figure 2-2.

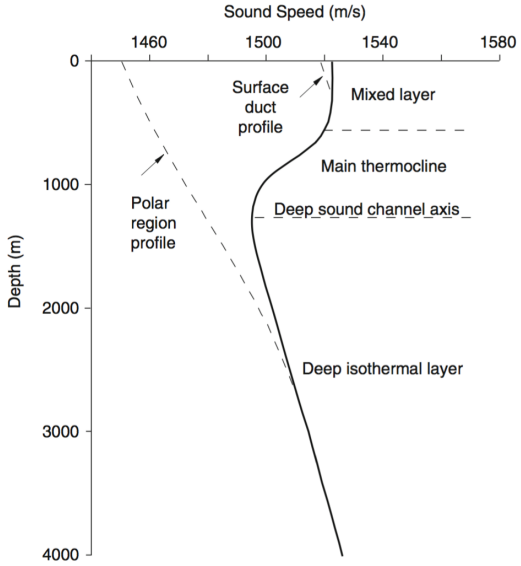

Figure 2-2: Generic Sound Speed Profiles [7]

Sound speed profiles are used to determine key characteristics in terms of an

environment's acoustic behavior. A key aspect of establishing sound speed profiles is accurately determining the sound speed. Sound speed within the ocean is dependent on the temperature, salinity, and depth of the water. The speed of sound is determined using an empirical function taking into account these three independent variables as defined in Equation 2.2 [7].

$$c = 1449.2 + 4.6T - 0.055T^2 + 0.00029T^3 + (1.34 - 0.01T)(S - 35) + 0.016z \quad (2.2)$$

where T is temperature, S is salinity, and z is depth. The characteristics of an environment's sound speed profile determines the behavior behind how a sound wave travels underwater. This behavior is best described with the use of Snell's Law which relates the angle of a sound wave's ray path to the sound speed as seen in Equation 2.3.

$$\frac{cos\theta(z)}{c(z)} = constant \quad (2.3)$$

It can be seen from Snell's Law that sound waves are attracted to lower speeds of sound, and vice-versa for higher speeds of sound [16]. This phenomena is illustrated in Figure 2-3.

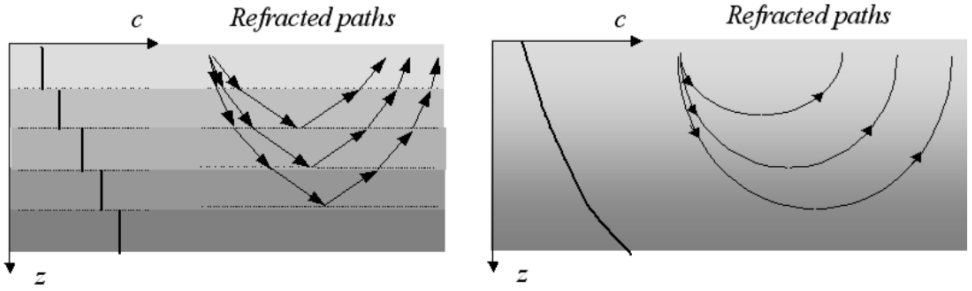

Figure 2-3: Theoretical Application of Snell's Law [9]

Snell's Law is used to model the direction which sound waves will travel and is essential for ray tracing and all subsequent analyses. An overview of this implementation and ray tracing is provided in the following section.

2.2 Ray Tracing

The ability to conduct ray tracing is a very powerful tool for underwater acoustic studies. Ray tracing allows multiple analyses to be conducted based on an environment's unique characteristics. It has many applications including high frequency and broadband problems, tomography, acoustic communications, active sonar, range-dependent problems, reverberation, and real-time and virtual experiments [16]. Figure 2-4 provides an example of ray tracing conducted on a sound speed profile from the Balearic Sea.

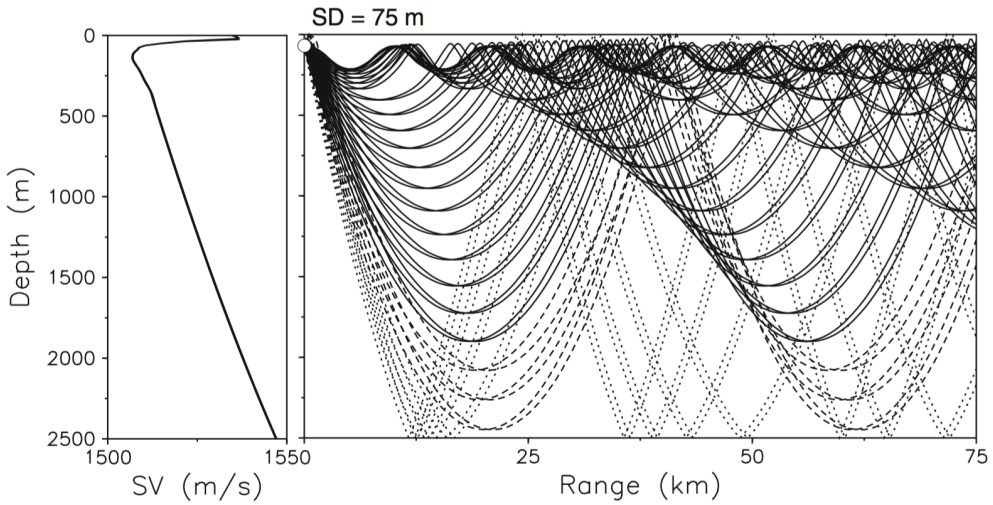

Figure 2-4: Ray Tracing Example from Balearic Sea [7]

Utilizing the principles discussed in the previous section associated with Snell's Law, it can be seen how the paths of individual rays travel based on the changing sound speeds. The trajectory and coordinates of each ray can be determined using mathematical derivations beginning with the Helmholtz equation, Equation 2.4 [7].

$$\nabla^2 p + \frac{\omega^2}{c^2(\mathbf{x})} p = -\delta(\mathbf{x} - \mathbf{x}_0) \tag{2.4}$$

where $\mathbf{x}$ = (x,y,z) in Cartesian coordinates, c($\mathbf{x}$) is the speed of sound, and ω is the angular velocity of the source. The Helmholtz equation is a time-independent form of the wave equation, Equation 2.1. By taking derivatives of the Ray Series equation,

$$p(\mathbf{x}) = e^{i\omega\tau(\mathbf{x})} \sum_{j=0}^{\infty} \frac{A_j(\mathbf{x})}{(i\omega)^j}, \tag{2.5}$$

substituting into Equation 2.4, and simplifying by terms of ω, the Eikonal equation and its associated transport equations of higher order are determined [7]. The Eikonal equation is expressed as follows:

$$|\nabla\tau|^2 = \frac{1}{c^2(\mathbf{x})} \tag{2.6}$$

Through the process of solving the Eikonal equation by the method of characteristics, the ray equations, in cylindrical coordinates, are determined [7]. The governing ray equations, in first-order form, are expressed as follows:

$$\frac{dr}{ds} = c\xi(s), \quad \frac{d\xi}{ds} = -\frac{1}{c^2}\frac{\partial c}{\partial r}, \tag{2.7a}$$

$$\frac{dz}{ds} = c\zeta(s), \quad \frac{d\zeta}{ds} = -\frac{1}{c^2}\frac{\partial c}{\partial z}, \tag{2.7b}$$

where $[r(s), z(s)]$ is the trajectory of the ray in the range-depth plane, and ξ(s) and ζ(s) serve as ancillary variables [7]. The tangent vector to the curve $[r(s), z(s)]$ is defined as $[dr/ds, dz/ds]$ and can be written as $t_{ray} = c[\xi(s), \zeta(s)]$ [7]. In order to complete the process of projecting the ray path, initial conditions are applied such that the rays start at the source position (r_0, z_0) with a specified take-off angle θ_0, thus resulting in the initial condition ray equations expressed as follows,

$$r = r_0, \quad \xi = \frac{cos\theta_0}{c(0)}, \tag{2.8a}$$

$$z = z_0, \quad \zeta = \frac{sin\theta_0}{c(0)}, \tag{2.8b}$$

This process of projecting ray paths utilizing the ray path governing equations and associated initial conditions is illustrated within Figure 2-5.

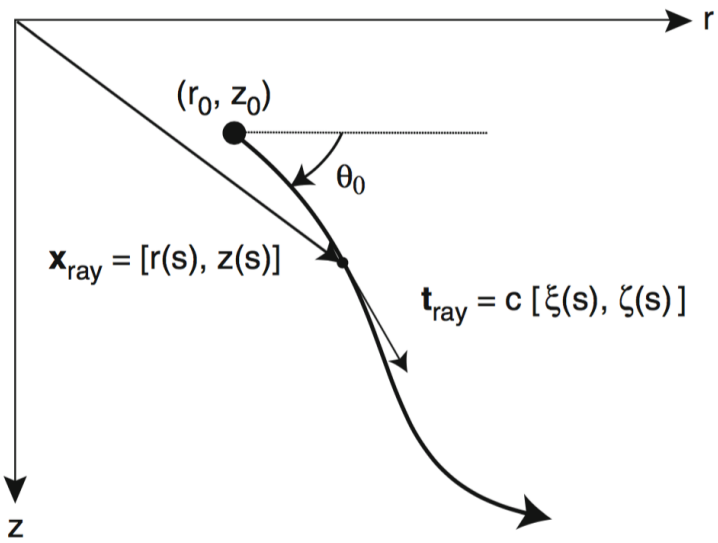

Figure 2-5: Ray Path Geometry [7]

By applying these principles, ray tracing programs can be developed to provide extremely useful tools for studying and analyzing the underwater acoustics environment. BELLHOP is one such program that proved to be essential for the analyses completed within this thesis. An overview of this program is provided within the following section.

2.3 Introduction to BELLHOP

BELLHOP is a ray tracing program created by Michael Porter of Heat, Light, and Sound Research, Inc., as a part of the Acoustic Toolbox online at the Ocean Acoustics Library [8] [11]. BELLHOP possesses the ability to produce a variety of useful output files as outlined below and illustrated within Figure 2-6.

1. **Inputs**

The primary input file required by BELLHOP is through the use of an environmental file, which contains sound speed profile information. The geometry of sources and receivers can be detailed within source beam pattern files with the use of angle-amplitude pairs, otherwise the source is assumed to be omnidirectional. Additionally, the top and bottom surfaces can be detailed and characterized through the use of several input files. The first is through the use of bathymetry and altimetry files, which are utilized for range-dependent surfaces. Secondly, users can characterize top and bottom surfaces with the use of top and bottom reflection coefficient files, respectively, which contain surface reflection coefficients and angle-reflection coefficient pairs defining the reflectivity [11]. As the backbone of BELLHOP, a detailed explanation of the environmental file input is provided within the following section, Section 2.3.1.

2. **Outputs**

The types of output files produced by BELLHOP are determined by the user within the environmental file. These options include ray tracing, pressure fields, and arrivals. Within the ray tracing option, typical ray tracing files can be created which illustrate a fan of rays emanating from a source, or eigenrays which include only the rays between the source and a specified receiver location. The pressure fields option has the ability to produce a variety of transmission loss plots including coherent, incoherent, and semi-coherent acoustic pressure fields. The arrivals option provides an arrival file containing amplitude-delay pairs defining the intensity and delay for each acoustic signal in the given environment [11]. These outputs, along with their respective inputs, are further detailed in Figure 2-6, which provides an overview of the BELLHOP input/ output structure.

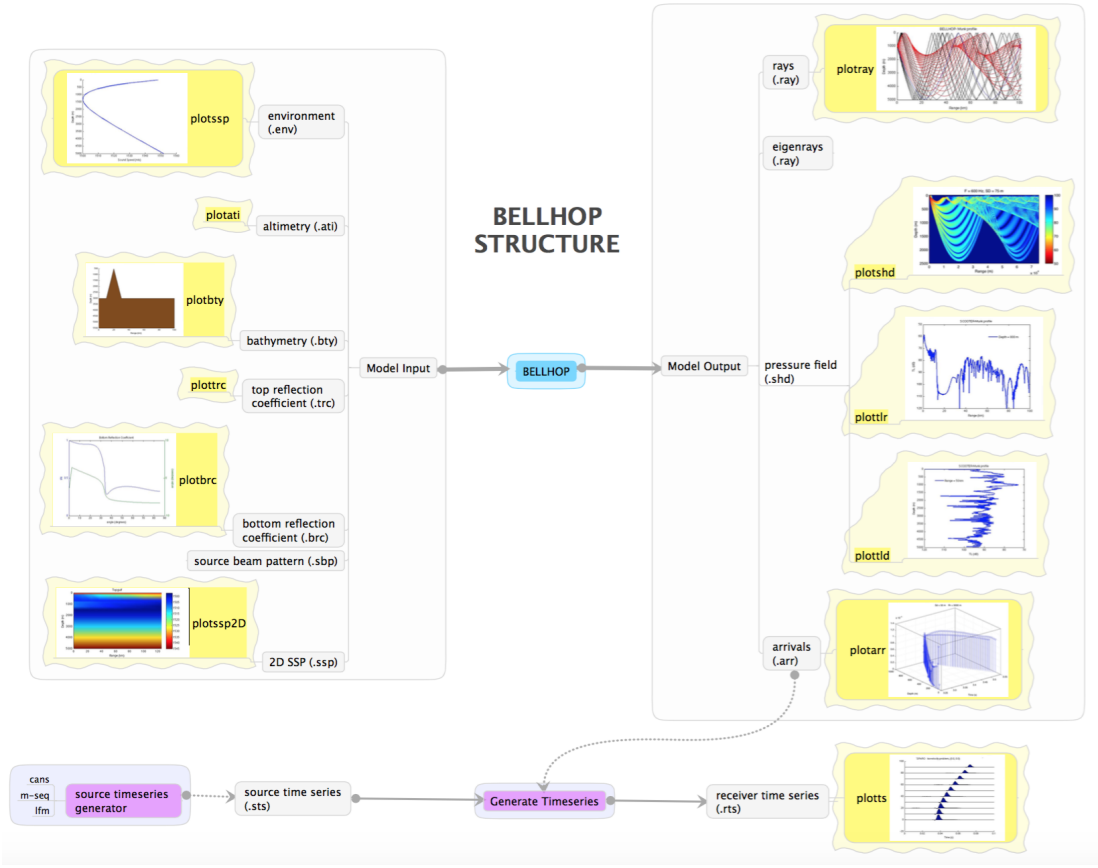

Figure 2-6: BELLHOP Structure [11]

2.3.1 Environmental File Overview

1: 'Arctic Analysis'

2: 50.0 !FREQ (Hz)

3: 1 !NMEDIA

4: 'CVW' ! SSPOPT (Analytic or C-linear interpolation)

5: 380 16.315456 3000

6: 16.315456 1431.40291 /

18.354888 1431.435676 /

20.39432 1431.468307 /

ETC

```
    3000          1499.5/
7:  'A' 0.0
8:  3000.0 1600.00 0.0 1.8 0.8 /
9:  1                                                    ! NSD
10: 30 /                                                 ! SD(1:NSD) (m)
11: 1 /                                                  ! NRD
12: 30 /                                                 ! RD(1:NRD) (m)
13: 151                                                  ! NRR
14: 0.0 15.0 /                                           ! R(1:NR ) (km)
15: 'A'                                                  ! 'R/C/I/S'
16: 1000                                                 ! NBEAMS
17: -20.3 20.3 /                                         ! ALPHA1, 2 (degrees)
18: 0.0 5500.0 101.0 ! STEP (m), ZBOX (m), RBOX (km)
```

Table 2.1: Environmental File Example

The information found within Table 2.1 provides the construct for the creation of an environmental file. Exclamation points are used as a means to provide comments as BELLHOP does not read anything to the right of an '!.'

Line 1 is simply a "title" line with no impact on the BELLHOP analysis.

Line 2 is the source frequency.

Line 3 is 'NMedia' and is always set to one in BELLHOP as it is included only for compatibility purposes with other programs within the Acoustic Toolbox.

Line 4 is used to describe the method of interpolation by BELLHOP to determine sound speed between each set SSP point provided in line 6, the type of surface, and the type of attenuation units. For this example, 'CVW' is set, which 'C' is curvilinear interpolation, 'V' is vacuum above the surface, and 'W' is attenuation units of dB/ wavelength. Additional options for the interpolation type include 'S' for cubic spline, 'N' for N2-linear, 'A' for analytic interpolation, and 'Q' for quadratic approximation to the sound speed field. Additional options for the types of surface include 'R' for perfectly rigid media above the surface, 'A' for acoustic halfspace, and 'F' reads

from a list of predetermined reflection coefficients provided from an input reflection coefficient file. Additional options for the type of attenuation units include 'F' for (dB/m)kHz, 'L' for units corresponding to the parameter loss, 'M' for dB/m, 'N' for Nepers/m, and 'Q' for the Q-factor [14].

Line 5 provides the number of SSP points listed in Line 6, the shallowest depth, and the deepest depth. For this example, 380 sound speed pairs of depth and velocity are provided in line 6, 16.315456 meters is the shallowest depth, and 3000 meters is the deepest depth.

Line 6 is the SSP data in terms of depth-velocity pairs. For this example, the 380 lines containing the depth-velocity pairs were abbreviated for illustrative purposes. The SSP data used to construct the environmental files utilized for this thesis were found at the website provided in [13]. Specifically, data from ITP 84 and 85 were used to construct the regional databases and test platforms, which will be discussed with greater detail in later chapters.

Line 7 is used to describe the bottom boundary. For this example, 'A' is acoustic halfspace. Additional options for bottom boundaries include 'V' for vacuum below the water column and 'R' for rigid below the water column [14].

Line 8 is also used to describe bottom boundary, including the bottom depth, density at the bottom boundary, and alpha at the bottom boundary. For this example, 3000 meters is the bottom depth, the next two numbers can be ignored, 1.8 is the bottom density, and 0.8 is the bottom alpha.

Line 9 is the number of sources x depth (array). For this example, there is one source.

Line 10 is the source depth. For this example, source depth is 30 meters.

Line 11 is the number of receivers x depth (array). For this example, there is one receiver for each depth stratum.

Line 12 is the receiver depth. For this example, receiver depth is 30 meters.

Line 13 is the number of receivers x range. For this example, 151 receivers are to be evenly spaced over 15.0 kilometers, the distance specified in line 14, from the source to the receiver range. This results in a receiver being located every 100 meters

from 0.0 to 15.0 kilometers in range.

Line 14 is the receiver range. For this example, the receiver range is from 0.0 to 15.0 kilometers.

Line 15 is the "RunType." For this example, 'A' is for arrivals, which result in the output of arrival files as discussed in the previous section. Additional options for the run type include 'E' for eigenrays, 'R' for ray tracing, 'C' for coherent acoustic pressure, 'I' for incoherent acoustic pressure, and 'S' for semi-coherent acoustic pressure[14].

To help illustrate the descriptions of lines 9 through 15, Figure 2-7 is provided. In this figure, the blue circle represents the source location (lines 9 and 10), while the red circles represent the receiver locations for all depth/ range combinations (lines 12, 13, and 14).

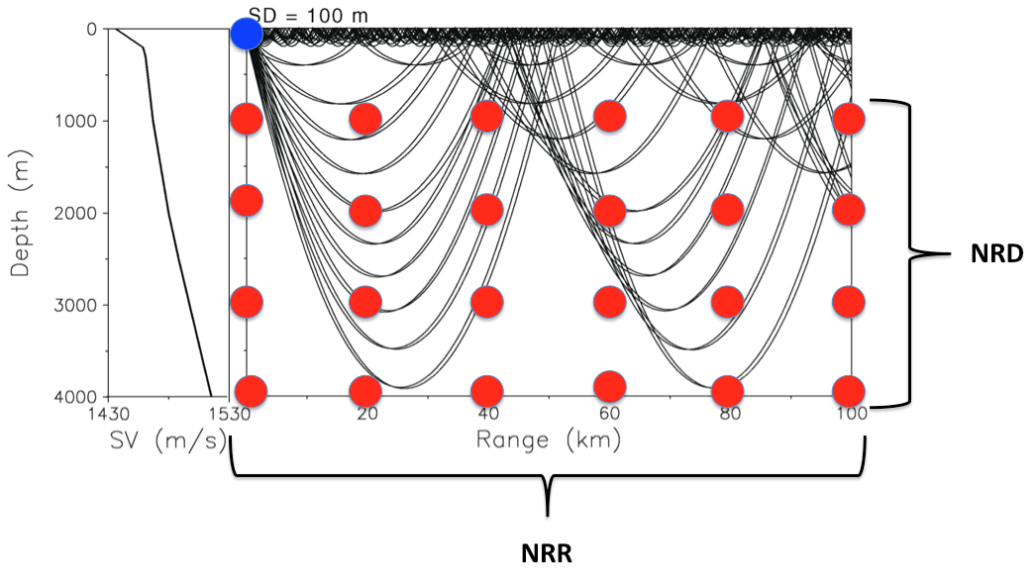

Figure 2-7: Source/Receiver Locations within Environmental File

Line 16 is "NBeams," which is the number of beams or launching angles. For this example, there are 1000 beams.

Line 17 describes the angular spread of the beams allocated in Line 16. For this example, the 1000 beams specified in line 16 are evenly distributed from -20.3 to 20.3 degrees.

Line 18 is the step size used to trace a ray, along with the depth and range of a box beyond which no rays are traced. For this example, the step size is 0.0 meters, and the box is at 5500 meters depth and 101.0 kilometers in range.

A further detailed explanation of all options for each line and their associated descriptions can be found within [11], which is a user guide written by Michael Porter, and within [14], which is written by Orlando Rodriguez of the Signal Processing Laboratory at the Universidade do Algarve.

Chapter 3

Development of Pattern Recognition Algorithm

3.1 Overview of Pattern Recognition

Pattern recognition is a very useful took that can be utilized to extract meaningful data patterns from seamlessly uncorrelated and unusable data sets. In their book, "Pattern Classification," authors Duda et. al provide a very helpful example highlighting the advantages of applying pattern classification and recognition techniques. This example covers the goal for a fish packing plant to automate the process of sorting incoming fish according to their species, salmon or sea bass [4]. Although fish possess many unique characteristics, length and lightness of color are the two most prominent distinguishing characteristics between salmon and sea bass which were used as the two classifiers in this example. Figures 3-1a and 3-1b provide examples of classifying the fish by one characteristic alone, either by length or lightness.

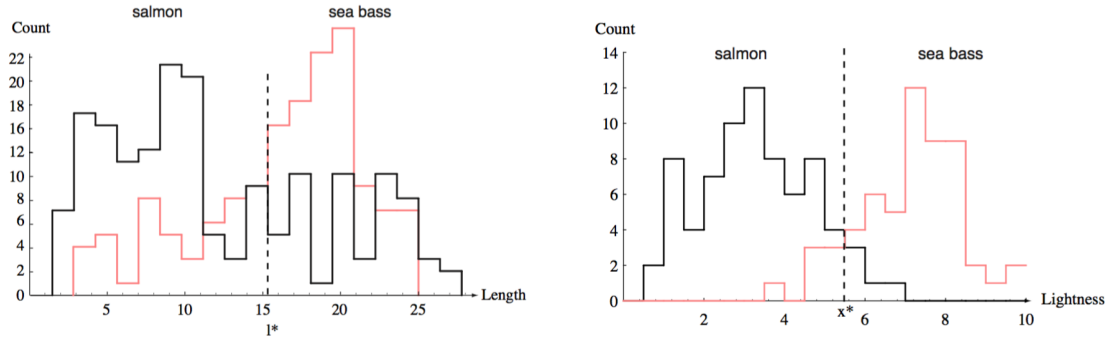

(a) Classifier #1: Length

(b) Classifier #2: Lightness

Figure 3-1: Example: Individual Fish Packing Classifiers [4]

Although both length and lightness individually provide obvious classifying trends, each also presents a great deal of sorting errors if used alone. Together, these two identifying features can be used to provide a more conclusive and accurate sorting criteria. Figure 3-2 provides a sorting criteria combining both length and lightness.

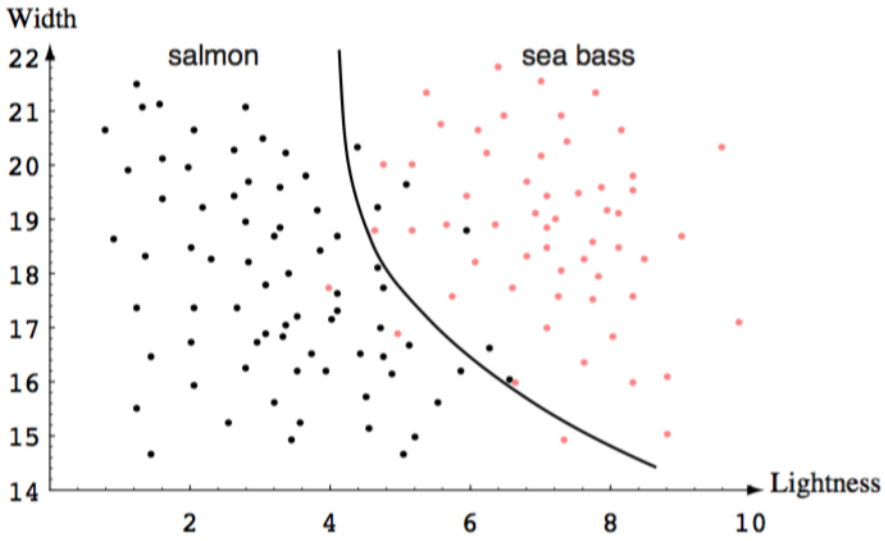

Figure 3-2: Example: Ideal Fish Sorting Criteria [4]

The dark line serves as the decision boundary. It can be seen that the overall classification error is lower than if only one feature were to be used as evident by the conclusive separation between the two species of fish. An ideal decision boundary

will represent the optimal balance between sorting accuracy and classifier simplicity [4]. This simple example demonstrates the advantages of effectively applying pattern classification and recognition techniques by highlighting the importance of selecting the appropriate classifiers and associated decision boundary.

This thesis employs the use of two pattern classifiers in order to perform contact tracking. These classifiers include the received acoustic signal's arrival time and amplitude, converted to transmission loss. These classifiers are discussed in further detail within Sections 3.3 and 3.4 for amplitude and arrival time, respectively.

3.2 Set Up

3.2.1 Assumptions

Listed below are the assumptions carried forth within this thesis.

1. The source (beacon) operates at a single frequency.
2. The ocean surface and bottom are treated as flat.
3. Only one receiver is being tracked.
4. Depths of 30, 150, and 500 meters are all encompassing for stratums associated with above, within, and below the Beaufort Duct, respectively.

3.2.2 Regional Databases

The acoustic data utilized for this thesis was acquired from an instrument employed in the Arctic Region called an Ice-Tethered Profiler (ITP). The ITP data was collected and made available by the Ice-Tethered Profiler Program based at the Woods Hole Oceanographic Institution [13]. An ITP system is comprised of a tethered wire rope that extends vertically down through an ice flow into the ocean with an underwater instrument that travels up and down the rope collecting acoustic data through the use of oceanographic sensors [13]. This system is depicted in Figure 3-3.

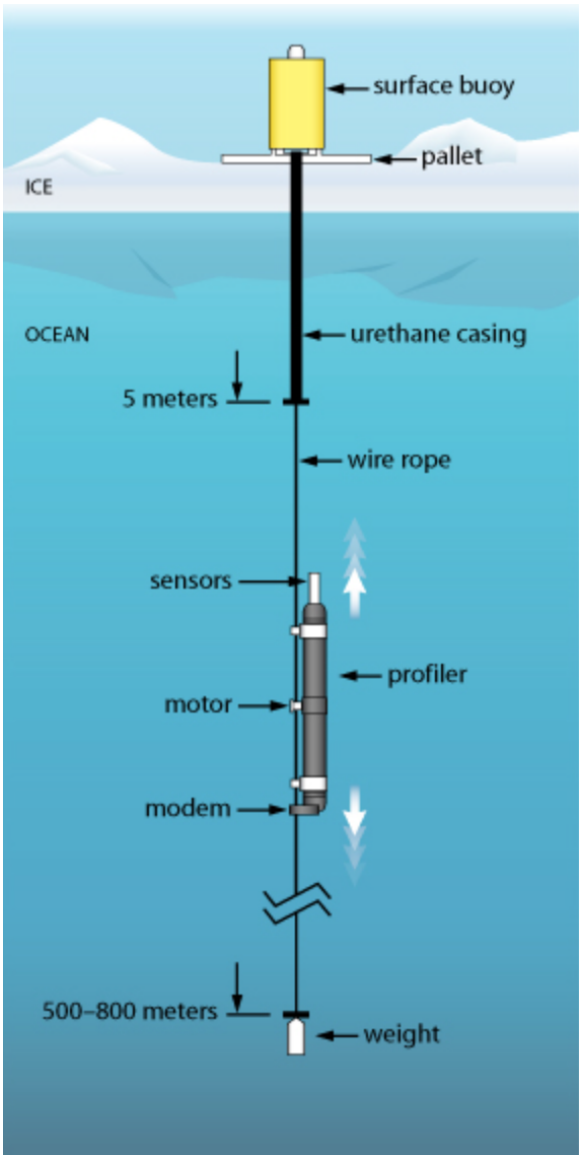

Figure 3-3: Ice-Tethered Profiler System [13]

These profilers are operated in various locations within the Arctic Region. As stated in Section 1.3.2, the intent for this thesis is to perform pattern recognition of received acoustic signals using regional databases depending on the location of the source, or beacon. Two regional databases were created from the ITP84 and ITP85 collected data sets. Specifically, these were created from ITP84grd0100 and ITP85grd0101. The ITP84 regional database is located in the south region, while the ITP85 regional database is located in the north region as depicted in Figure 3-4.

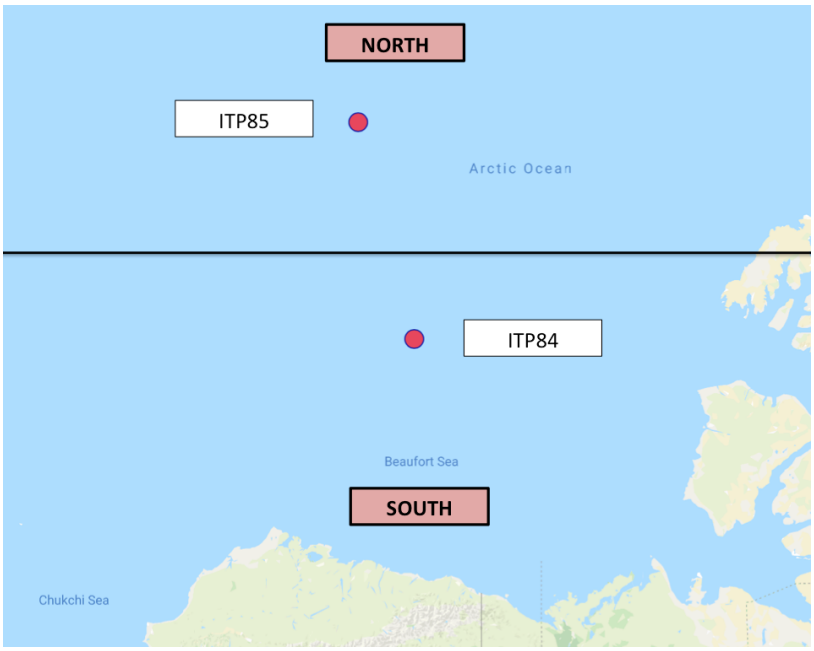

Figure 3-4: Regional Database Locations

The data from the ITPs were used to create sound speed profiles. These sound speed profiles were then input into BELLHOP in order to produce ray tracing and arrival information, including arrival times and signal amplitude, for various depths and ranges. The regional databases are comprised of the signals' arrival times and amplitudes converted into transmission losses. The databases contain this information for all nine depth combinations of the source and receiver with respect to the Beaufort Duct as previously described in Section 1.2. Depths of 30, 150, and 500 meters were chosen to represent the locations above, within, and below the Beaufort Duct, respectively. The nine combinations of source depth (Sd) and receiver depth (Rd) are as follows:

1. Sd = 30m; Rd = 30m
2. Sd = 30m; Rd = 150m
3. Sd = 30m; Rd = 500m
4. Sd = 150m; Rd = 30m
5. Sd = 150m; Rd = 150m

6. Sd = 150m; Rd = 500m

7. Sd = 500m; Rd = 30m

8. Sd = 500m; Rd = 150m

9. Sd = 500m; Rd = 500m

The "fingerprint" data comprised of arrival times and transmission losses that make up the regional databases are provided for all nine of these source and receiver depth combinations along a range spectrum of 0 to 15,000 meters in 100 meter increments. This results in each regional database containing 150 "fingerprints" for both arrival times and transmission losses at each source/ receiver depth combination for a total of 1,350 arrival time and transmission loss "fingerprints" per database, or 2,700 total "fingerprints" per database. Figure 3-5 is an example of the transmission loss and arrival time "fingerprint" data found in the ITP84 regional database for both a source and receiver depth of 30 meters.

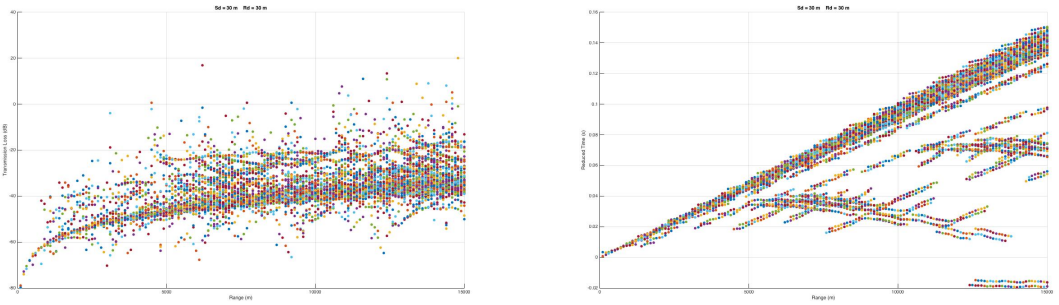

(a) TL Data **(b)** Arrival Time Data

Figure 3-5: ITP84, Sd=30m, Rd=30m: "Fingerprint" TL and Arrival Time Data

An example snippet of several "fingerprints" from the ITP84 regional database can be found within Figure 3-6. This data represents the same graphical information found within Figure 3-5 for both the source and receiver at 30 meters depth, but only covering 2,400, 2,500, and 2,600 meters in range as highlighted in Figures 3-6a and 3-6b.

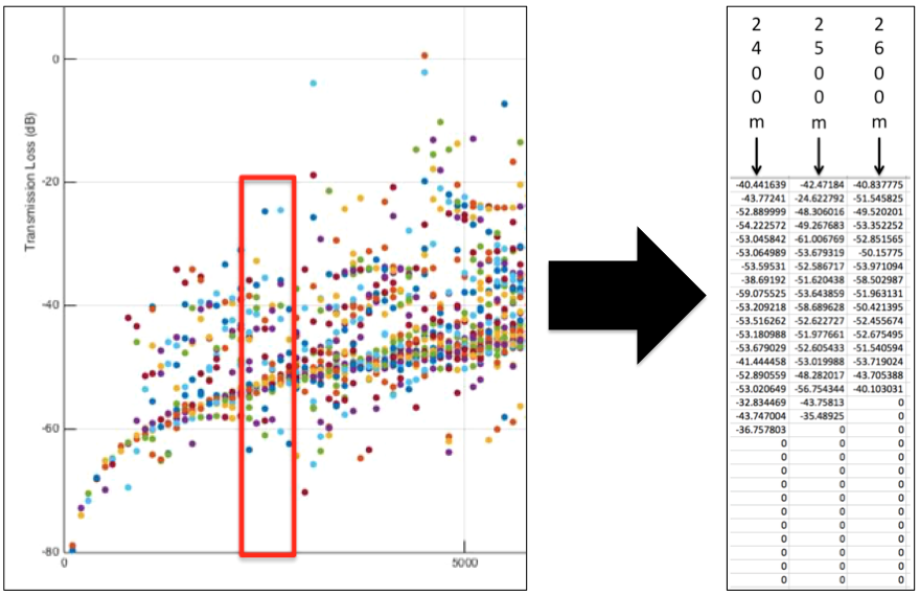

(a) "Fingerprint" TL Data Sample

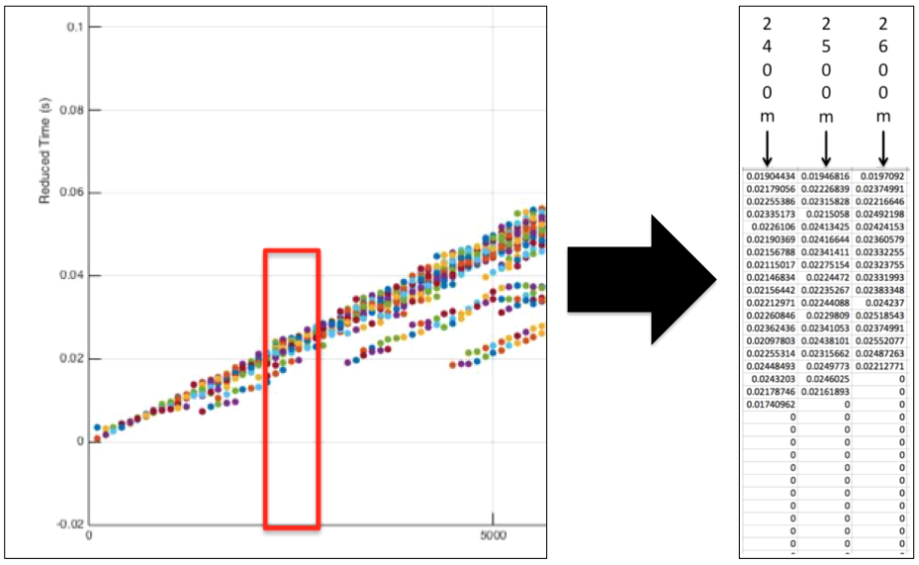

(b) "Fingerprint" Arrival Time Data Sample

Figure 3-6: ITP84, Sd=30m, Rd=30m: "Fingerprint" TL and Arrival Time Data Sample

All transmission loss and arrival time "fingerprint" data for both ITP84 and ITP85 regional databases can be found in Appendix B.

Surface Bounces

Due to the fact that BELLHOP treats the surface as perfectly reflective and does not account for surface bounce transmission losses, this was accounted for by deducting a certain amount of the signal's amplitude for each surface bounce that each sound signal undergoes. In his book "Sound Propagation in the Sea," author R.J. Urick compiled a table of surface loss measurements taken from various studies [17]. A general conclusion from these studies is that the surface loss is less than 1 dB at frequencies less than 1kHz [17]. The analyses performed within this thesis used source frequencies less than 1kHz, therefore surface losses were assumed to be less than 1 dB per surface bounce. This deduction value was built as a user input into the pattern recognition code and can easily be adjusted as necessary.

3.2.3 Test Platforms

In order to test and evaluate the developed pattern recognition program, test platforms were created for each ITP84 and ITP85 database. Table 3.1 provides the coordinates for all regional database and test platform locations.

	ITP	Longitude (E+)	Latitude (N+)
Regional Databases	ITP84grd0100	146.0378	75.3622
	ITP85grd0100	150.2457	78.9751
Test Platforms	ITP84grd0110	-146.6002	75.1814
	ITP85grd0101	-149.8379	78.9462

Table 3.1: ITP Location Coordinates

These test platforms were used to develop test inputs for the program. They were also chosen from the ITP84 and ITP85 data sets. Specifically, they were created from ITP84grd0110 and ITP85grd0101. These two were chosen because they were located within the general proximity of the regional database locations and provided enough variation in the environment to produce robust testing standards. Figure 3-7 shows the locations of the test platforms with respect to the regional databases.

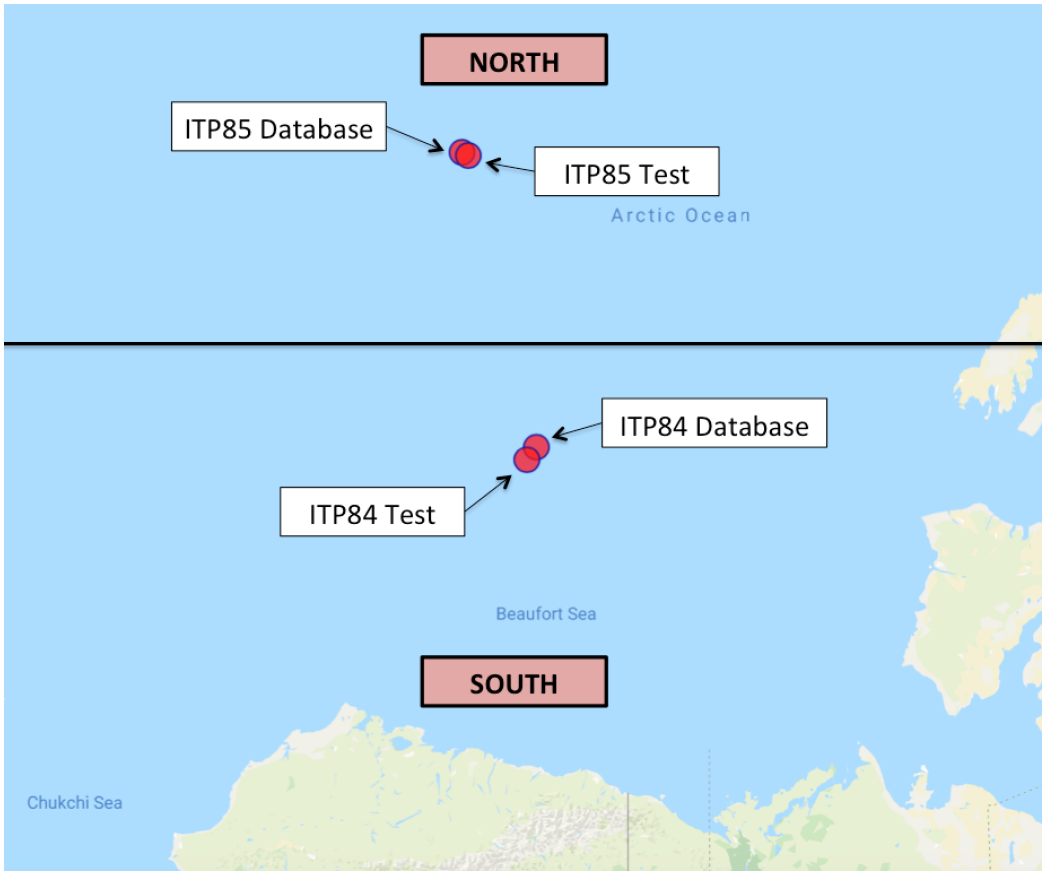

Figure 3-7: Regional Database and Test Platform Locations

A side-by-side comparison of the sound speed profiles for the regional databases and their respective test platforms can seen below in Figures 3-8 and 3-9.

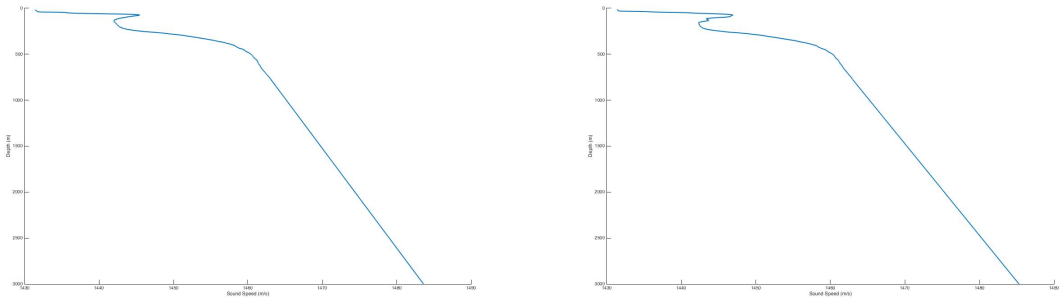

(a) Database **(b)** Test Platform

Figure 3-8: ITP84 Database and Test Platform SSP Comparison

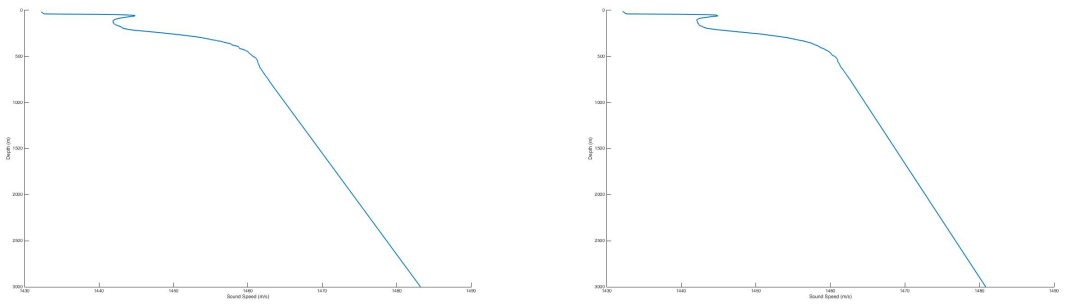

(a) Database **(b)** Test Platform

Figure 3-9: ITP85 Database and Test Platform SSP Comparison

Although the general shape of these SSPs are very similar, the slight variations create substantial differences in arrival patterns. These differences allow for excellent pattern recognition testing which will be discussed in further detail within the ensuing sections.

3.2.4 Program Inputs

The inputs for the developed pattern recognition program include various direct user inputs and parameters from the received acoustic signals. These include the following:

1. **Source Location**

   It is assumed that the location of the source, or beacon, is known. This is important as this determines which regional database will be used for carrying out the pattern recognition algorithm. For the purposes of this thesis, this location is simply either the south or north region, as ITP84 and ITP85 represent the south and north regions, respectively.

2. **Source Depth**

   It is assumed that the depth of the source, or beacon, is known. This is important because it narrows down the possible depth combinations of the source

and receiver from nine to three, which decreases the program run time resulting in a more efficient, and overall better, contact tracking program.

3. **Confidence Filter**

   This input is provided by the user. It determines the confidence filter cutoff limit utilized in the amplitude (transmission loss) portion of the recognition algorithm. A lower confidence filter limit results in less ranges being filtered from the analysis, while a higher confidence filter results in more ranges being filtered from the analysis. The key is to find a balanced confidence filter that is not too high, nor too low. If the confidence filter is set too high, there exists an increased possibility that the correct location of the contact will be filtered and removed from the analysis. If the confidence filter is set too low, a higher number of contact locations will be included and analyzed for the remainder of the recognition algorithm, resulting in an increased possibility of incorrectly selecting the location of the contact. This will be discussed in greater detail in Section 3.3, which provides a detailed explanation of the confidence interval portion of the analysis.

4. **Arrival Transmission Loss Data**

   This input is directly from the received acoustic signal. It is simply the converted transmission loss from the signal's amplitude. For the purposes of this thesis and all conducted simulations, this input is received from either the ITP84 or ITP85 test platforms.

5. **Arrival Time Data**

   This input is directly from the received acoustic signal. It is simply the arrival time converted to reduced time, which measures the travel time of the signal from the source to the receiver. For the purposes of this thesis and all conducted

simulations, this input is received from either the ITP84 or ITP85 test platforms.

3.3 Amplitude Analysis

The first classifier utilized for the conduct of this thesis is the amplitude information associated with the received acoustic signal. Each received signal possesses a unique amplitude defining its relative strength. Figure 3-10 shows an example of the arrival amplitudes associated with the ITP84 regional database for a source and receiver depth of 30 meters.

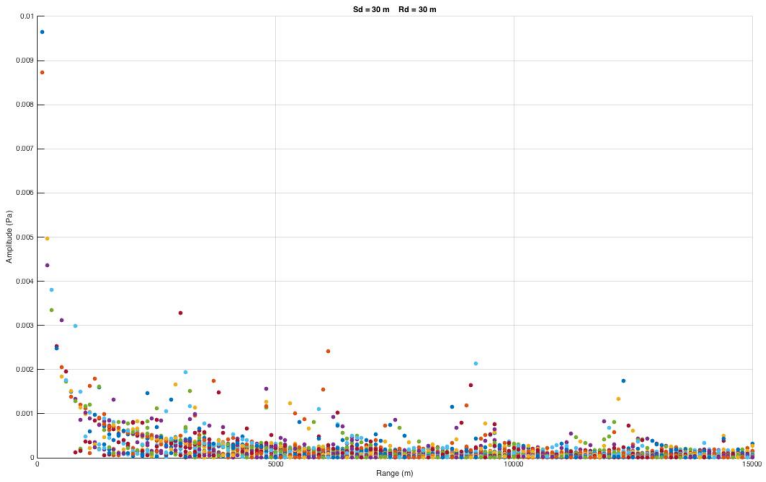

Figure 3-10: Arrival Amplitudes for ITP84, Sd = 30m, Rd = 30m

Signal amplitudes prove to be an excellent classifier for use in a pattern recognition tracking program due to geometrical spreading losses. At increased distances from a source, the sound signal strength decreases based on laws associated with either spherical or cylindrical spreading losses as depicted in Figure 3-11.

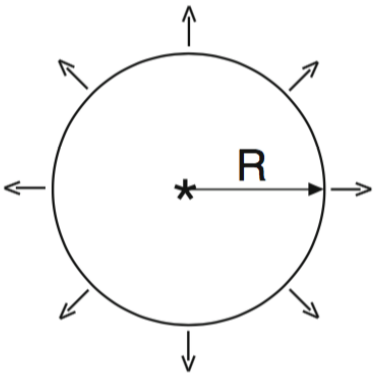

(a) Spherical Spreading

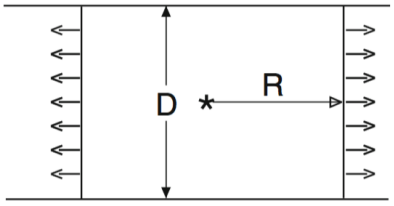

(b) Cylindrical Spreading

Figure 3-11: Geometrical Spreading Losses [7]

The intensity degradation associated with spherical and cylindrical spreading losses can be found in Equations 3.1a and 3.1b, respectively [7].

$$I \propto \frac{1}{4\pi R^2} \tag{3.1a}$$

$$I \propto \frac{1}{2\pi RD} \tag{3.1b}$$

In order to track these losses, the arrival amplitudes received, such as those presented in Figure 3-10, were converted to transmission losses (TL) in accordance with Equation 3.2.

$$TL = -20 \log \frac{|p(r,z)|}{|p_o|} \tag{3.2}$$

where TL is transmission loss in dB re 1 m, and p is pressure in Pascals. Based on these identified losses, each individual range distance from a source will possess its own unique transmission loss "fingerprint." The transmission loss "fingerprints" comprise half of all regional databases which are utilized within the developed pattern recognition algorithm. The associated arrival transmission loss plot of the converted

amplitudes shown within Figure 3-10 can be found in Figure 3-12.

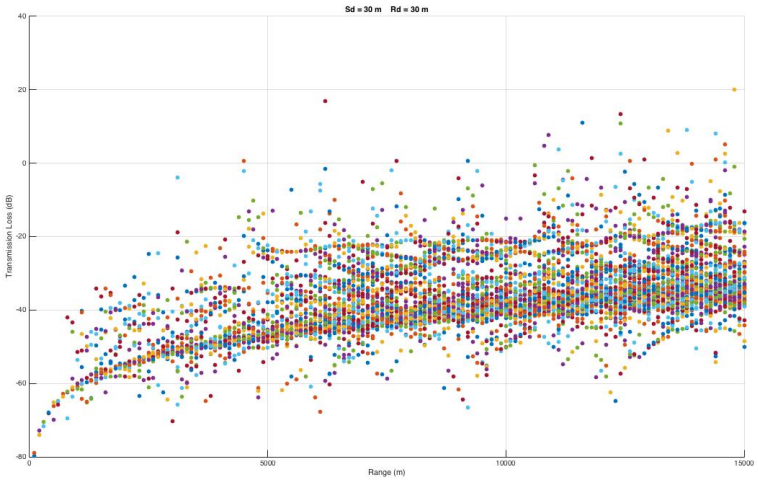

Figure 3-12: Arrival TL for ITP84, Sd = 30m, Rd = 30m

3.3.1 Developed Algorithm

The backbone of the amplitude portion of the pattern recognition analysis is the use of confidence intervals. A confidence interval is a statistical tool used to determine the likelihood that a value, μ, is located within a specified interval of the form $L \leq \mu \leq U$, where 'L' and 'U' are the lower and upper confidence interval limits, respectively, dependent upon the numerical value of the data set's sample mean, $\bar{X}$ [10]. The goal of this analysis is to determine the confidence level, or certainty, that the input's mean transmission loss is equal to each "fingerprint's" mean transmission loss value.

Based on source location and depth, various confidence intervals were determined for all possible remaining contact locations within the associated regional database. These various confidence intervals ranged between 10% and 90%, in 10% intervals. This was accomplished by assuming the transmission loss "fingerprints" for each location were normally distributed. Based on this assumption, the location's mean transmission loss was determined thereby making it possible to determine the various lower and upper limits for each incremental confidence interval. All confidence

intervals were determined following the format in Equation 3.3

$$P(L \leq \mu \leq U) = 1 - \alpha \tag{3.3}$$

where $0 \leq \alpha \leq 1$, and α is the certainty that the value μ falls within the specified confidence interval [10]. The term μ is the mean input transmission loss value determined from the received signal's transmission loss data, which were also assumed to be normally distributed.

The goal for determining the various confidence intervals at each possible contact location is to narrow down the field of possible contact locations by filtering out improbable solutions. To help clarify this concept, Figure 3-13 provides an illustration of both a 90% and 10% confidence interval, which are at opposite ends of the determined confidence intervals spectrum.

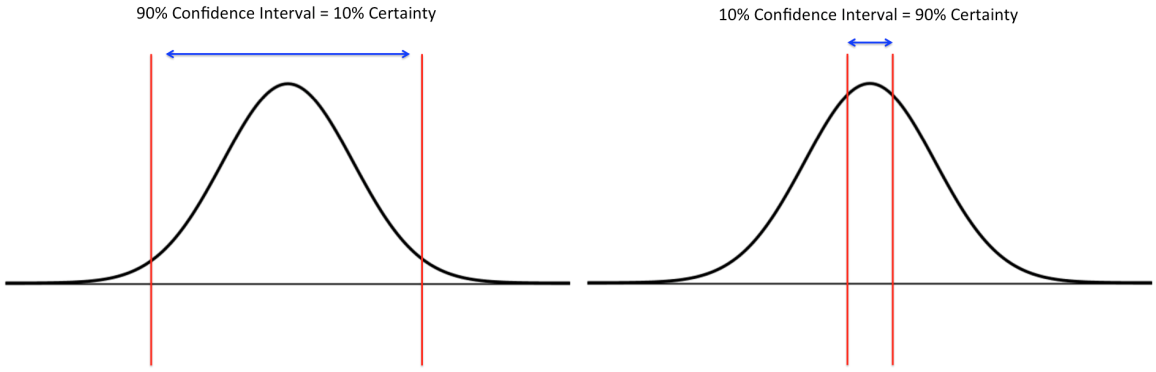

(a) 90% C.I. **(b)** 10% C.I.

Figure 3-13: Confidence Interval Illustrations

The 90% confidence interval is broad and includes a majority of possible solutions, therefore only providing a 10% certainty of the predicted contact's location. As the confidence interval is decreased and the field of possible solutions becomes more limited, the certainty of determining the correct location of the contact increases. The 10% confidence interval is more exclusive and includes a small portion of possible solutions, therefore providing a 90% certainty of the predicted contact's location.

This analysis aims to determine the certainty value of the match between the inputs and "fingerprint" transmission loss data. By determining the certainty values,

a decision boundary (i.e. confidence filter value) can be applied in order to separate feasible and infeasible solutions. This was accomplished by determining the lowest confidence interval, ranging from 0% to 100%, that the mean input transmission loss value falls within for all available "fingerprints." Since certainty is equal to *1-(Confidence Interval)*, determining the lowest confidence intervals for each "fingerprint" will determine the highest certainty for each as well. The certainty value provides an indication of the possible receiver locations. A higher certainty means there is a higher confidence that the input data matches the "fingerprint" data therefore increasing the likelihood that the "fingerprint's" location is the exact location of the receiver. Conversely, a lower certainty means there is less confidence that the input data matches the "fingerprint" data therefore decreasing the likelihood that the receiver is located at the "fingerprint's" location.

Upon completion of determining the certainty for each possible contact location, a confidence filter is applied. This filter eliminates all possible solutions that fall beneath this value from the remainder of the analysis. The goal for this filter is to not be too limiting, nor too encompassing. If the filter value is too low and therefore inclusive, this increases the chances that the contact's location will be falsely predicted in later analyses as there is a larger field of possible solutions. If the filter value is too high and therefore limiting, this increases the chances that the actual contact's location will be prematurely filtered and removed from future analyses and consideration. A balanced confidence filter that falls between these two extremes is ideal. After this filter is applied, the remaining possible solutions are then fed to the arrival time portion of the pattern recognition analysis as discussed in Section 3.4.

3.3.2 Demonstration

To help clarify the concepts associated with the amplitude analysis, this section provides a demonstration of its application. This demonstration is performed in the northern region with the use of the ITP85 regional database. The known source depth is 30 meters. For the purposes of this demonstration, the receiver's (contact) location is known to be at a depth of 30 meters and 15,000 meters in range from the source,

therefore the "fingerprint" information associated with the ITP85 test platform for Sd = 30m, Rd = 30m, and Rr=15,000m serve as the inputs.

The input containing the source's location within the northern region informs the pattern recognition algorithm to utilize the ITP85 regional database vice the ITP84. The input containing the source's depth at 30 meters automatically reduces the possible source/ receiver depth combinations from nine to three. This informs the pattern recognition algorithm to utilize the "fingerprint" data associated with the following three source/ receiver combinations within the ITP85 regional database for carrying out the full pattern recognition tracking analysis:

1. ITP85: Sd = 30m, Rd = 30m
2. ITP85: Sd = 30m, Rd = 150m
3. ITP85: Sd = 30m, Rd = 500m

Based on the input of the received signal's transmission loss data, the certainty value for each possible location listed for the above three source/ receiver depth combinations within the ITP85 regional database is determined as seen in Figure 3-14. This is accomplished by finding the lowest confidence interval that the received signal's data falls into for all possible solutions.

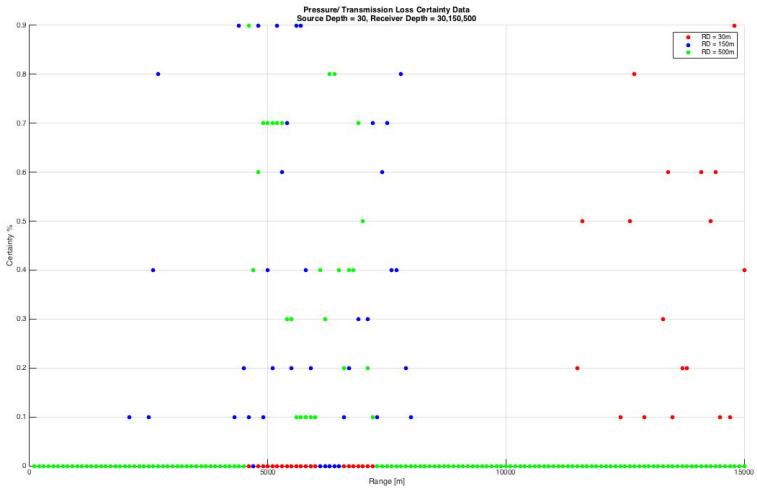

Figure 3-14: Demo: Unfiltered TL Data for ITP85, Sd=30

It can be seen from this figure that the output of this analysis provides a certainty value for each possible location associated with depth and range. The next step within this analysis is to apply a confidence filter. For this demonstration, the confidence filter was set to 0.2. This means that all possible locations with a certainty value of 0.2 or less are filtered and removed from further analysis. Figure 3-15 provides the filtered TL analysis results for this demonstration.

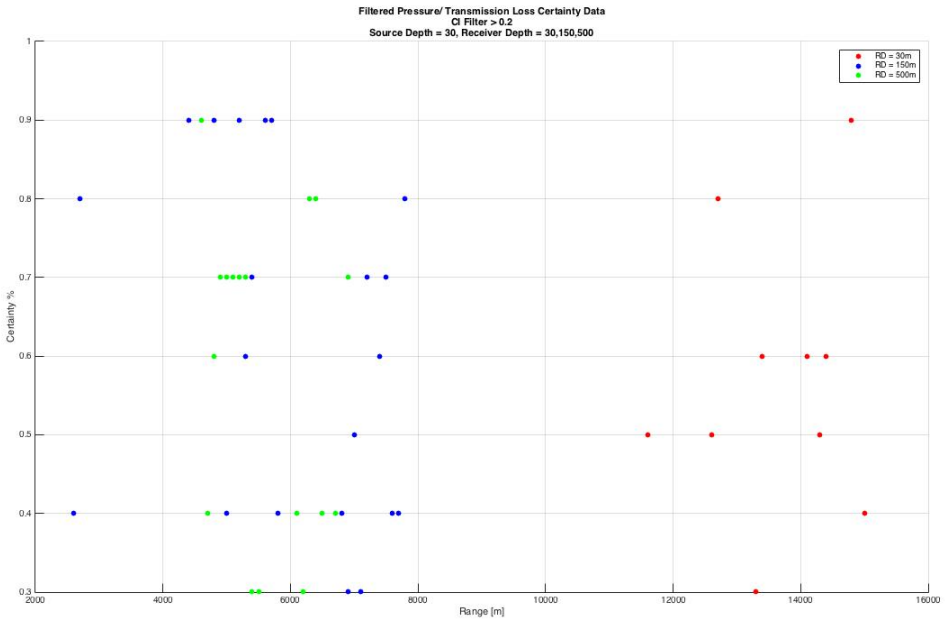

Figure 3-15: Demo: Filtered TL Data for ITP85, Sd=30

These filtered locations are then utilized for the next portion of the pattern recognition algorithm, which is the arrival time analysis as detailed in Section 3.4.

3.4 Arrival Time Analysis

The second classifier utilized for the conduct of this thesis is the arrival time information associated with the received acoustic signal. Each received signal possesses a unique arrival time dependent on the travel time and distance between the source and the receiver. Figure 3-16 shows an example of the arrival times associated with the ITP84 regional database for a source and receiver depth of 30 meters.

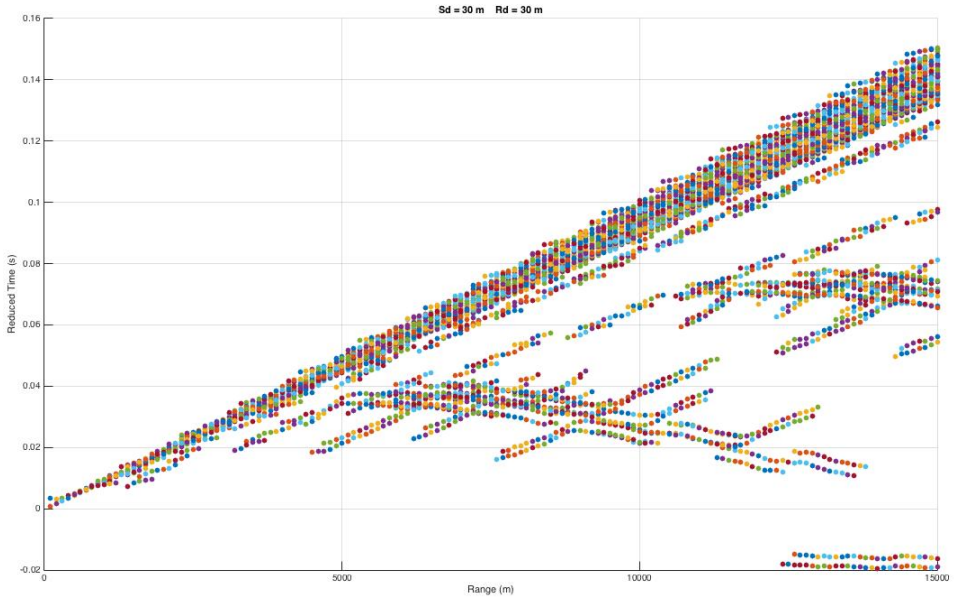

Figure 3-16: Arrival Times for ITP84, Sd = 30m, Rd = 30m

The signal arrival times prove to be an excellent classifier for use in a pattern recognition tracking program due to the fact that each receiver location possesses a distinct travel time pattern associated with its range from the source. By understanding and utilizing these unique arrival patterns, a recognition tracking program has the ability to overcome the challenges related to fading and improper ray path identification.

3.4.1 Developed Algorithm

Pattern recognition is accomplished for the arrival time data by computing a correlation coefficient between the received signal's arrival time inputs and all filtered arrival time "fingerprints" within the associated regional database. The correlation coefficient is a measure of the linear relationship between two variables (i.e. arrival time input and an arrival time "fingerprint"). The equation used to calculate the correlation coefficient can be seen in Equation 3.4 [10].

$$\rho_{(X_1,X_2)} = \frac{Cov(X_1X_2)}{\sqrt{{\sigma_1}^2, {\sigma_2}^2}} \tag{3.4}$$

where 'Cov' is the covariance between the two random variables, X_1 and X_2, and σ is the standard deviation of each associated data set. The output of this equation provides a value between -1.0 and 1.0. A negative score means an inverse relationship, which is irrelevant and nonexistent for the work completed within this thesis. A high correlation coefficient value close to 1.0 indicates a strong linear relationship between the inputs and "fingerprints," whereas a low correlation coefficient value close to 0.0 indicates a very poor, or nonexistent, relationship between the inputs and "fingerprints." Calculating the correlation coefficient provides an intuitive score that reflects the relative strength of the linear relationship between the input and each "fingerprint" [10]. This means that the higher the correlation coefficient, the more likely there is a match between the input and associated "fingerprint." A higher correlation coefficient indicates a likely range and location of the receiver, or contact, being tracked.

3.4.2 Demonstration

To help clarify the concepts associated with the arrival time analysis, the demonstration introduced in Section 3.3.2 is continued here with the arrival time portion of the pattern recognition algorithm. This demonstration is conducted within the northern region associated with the ITP85 regional database for a source depth of 30 meters. The inputs include the data received from the ITP85 test platform for Sd=30m, Rd=30m, and Rr=15,000m.

For the purposes of this demonstration, Figure 3-17 is provided to show the calculated correlation coefficients between the input arrival times and all possible receiver locations associated with the source at a depth of 30 meters.

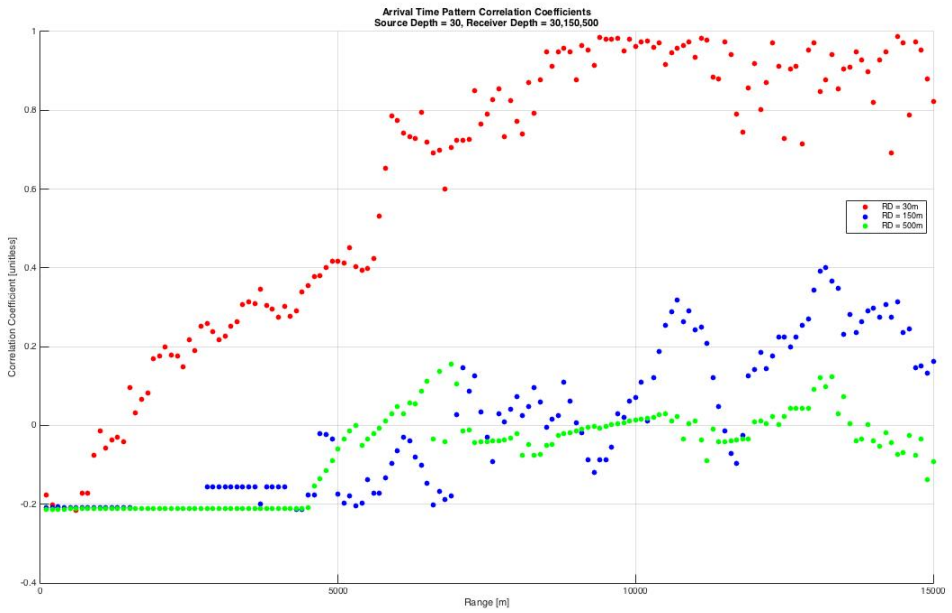

Figure 3-17: Demo: Unfiltered Arrival Time Data for ITP85, Sd=30

It can be seen from this figure that the receiver depths above the Beaufort Duct at 30 meters dominate the data set, especially at ranges greater than approximately 9,000 meters, which makes sense and is expected since it is known that the actual location of the inputs are at Rd=30m and Rr=15,000m.

The pattern recognition algorithm is not designed to calculate the correlation coefficient between the inputs and all possible "fingerprints" as seen in Figure 3-17. It is only provided here for illustrative purposes.

The arrival time analysis is conducted only on the filtered locations provided from the amplitude analysis portion of the recognition algorithm as seen in Figure 3-15. Figure 3-18 shows the arrival time analysis completed for the filtered data fed from the amplitude analysis.

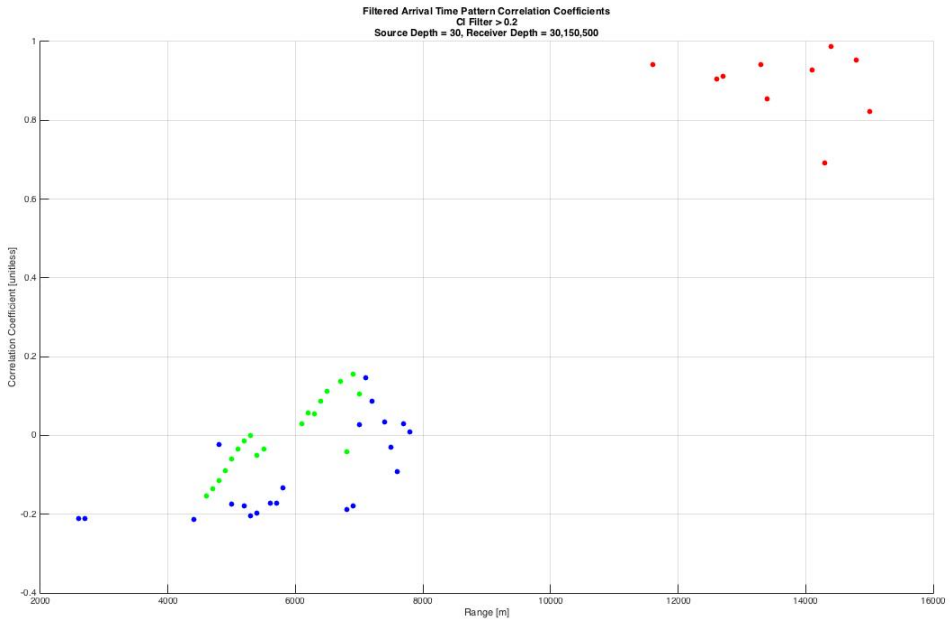

Figure 3-18: Demo: Filtered Arrival Time Data for ITP85, Sd=30

The next section, Section 3.5, will show the effect of combining these two classifiers and analyses. Together, these two classifiers create a very effective pattern recognition criteria.

3.5 Combined Analysis

While the individual analyses for both classifiers, amplitude and arrival times, provide relatively decent pattern recognition criteria for determining the receiver's location, they still possess a great deal of error and uncertainty. On their own, they are not accurate enough to present reliable solutions. Combined together, they form a very effective and robust pattern recognition algorithm. This is accomplished by beginning with the amplitude analysis discussed in Section 3.3 involving transmission losses and determining location certainties. The application of the confidence filter then removes improbable solutions from future analyses and consideration. These filtered solutions are then provided to the arrival time analysis portion of the pattern recognition algorithm as discussed in Section 3.4 involving the determination of

correlation coefficients. The process of combining these two analyses with the implementation of the confidence filter proves to be very effective at removing improbable solutions that would otherwise be considered and possibly selected as the final solution. This is expanded upon in further detail in Section 3.5.1 with the continuation of the demonstration from Sections 3.3.2 and 3.4.2.

After the completion of the arrival time analysis, the final candidate solutions are assigned an accuracy score. This accuracy score can be thought of as the decision boundary as it determines the relative weighted importance between the amplitude and arrival time analyses. For the purposes of this thesis, these two analyses were assigned equal importance as the accuracy score is simply the average of the two values. The output of the amplitude analysis provides a certainty value between 0.0 and 1.0, while the arrival time analysis provides a strength of relationship value (correlation coefficient) also between 0.0 and 1.0. Since both of these scores are between 0.0 and 1.0 and measure accuracy, where a higher score means a higher degree of pattern matching between the inputs and the associated "fingerprint," they were provided equal weight importance in determining the overall accuracy score. The accuracy score is calculated as shown in Equation 3.5.

$$Accuracy = \frac{\alpha + \rho_{(X_1,X_2)}}{2.0} 100\% \tag{3.5}$$

where α is the certainty value determined from the amplitude analysis and ρ is the correlation coefficient determined from the arrival time analysis. These final accuracy scores provide a system for scoring the pattern matching between the inputs and candidate "fingerprint" solutions. A flow diagram illustrating the inputs, analyses, and outputs of the combined pattern recognition algorithm is shown in Figure 3-19.

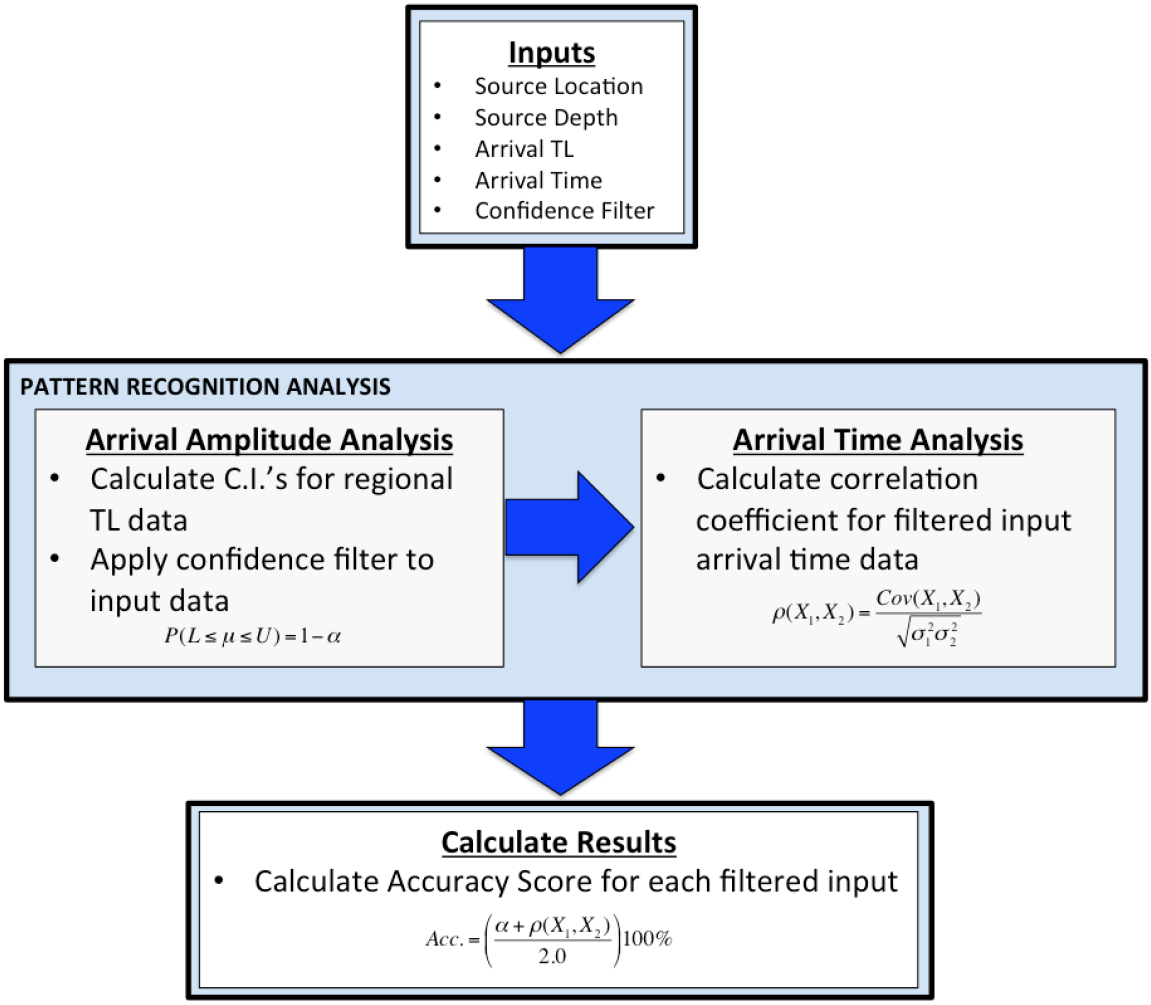

Figure 3-19: Pattern Recognition Flow Diagram

3.5.1 Demonstration

To further help clarify these concepts, the demonstration introduced in Sections 3.3.2 and 3.4.2 is continued here. This demonstration is conducted within the northern region associated with the ITP85 regional database for a source depth of 30 meters. The inputs include the data received from the ITP85 test platform for Sd=30m, Rd=30m, and Rr=15,000m. Upon completion of determining the correlation coefficients for all filtered data within the arrival time analyses, these correlation coefficients along with their respective certainty values determined from the amplitude analysis are fed to the results portion of the pattern recognition algorithm as illusrated in Figure 3-19. These scores are used to determine the overall accuracy score introduced in

Equation 3.5. Figure 3-20 presents the final results for this demonstration with the determination of all applicable accuracy scores.

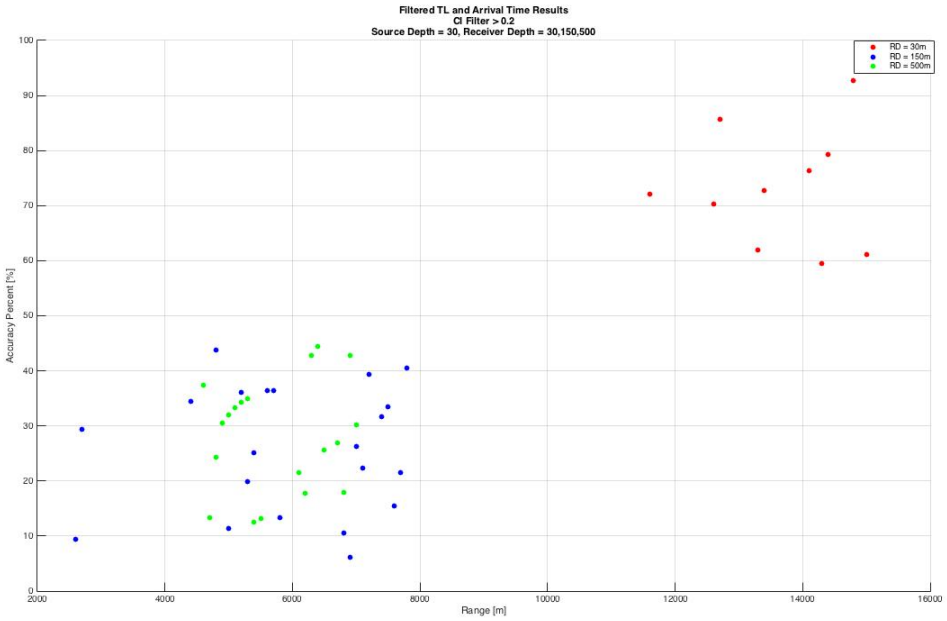

Figure 3-20: Demo: Accuracy Scores for ITP85, Sd=30

It can be seen from Figure 3-20 that the pattern recognition algorithm determined that the highest accuracy scores were located with a receiver depth of 30 meters, and range somewhere between roughly 14,300 and 14,500 meters, which is very close to the actual location of the receiver at a depth of 30 meters and range of 15,000 meters. This solution is excellent, and the error is expected, as a limitation within this program is that the range is limited to 15,000 meters therefore no data is analyzed beyond that range. This removes any possibility of producing a more collective field of solutions around 15,000 meters.

This demonstration helps highlight the importance of utilizing both classifiers, amplitude and arrival time. As seen in Figure 3-14, the amplitude analysis itself guides the tracking program in the general direction of the receiver, but is far from providing any clear solutions. This analysis has proved to be excellent for the purposes of implementing a filter in order to remove infeasible solutions from obscuring the good data, and effectively from achieving the correct results.

If the arrival time analysis was utilized on its own, with no confidence filter applied from the amplitude analysis, it can be seen from Figure 3-17 that an array of possible solutions exist between 9,000 and 15,000 meters. This field of possible solutions is too broad, making it impossible to pick an accurate receiver location. The combination of these two analyses alleviates this issue by removing infeasible solutions from contention, therefore filtering all of those seemingly good arrival time data points between 9,000 and 12,000 meters, and narrowing in on the actual solution at 15,000 meters in range.

Figure 3-21 is provided to illustrate this flow of data and highlight the effectiveness of combining these two classifiers within the the pattern recognition algorithm.

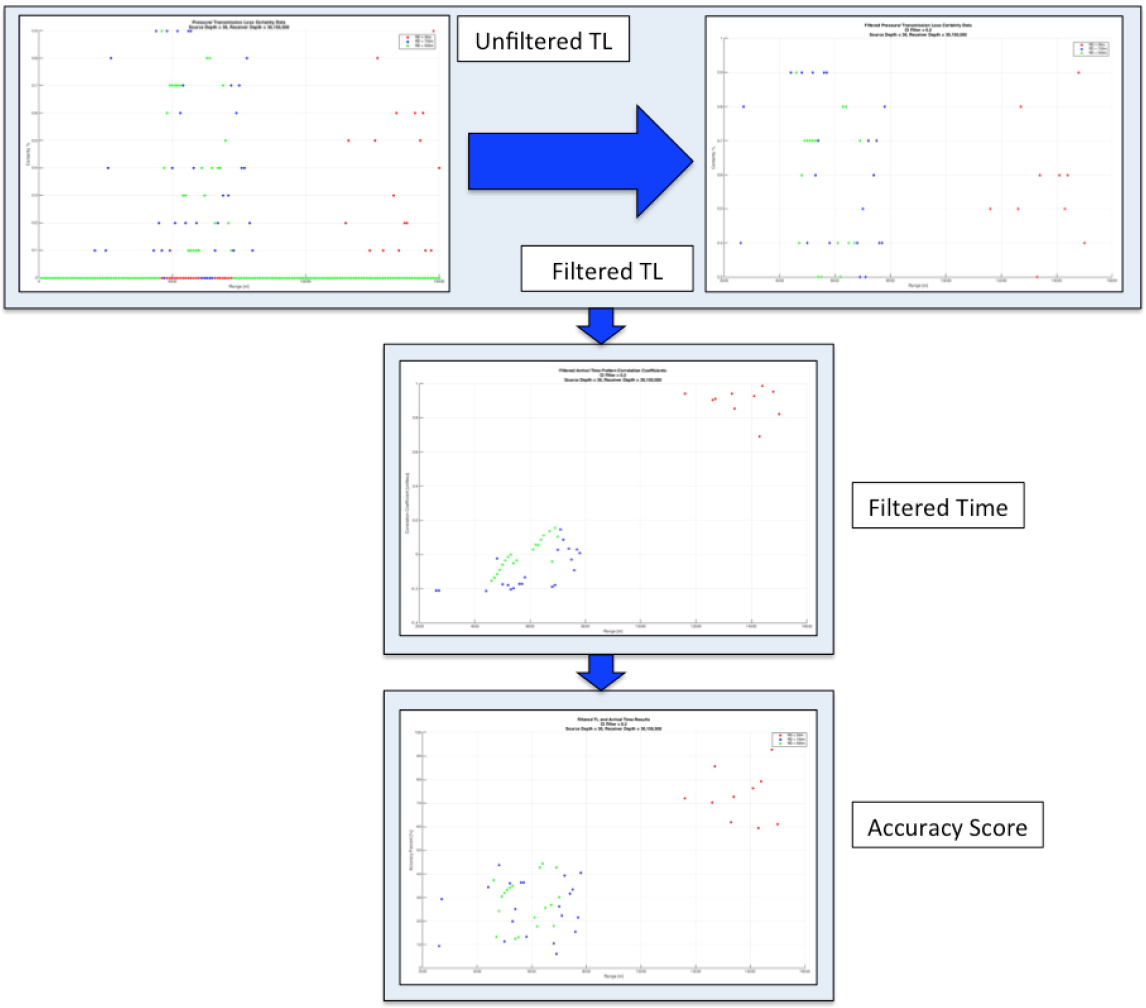

Figure 3-21: Demo: Results Flow Diagram

The following chapter, Chapter 4, applies these analyses and results to several simulations involving target tracking at various ranges.

THIS PAGE INTENTIONALLY LEFT BLANK

Chapter 4

Test and Evaluation

This chapter aims to apply the pattern recognition analyses presented in Chapter 3 to conduct several tracking simulations involving different combinations of source and receiver depths at various ranges. These simulations involve the following parameters:

1. ITP85, Confidence Filter=0.2, Sd=30m, Rd=30m
2. ITP84, Confidence Filter=0.6, Sd=30m, Rd=150m
3. ITP85, Confidence Filter=0.5, Sd=150m, Rd=30m
4. ITP84, Confidence Filter=0.6, Sd=500m, Rd=500m

These four locations and source/ receiver depths were chosen in order to provide an encompassing and conclusive set of simulations that are representative of the various geographical locations and depth combinations with respect to the Beaufort Duct. The confidence filter was also varied to demonstrate the effect of changing its filter amount upon the overall results.

4.1 Simulation #1: ITP85, Sd=30m, Rd=30m

The first simulation conducted was for a source (beacon) and receiver (AUV being tracked) both located above the Beaufort Duct, at depths of 30 meters, respectively,

within the north region, therefore utilizing the ITP85 regional database. This simulation was used to evaluate the position of the AUV as it closed in range to the beacon from 14,000 to 2,000 meters, in 2,000 meter intervals. The confidence filter was set to 0.2. The pattern recognition algorithm presented in Chapter 3 was applied for each range interval. Figure 4-1 provides a representative flow diagram of this pattern recognition process for the 14,000 meter range data utilized within this simulation.

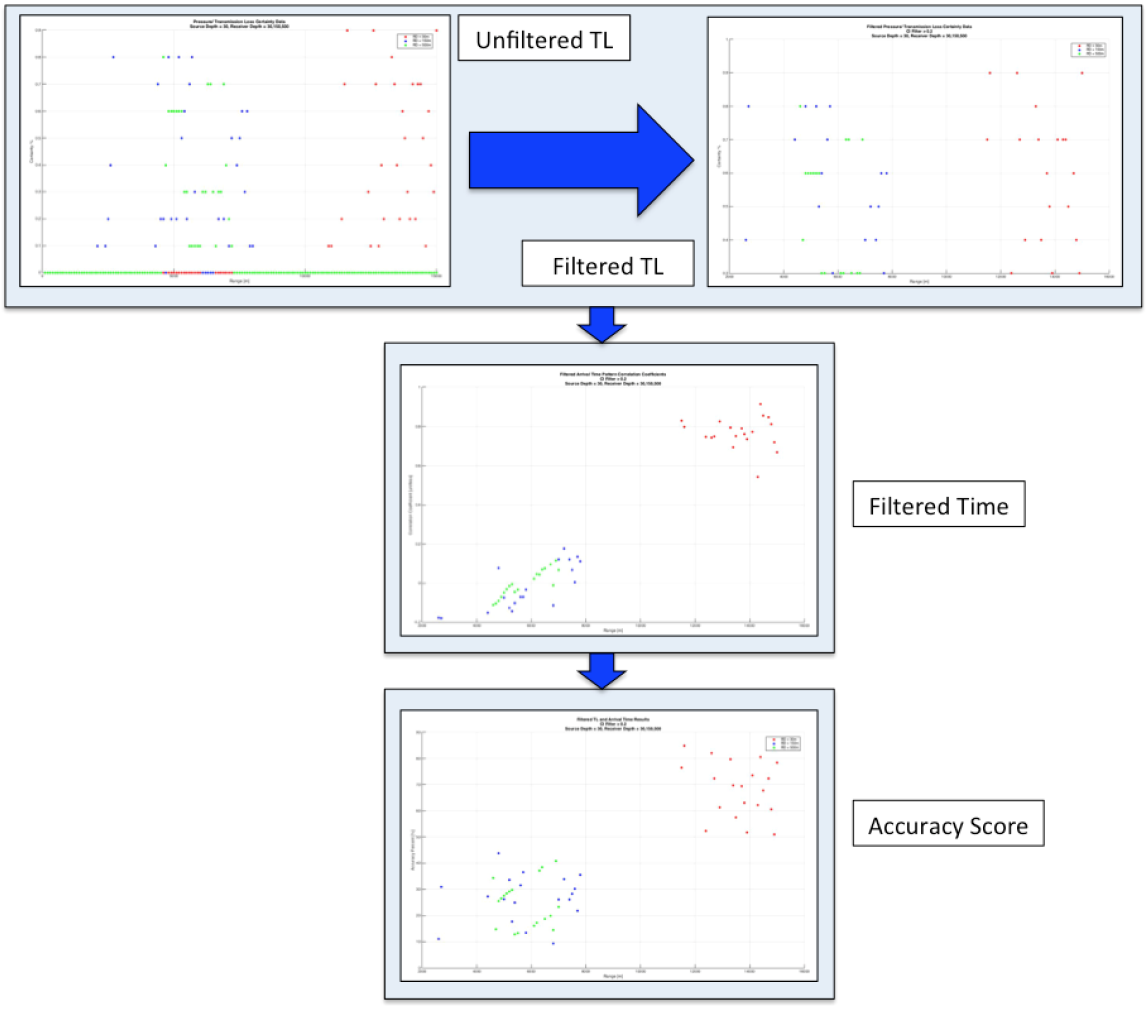

Figure 4-1: Simulation #1: Pattern Recognition Flow Diagram for 14k Range Data

The detailed results associated with the pattern recognition analyses completed for all sets of range data implemented within each simulation can be found in Appendix A. The cluster of data with the highest overall accuracy scores were then utilized to determine a predicted range to the AUV. This is highlighted in Figure 4-2 for the example associated with the 14,000 meter range data as this cluster of data is enclosed within the black circle.

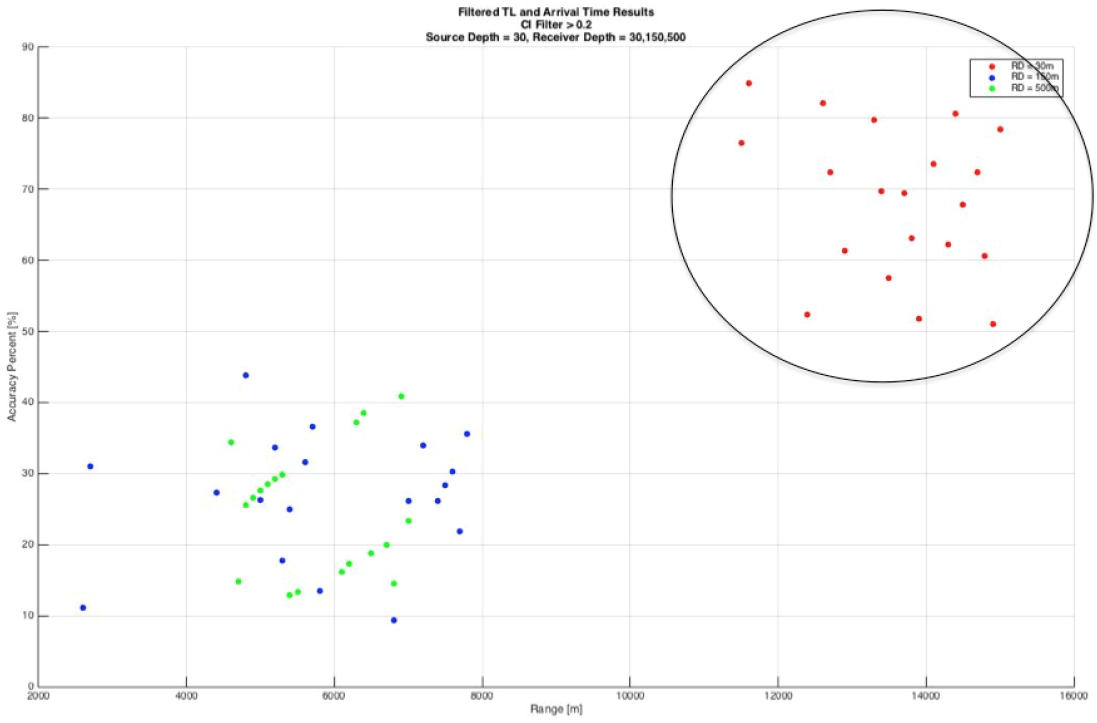

Figure 4-2: Simulation #1: Accuracy Scores for 14k Range Data

With the cluster of data selected, as seen in Figure 4-3 for the 14,000 meter range data, the next step is to use this data to determine the predicted range to the AUV.

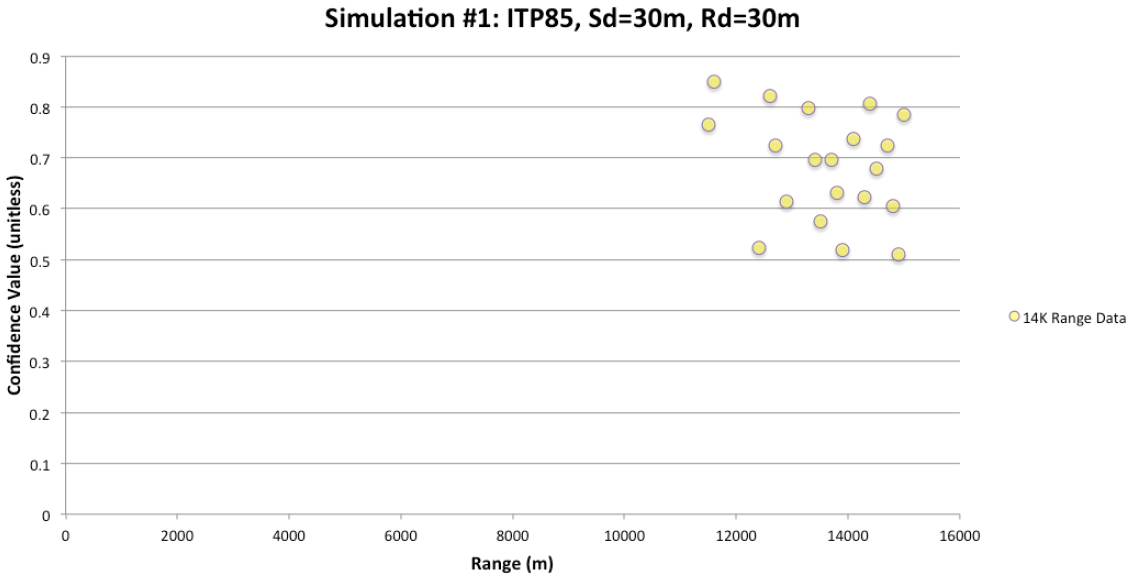

Figure 4-3: Simulation #1: Selected Accuracy Scores for 14k Range Data

The predicted ranges were determined by calculating the centroid of each respective data cluster. The x-value of the centroid is the predicted range to the AUV. Equation 4.1 shows how this predicted range was calculated:

$$PredictedRange = \frac{\Sigma C_i \cdot R_i}{\Sigma C_i} \tag{4.1}$$

where C_i are all individual accuracy scores within the data cluster and R_i are the respective ranges. The confidence value associated with each predicted range is calculated by simply swapping the C_i's and R_i's, as this value represents the y-value of the centroid. This calculation is shown in Equation 4.2.

$$ConfidenceValue = \frac{\Sigma R_i \cdot C_i}{\Sigma R_i} \tag{4.2}$$

This method of utilizing the data's centroid as the target's range predictor is highly effective due to the fact that it takes into account the relative weight associated with each data point thereby helping reduce the overall error. The pattern recognition algorithm is excellent at hovering around the correct location, but simply choosing the range with the highest overall accuracy score tends to present a great deal of risk in regards to the range prediction due to existing inherent imperfections in such a

pattern recognition analysis. Utilizing all data points with the centroid determination provides a more robust and accurate overall result as all filtered data's accuracy scores are taken into account. This is an additional benefit to the implementation of the confidence filter. For example, the 14,000 meter example presented above possesses the highest overall accuracy score at 11,900 meters, which presents a great deal of error if used alone as it is 2,100 meters below the actual range. Conversely, the cluster of data as a whole centers around the the actual range at 14,000 meters. By the finding the weighted sum of the data, or the centroid, all data points are effectively utilized to find a more accurate predicted range at 13,600 meters, which is a very good estimation of the AUV's actual range.

The predicted range for the 14,000 meter range data can be seen in Figure 4-4.

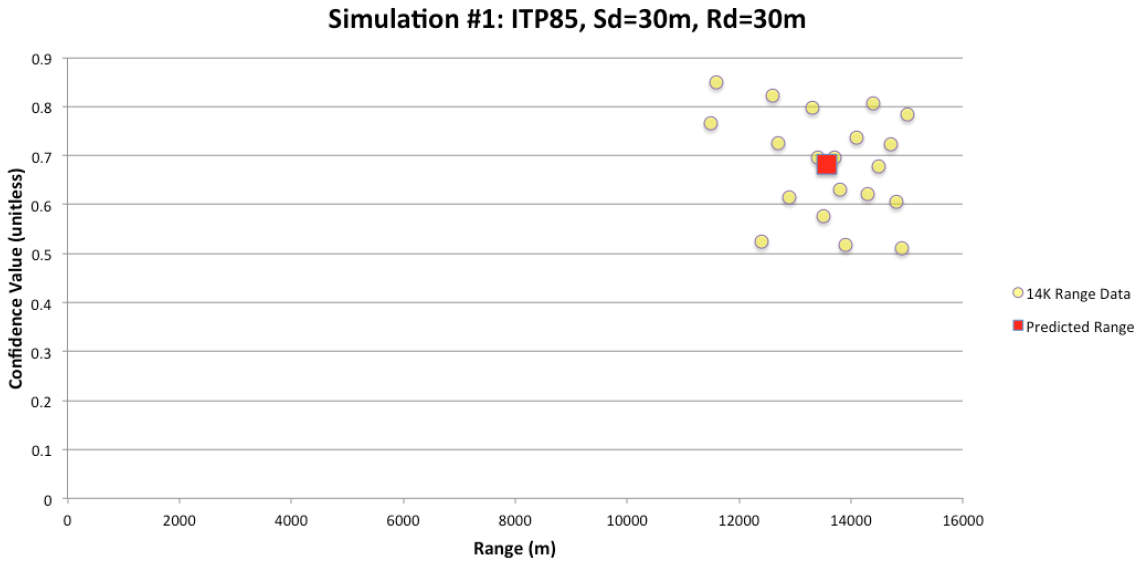

Figure 4-4: Simulation #1: Predicted Range for 14k Range Data

This same process was completed at all 2,000 meter range intervals as the AUV's range closes in on the beacon from 14,000 to 2,000 meters. Figure 4-5 shows the selected clusters of accuracy score data taken from each range interval.

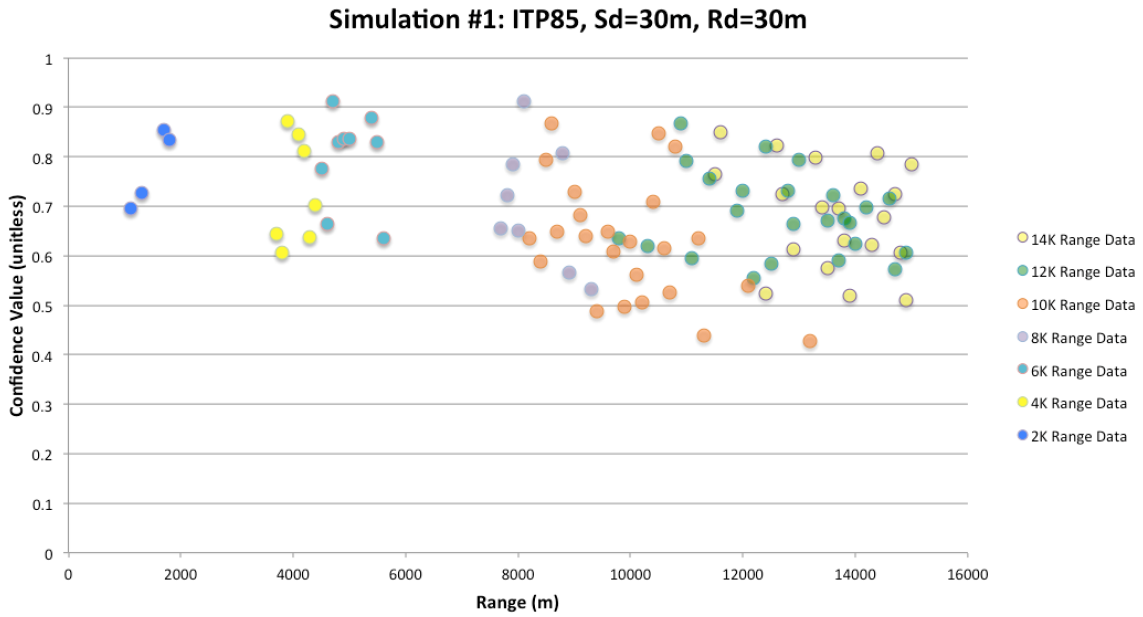

Figure 4-5: Simulation #1: Selected Accuracy Scores

Figure 4-6 shows the predicted ranges for all sources of range data as the AUV closes in range.

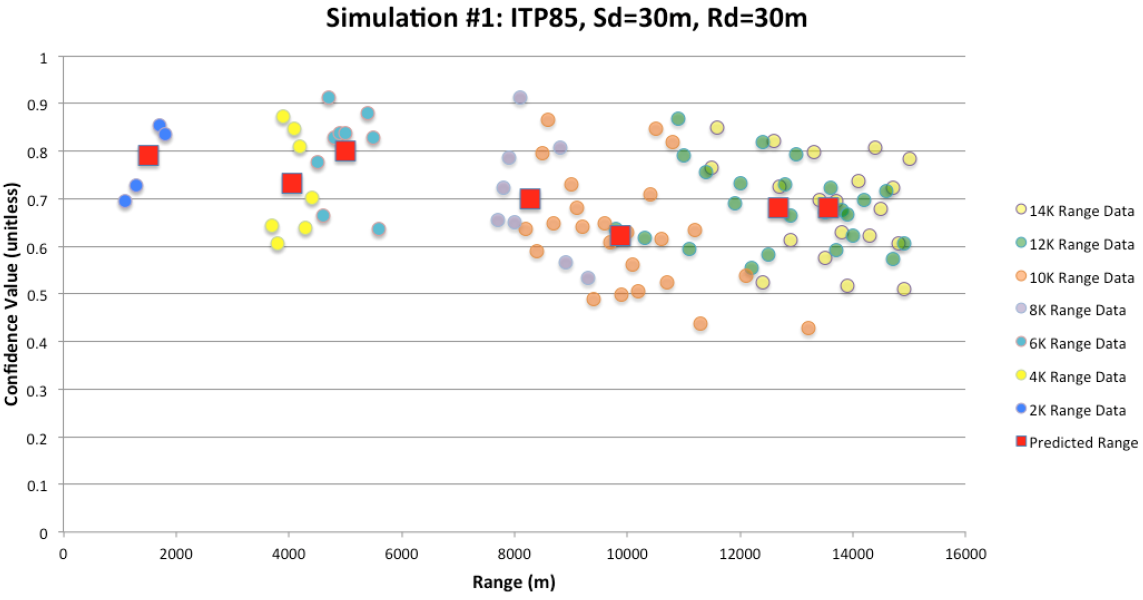

Figure 4-6: Simulation #1: Predicted Ranges

In order to provide a measure of overall predicted range accuracy, Figure 4-6 shows these same results, but along with the addition of the actual range of the AUV at

each interval, and a trend line illustrating the confidence value trend associated with each range data set.

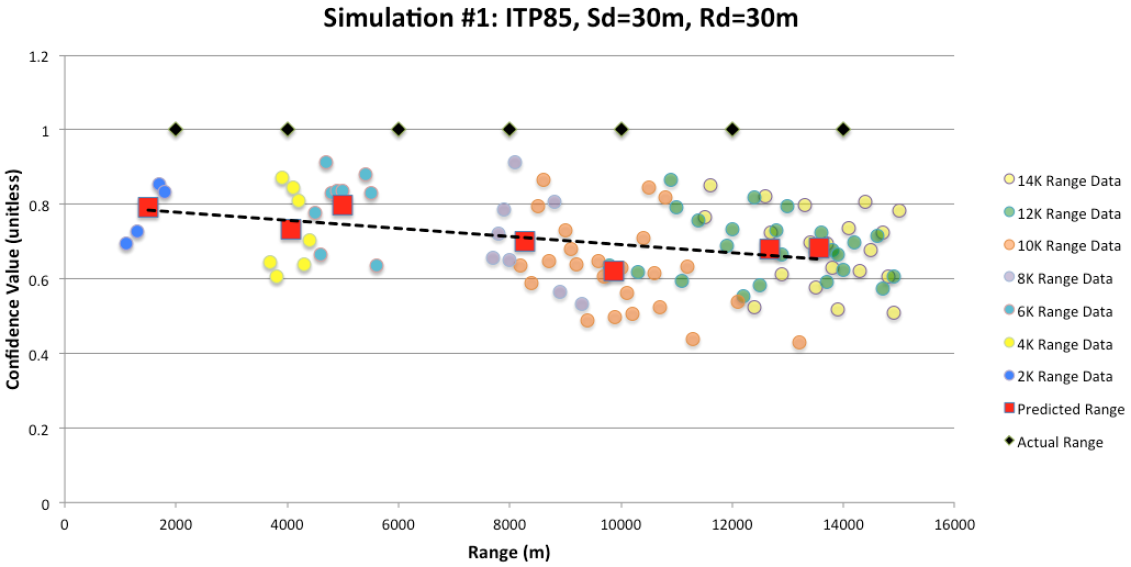

Figure 4-7: Simulation #1: Full Results

A summary of this simulation's results can be found in Table 4.1 with the determination of the error associated with each predicted range.

Actual Ranges (m)	Predicted Ranges (m)	Error (m)
14000	13557.65	442.35
12000	12675.19	675.19
10000	9875.20	124.80
8000	8269.82	269.82
6000	4995.94	1004.06
4000	4061.94	61.94
2000	1499.25	500.75

Table 4.1: Simulation #1: Summary of Results

These results show a very promising trend associated with the tracking capability of the developed pattern recognition algorithm. With the exception of the the 6,000 meter range data, all range predictions are well within 1,000 meters of the actual range. Due to the fact that the test data will never exactly match the regional data, inherent errors will inevitably exist. The goal for this algorithm is to minimize these errors, which this simulation proves is well within the bounds of possibilities.

4.2 Simulation #2: ITP84, Sd=30m, Rd=150m

The second simulation was conducted in the southern region therefore utilizing the ITP84 regional database with the source located above the Beaufort Duct at a depth of 30 meters and the receiver located within the Beaufort Duct at a depth of 150 meters. This simulation was used to evaluate the position of the AUV as it closes in range to the beacon from 12,000 to 6,000 meters, in 2,000 meter intervals. The confidence filter was set to 0.6. Figure 4-8 shows the selected clusters of accuracy score data taken from each range interval.

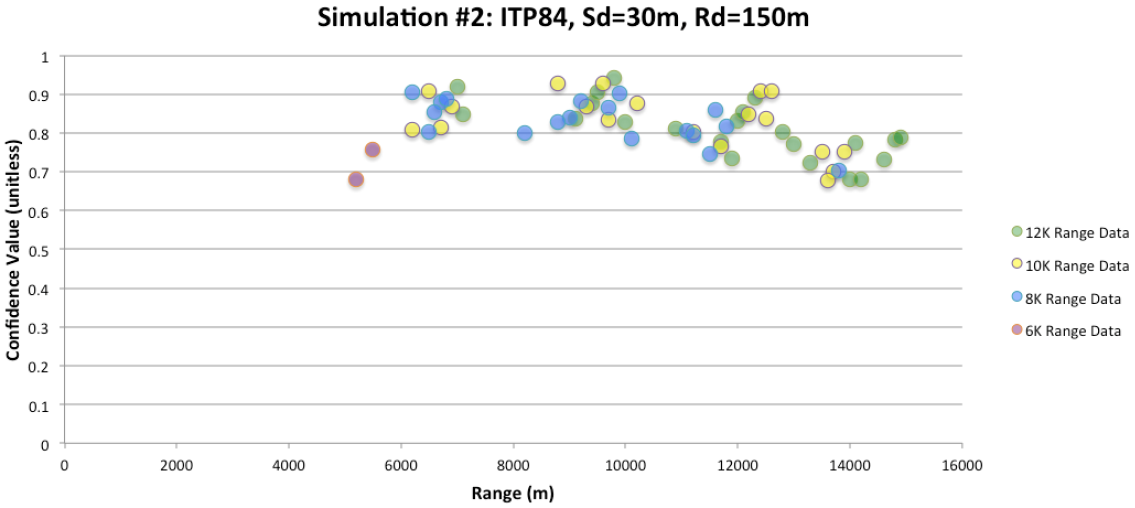

Figure 4-8: Simulation #2: Selected Accuracy Scores

Figure 4-9 shows the predicted ranges for all sources of range data as the AUV closes in range.

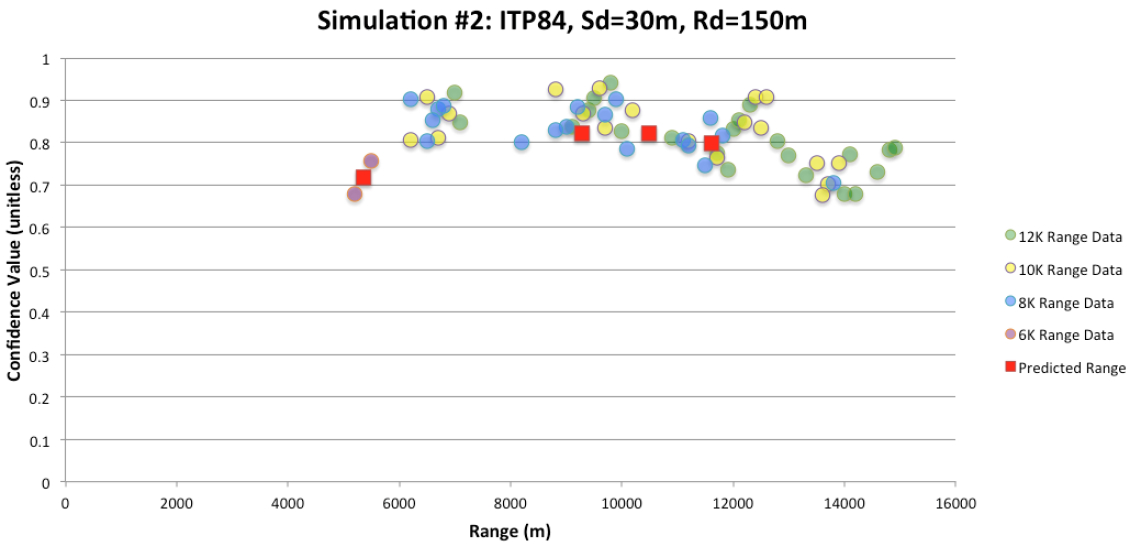

Figure 4-9: Simulation #2: Predicted Ranges

A plot of the full results, including both predicted and actual ranges, can be found in Figure 4-10.

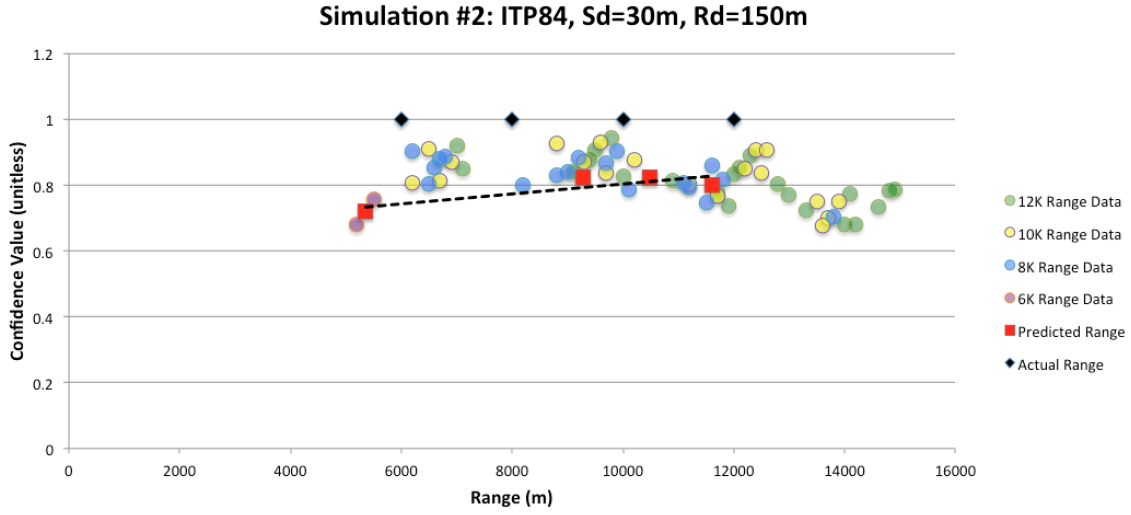

Figure 4-10: Simulation #2: Full Results

A summary of this simulation's results can be found in Table 4.2 with the determination of the error associated with each predicted range.

Actual Ranges (m)	Predicted Ranges (m)	Error (m)
12000	11601.93	398.07
10000	10478.90	478.90
8000	9286.96	1286.96
6000	5358.01	641.99

Table 4.2: Simulation #2: Summary of Results

Aside from the range data at 8,000 meters, these results present a highly accurate range prediction model. Errors can be attributed to inherent imperfections and differences between the test data and regional database.

4.3 Simulation #3: ITP85, Sd=150m, Rd=30m

The third simulation was conducted in the northern region therefore utilizing the ITP85 regional database with the source located within the Beaufort Duct at a depth of 150 meters and the receiver located above the Beaufort Duct at a depth of 30 meters. This simulation was used to evaluate the position of the AUV as it closes in range to the beacon from 10,000 to 2,000 meters, in 2,000 meter intervals. The confidence filter was set to 0.5. Figure 4-11 shows the selected clusters of accuracy score data taken from each range interval.

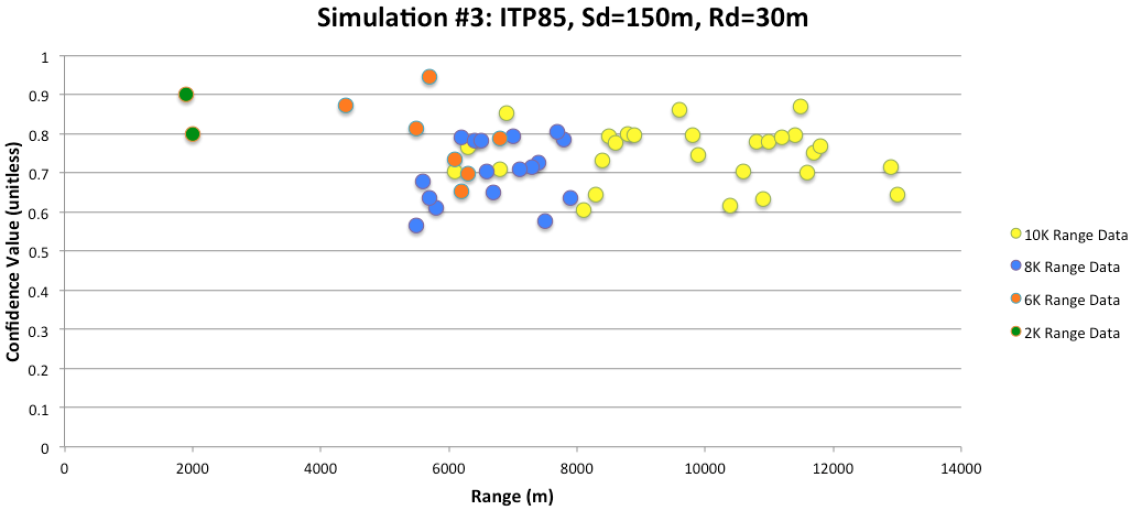

Figure 4-11: Simulation #3: Selected Accuracy Scores

Figure 4-12 shows the predicted ranges for all sources of range data as the AUV closes in range.

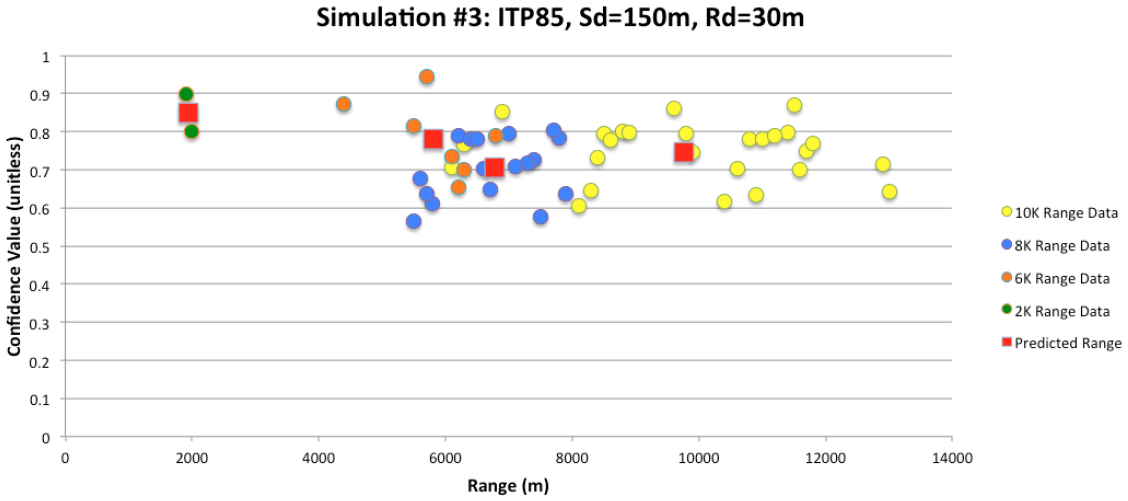

Figure 4-12: Simulation #3: Predicted Ranges

A plot of the full results, including both predicted and actual ranges, can be found in Figure 4-13.

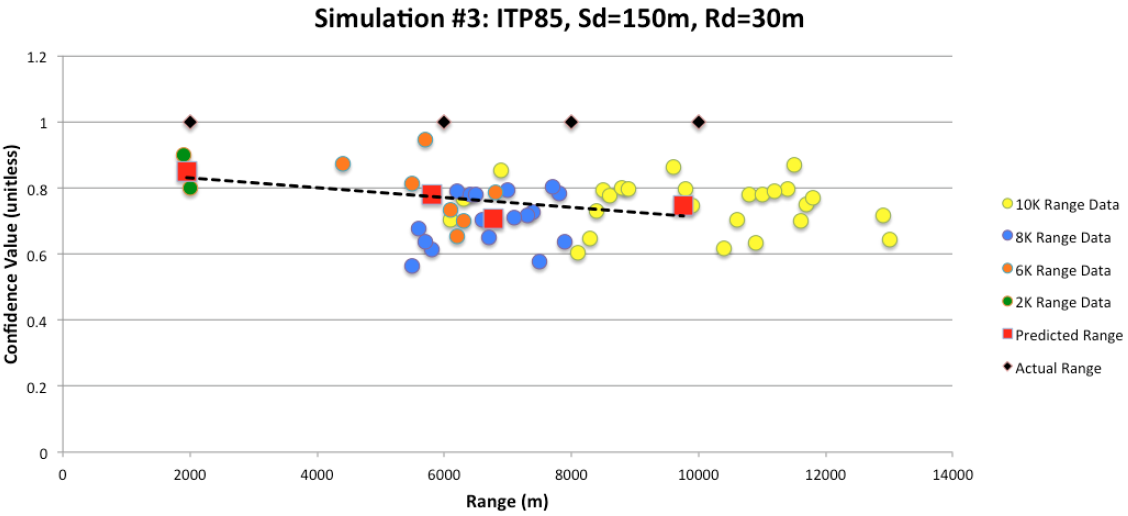

Figure 4-13: Simulation #3: Full Results

A summary of this simulation's results can be found in Table 4.3 with the determination of the error associated with each predicted range.

Actual Ranges (m)	Predicted Ranges (m)	Error (m)
10000	9761.24	238.76
8000	6774.31	1225.69
6000	5810.98	189.02
2000	1947.05	52.95

Table 4.3: Simulation #3: Summary of Results

With the exception of the 8,000 meter range data, all range predictions are within 250 meters of the actual range highlighting the effectiveness of the tracking algorithm.

4.4 Simulation #4: ITP84, Sd=500m, Rd=500m

The fourth simulation was conducted in the southern region therefore utilizing the ITP84 regional database with both the source and receiver located below the Beaufort Duct at depths of 500 meters, respectively. This simulation was used to evaluate the position of the AUV as it closes in range to the beacon from 12,000 to 2,000 meters, in 2,000 meter intervals. The confidence filter was set to 0.6. Figure 4-14 shows the selected clusters of accuracy score data taken from each range interval.

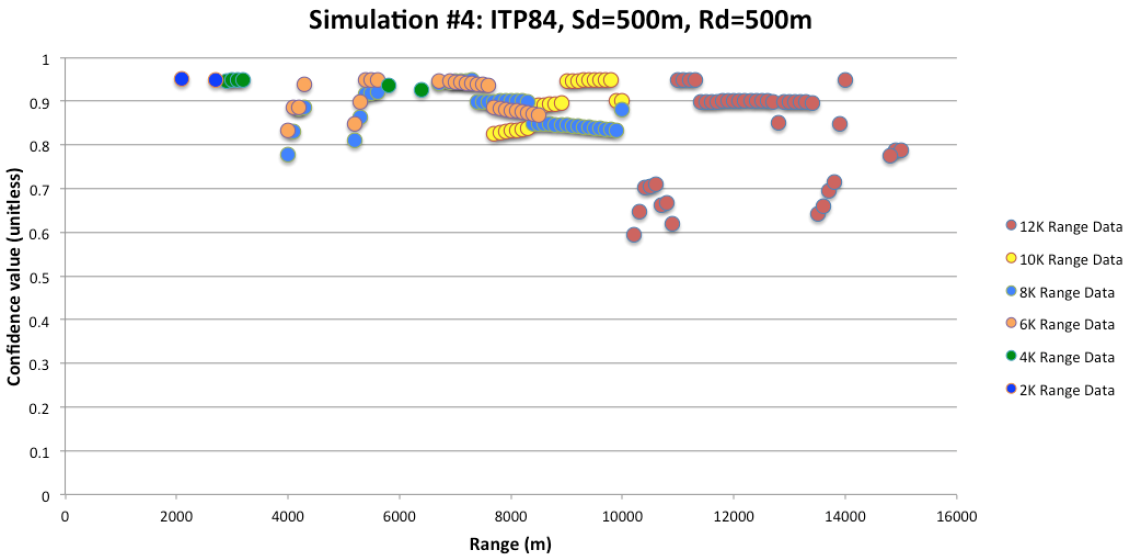

Figure 4-14: Simulation #4: Selected Accuracy Scores

Figure 4-15 shows the predicted ranges for all sources of range data as the AUV

closes in range.

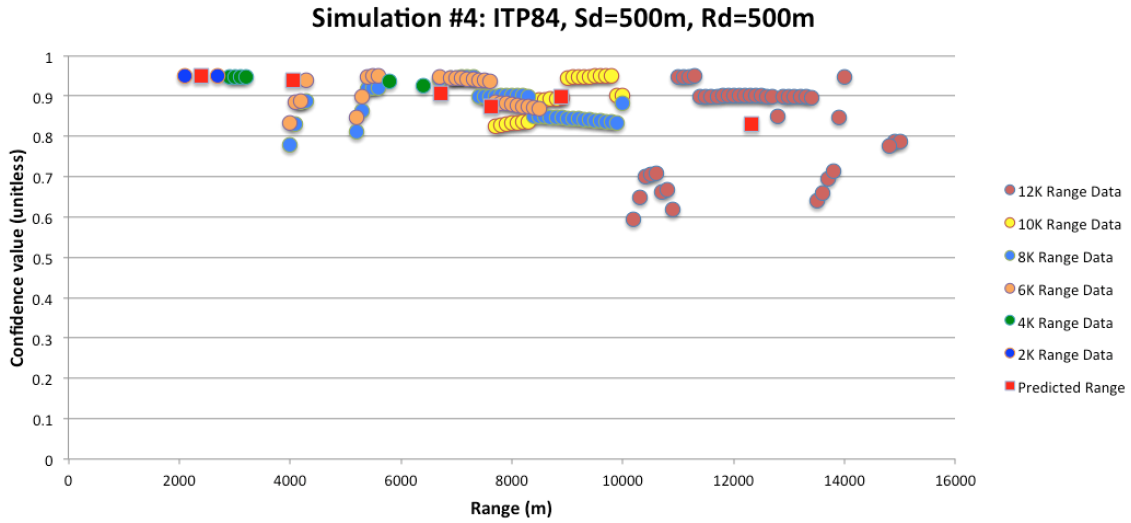

Figure 4-15: Simulation #4: Predicted Ranges

A plot of the full results, including both predicted and actual ranges, can be found in Figure 4-16.

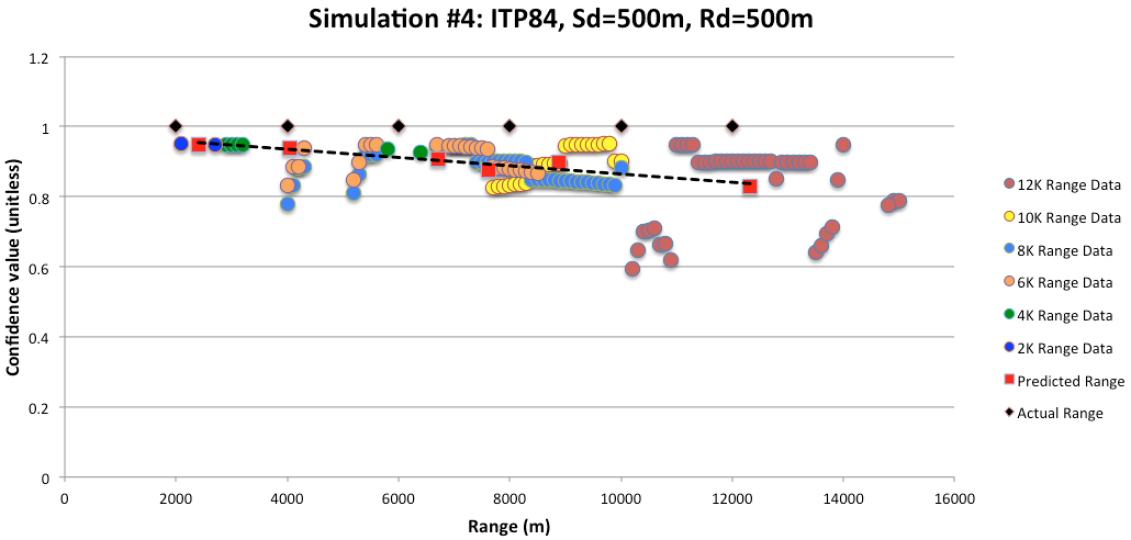

Figure 4-16: Simulation #4: Full Results

A summary of this simulation's results can be found in Table 4.4 with the determination of the error associated with each predicted range.

Actual Ranges (m)	Predicted Ranges (m)	Error (m)
12000	12327.94	327.94
10000	8880.92	1119.08
8000	7617.62	382.38
6000	6708.53	708.53
4000	4053.77	53.77
2000	2399.90	399.90

Table 4.4: Simulation #4: Summary of Results

In similar fashion to the previous three simulations, these results highlight the effectiveness of the developed pattern recognition algorithm as all range data predictions track along with the actual range values. Aside from 10,000 meters, all range data predictions are well within 1,000 meters of their respective actual ranges. Similarly, errors can be attributed to inherent imperfections and differences between the test data and regional databases.

4.5 Summary of Results

Through the conduct of these four simulations, the developed pattern recognition algorithm's effectiveness was validated. This was accomplished by accurately determining the position of the AUV as it closed in range for various combinations of source/ receiver depths with respect to the Beaufort Duct in two different geographical regions within the Arctic. This highlighted the robustness associated with successfully implementing a pattern recognition tracking program across various unique depth stratums with distinct characteristics.

Chapter 5

Conclusion and Recommendations

5.1 Conclusion

The overall conclusion of this thesis is that pattern recognition can be successfully applied to a high multipath environment in order to conduct long-range contact tracking. This type of analysis overcomes the difficulties associated with fading and improper ray path identification by taking advantage of the environment's unique characteristics. The developed pattern recognition algorithm utilizes a combined signal amplitude and arrival time analysis. These two classifiers, together, provide a robust and accurate tracking program as seen from the simulation results presented in Chapter 4.

Error is inherent within a pattern recognition analysis as the testing data will never exactly match the global data. The goal for this thesis was to minimize these errors in order to accurately predict the range to a contact. This was successfully accomplished as the two classifiers, amplitude and arrival time, individually produce valid results that are more robust and accurate when coupled together through the implementation of a confidence filter. Overall, this thesis presents a unique and effective method to conduct long-range underwater contact tracking.

5.2 Future Work

Based on the results of this thesis, four major areas of study were identified and recommended for future work.

1. **Develop more robust regional databases**

   This thesis employed the use of a single sound speed profile within each region (north and south) to perform all pattern recognition. This provided excellent results, but further development of better, more robust regional databases could prove to be beneficial. This could be accomplished by altering the size of the regions such as decreasing the size in order to minimize the inherent errors between the input data and their associated "fingerprint" databases. Additionally, utilizing multiple sound speed profiles could prove to be advantageous. This could be accomplished by either employing multiple sound speed profiles or combining the characteristics of multiple sound speed profiles into one aggregate sound speed profile.

2. **Refine pattern recognition algorithm**

   Although this thesis effectively employed the use of two classifiers, amplitude and arrival time, it is possible that additional classifiers exist which could improve the overall accuracy of the analysis. Furthermore, continued evaluation of the decision boundaries contained within each classifier's respective analysis could prove to increase the tracking accuracy of the developed program.

3. **Expand application to other environments**

   An environment's unique characteristics is what makes pattern recognition possible. This thesis successfully applied this concept to develop a pattern recognition algorithm within the Arctic Region where the Beaufort Duct exists. It

proved the feasibility of applying such a pattern recognition analysis to this environment, but furthermore, could prove to be beneficial in other parts of the world. Every environment is unique in its own distinct way. These characteristics could be used to develop similar pattern recognition programs for the purpose of conducting underwater contact tracking all across the globe.

4. **Broaden applications to additional contact tracking scenarios**

   The simulations conducted within this thesis are assumed to be applied to a time synchronized, OWTT tracking system where the location of the source is known. This reduces computational time and costs, while aiding to increase the fidelity associated with such tracking systems. Due to the fact that the developed algorithm utilizes relative travel times associated with the received acoustic signals, and relies solely on "fingerprint" patterns at all range and depth combinations between the source and receiver, applications can be expanded upon to include scenarios where the location of the source is unknown. This can include the tracking of unknown and unidentified submerged contacts, such as submarines or AUVs. This capability has the potential to greatly expand applications to a wide array of useful and relevant contact tracking scenarios.

THIS PAGE INTENTIONALLY LEFT BLANK

Appendix A

Detailed Results

A.1 Simulation #1 Results

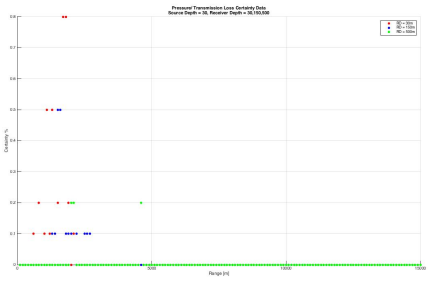

(a) Unfiltered TL

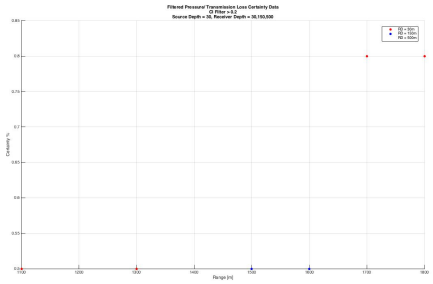

(b) Filtered TL

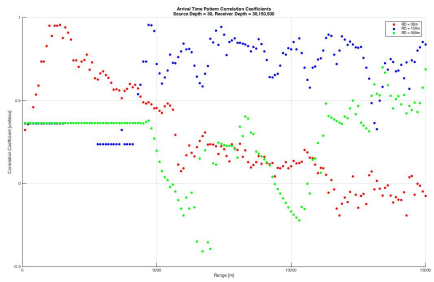

(c) Unfiltered Arrival Time

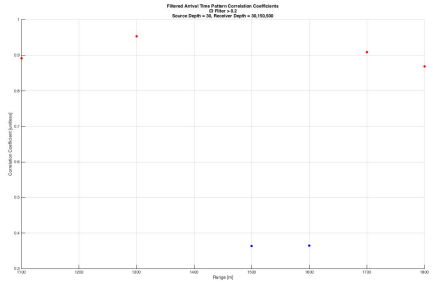

(d) Filtered Arrival Time

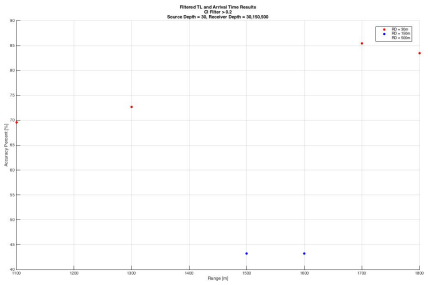

(e) Final Results

Figure A-1: Simulation #1 Results: 2k Range Data

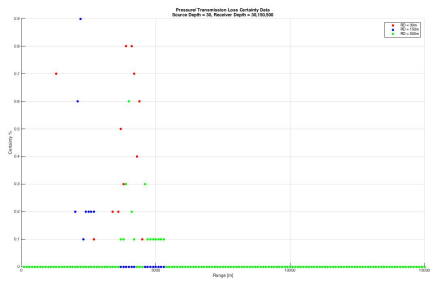

(a) Unfiltered TL

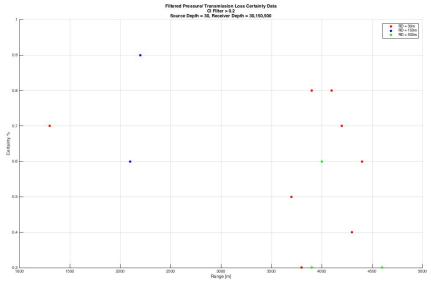

(b) Filtered TL

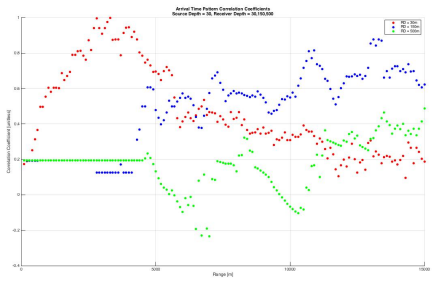

(c) Unfiltered Arrival Time

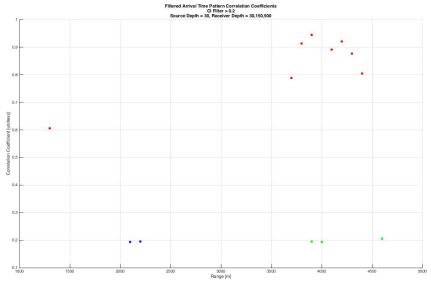

(d) Filtered Arrival Time

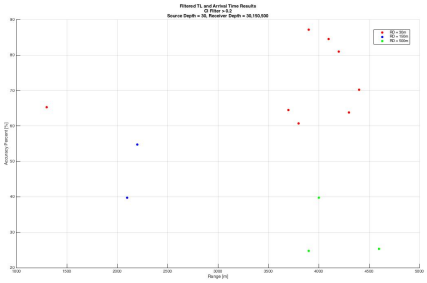

(e) Final Results

Figure A-2: Simulation #1 Results: 4k Range Data

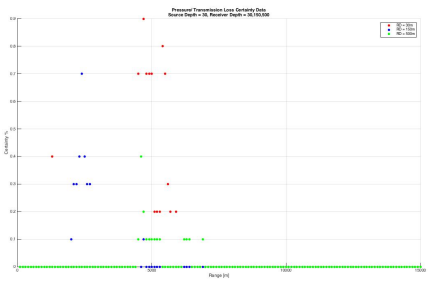

(a) Unfiltered TL

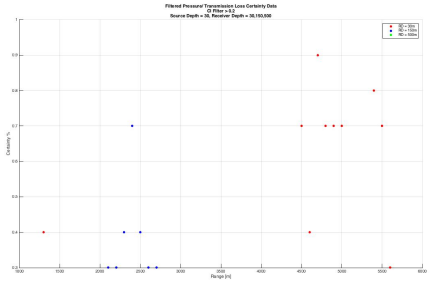

(b) Filtered TL

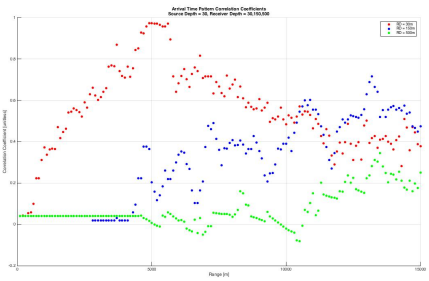

(c) Unfiltered Arrival Time

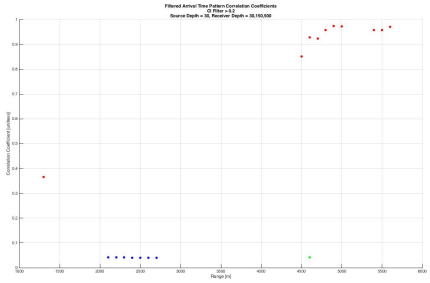

(d) Filtered Arrival Time

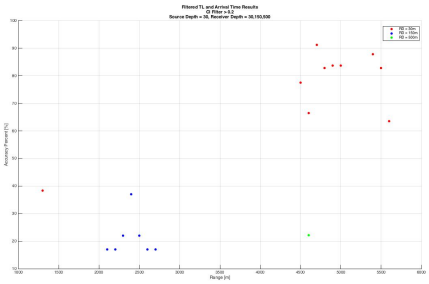

(e) Final Results

Figure A-3: Simulation #1 Results: 6k Range Data

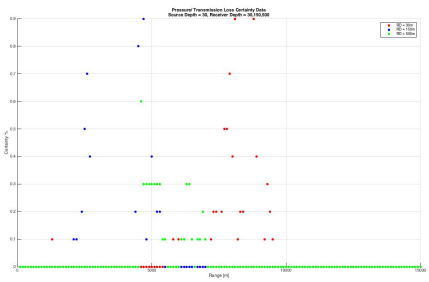

(a) Unfiltered TL

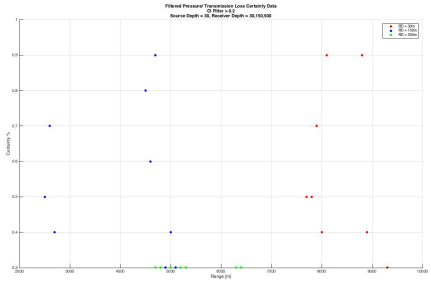

(b) Filtered TL

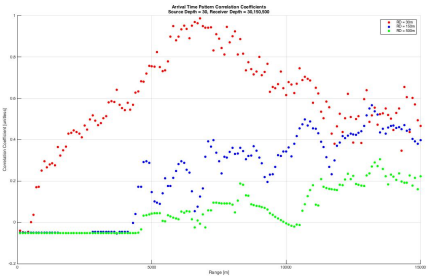

(c) Unfiltered Arrival Time

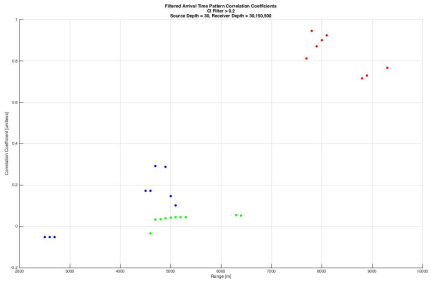

(d) Filtered Arrival Time

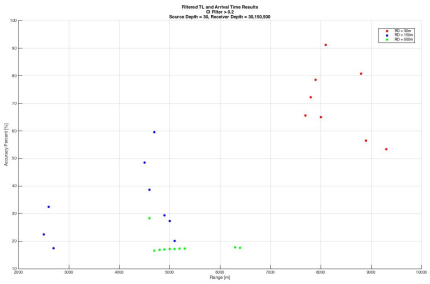

(e) Final Results

Figure A-4: Simulation #1 Results: 8k Range Data

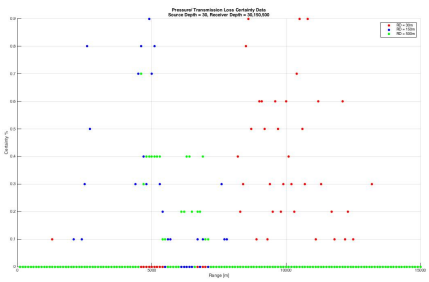

(a) Unfiltered TL

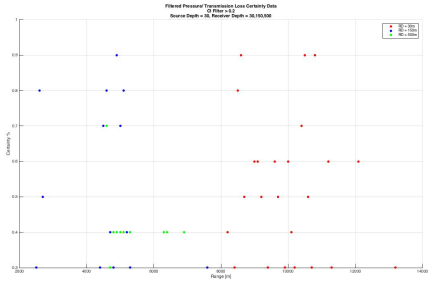

(b) Filtered TL

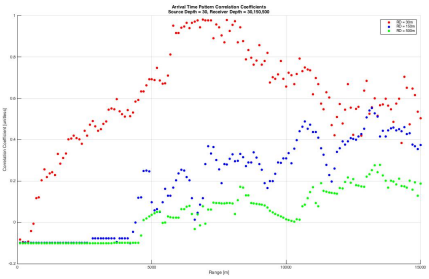

(c) Unfiltered Arrival Time

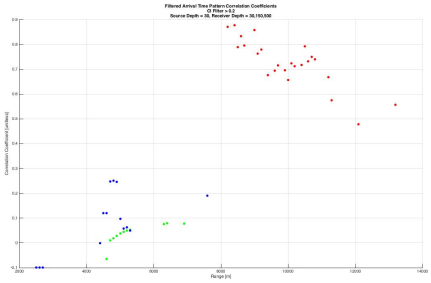

(d) Filtered Arrival Time

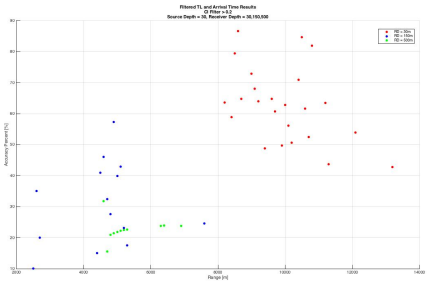

(e) Final Results

Figure A-5: Simulation #1 Results: 10k Range Data

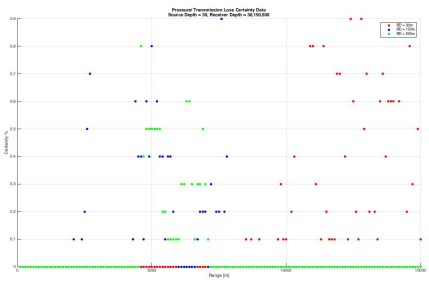

(a) Unfiltered TL

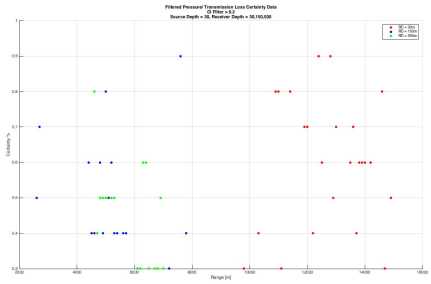

(b) Filtered TL

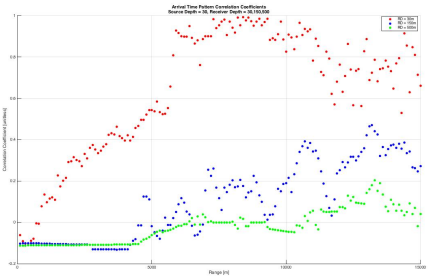

(c) Unfiltered Arrival Time

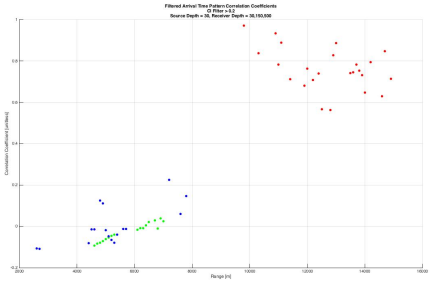

(d) Filtered Arrival Time

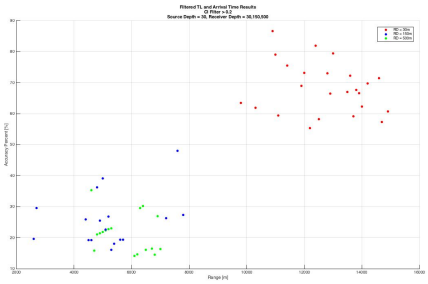

(e) Final Results

Figure A-6: Simulation #1 Results: 12k Range Data

(a) Unfiltered TL

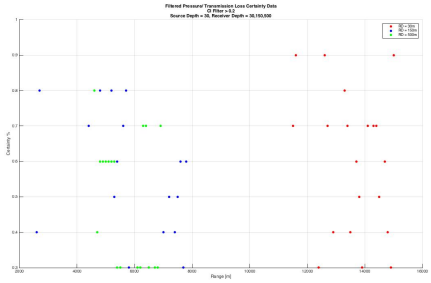

(b) Filtered TL

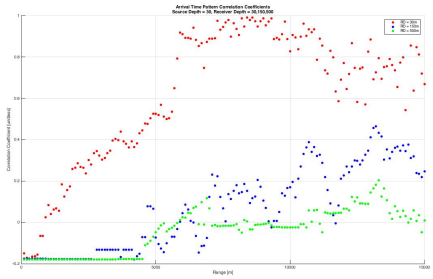

(c) Unfiltered Arrival Time

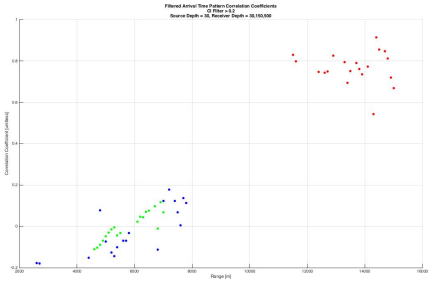

(d) Filtered Arrival Time

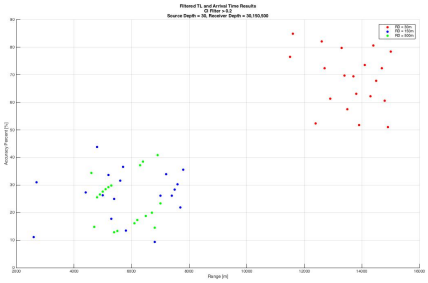

(e) Final Results

Figure A-7: Simulation #1 Results: 14k Range Data

A.2 Simulation #2 Results

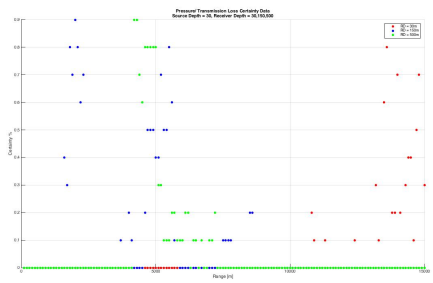

(a) Unfiltered TL

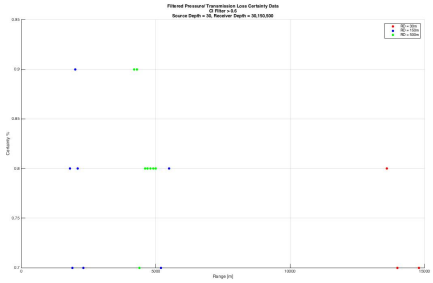

(b) Filtered TL

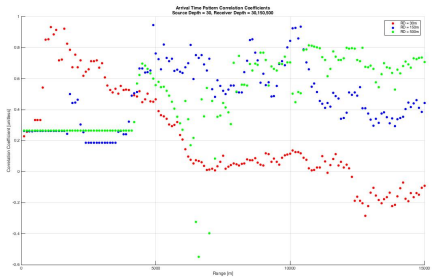

(c) Unfiltered Arrival Time

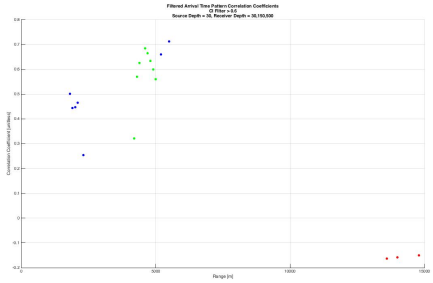

(d) Filtered Arrival Time

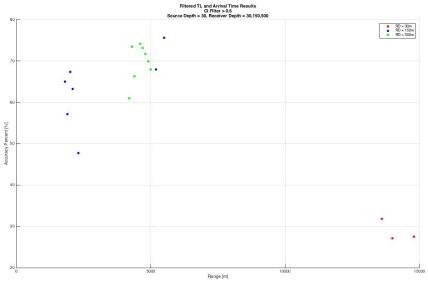

(e) Final Results

Figure A-8: Simulation #2 Results: 6k Range Data

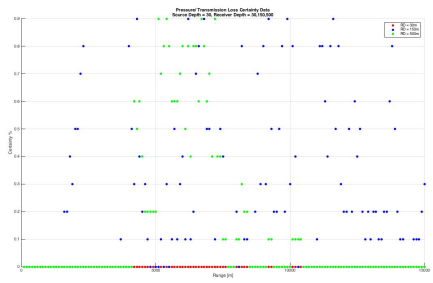

(a) Unfiltered TL

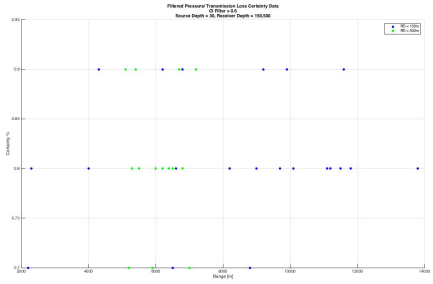

(b) Filtered TL

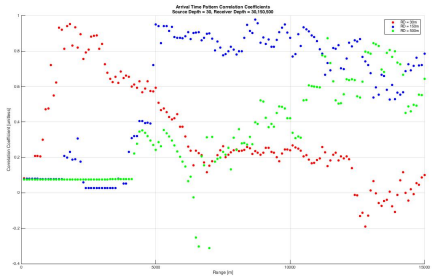

(c) Unfiltered Arrival Time

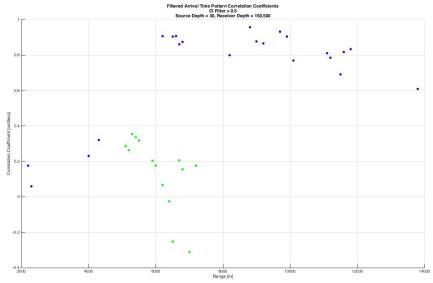

(d) Filtered Arrival Time

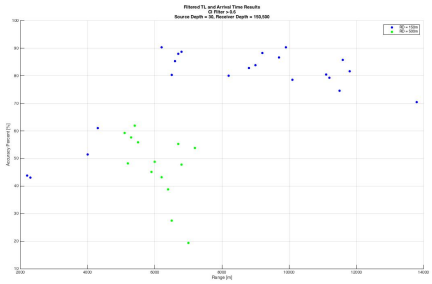

(e) Final Results

Figure A-9: Simulation #2 Results: 8k Range Data

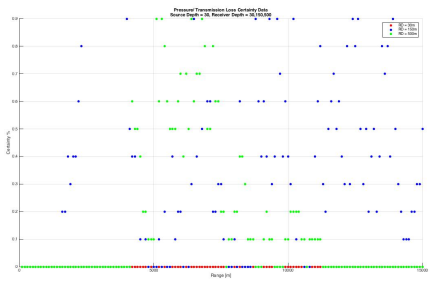

(a) Unfiltered TL

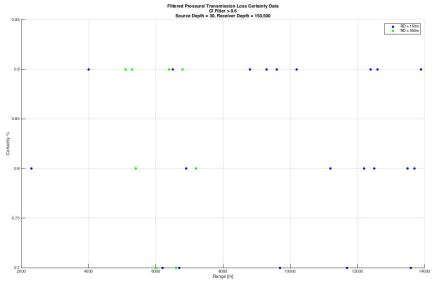

(b) Filtered TL

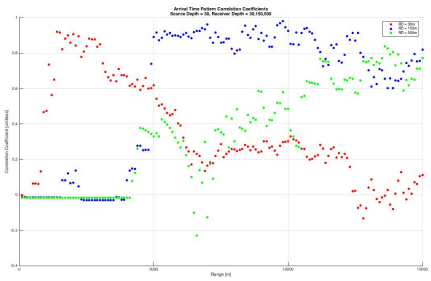

(c) Unfiltered Arrival Time

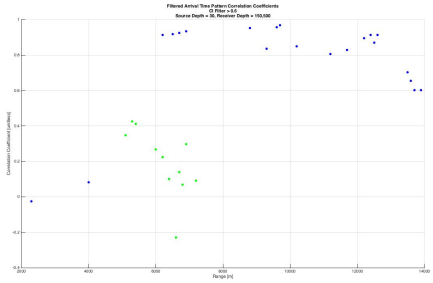

(d) Filtered Arrival Time

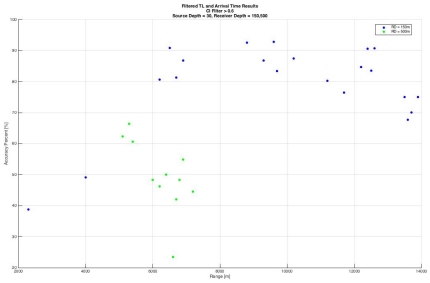

(e) Final Results

Figure A-10: Simulation #2 Results: 10k Range Data

(a) Unfiltered TL

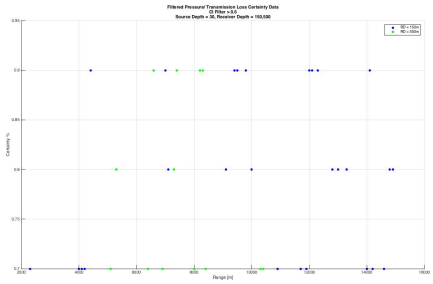

(b) Filtered TL

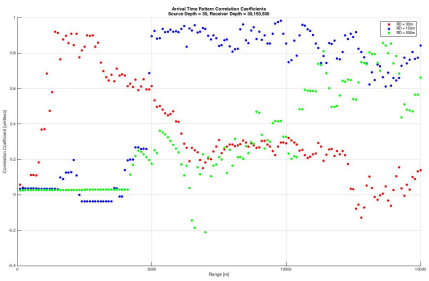

(c) Unfiltered Arrival Time

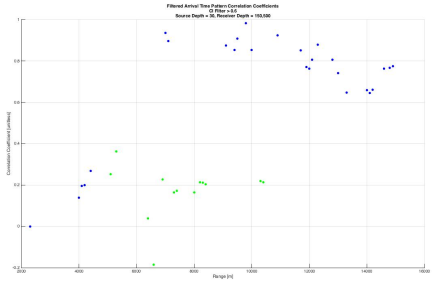

(d) Filtered Arrival Time

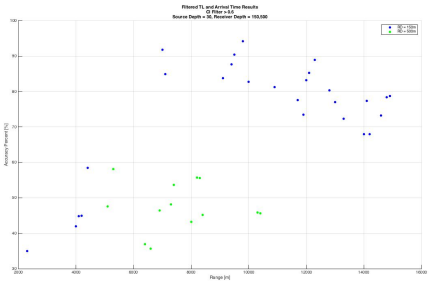

(e) Final Results

Figure A-11: Simulation #2 Results: 12k Range Data

A.3 Simulation #3 Results

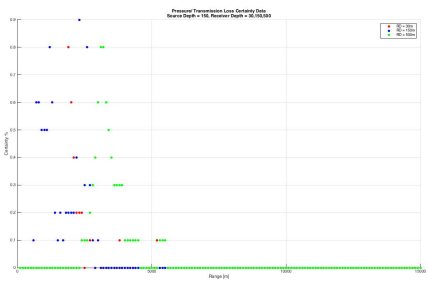

(a) Unfiltered TL

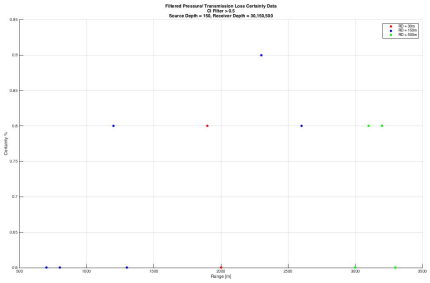

(b) Filtered TL

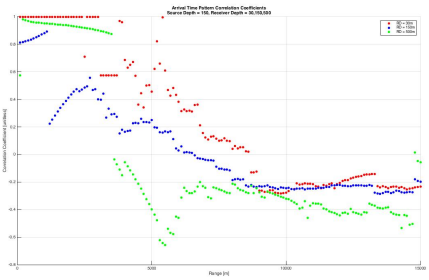

(c) Unfiltered Arrival Time

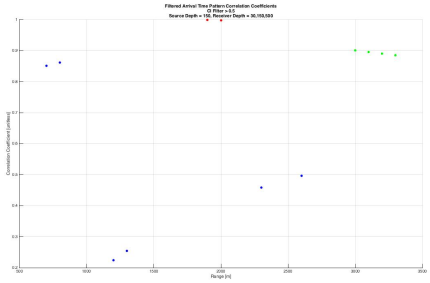

(d) Filtered Arrival Time

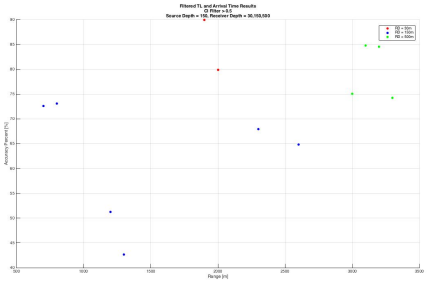

(e) Final Results

Figure A-12: Simulation #3 Results: 2k Range Data

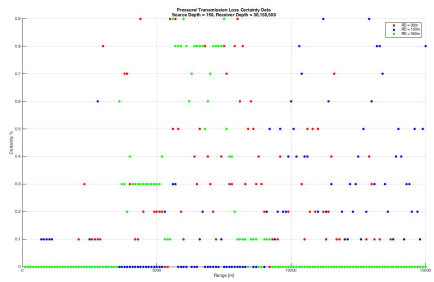

(a) Unfiltered TL

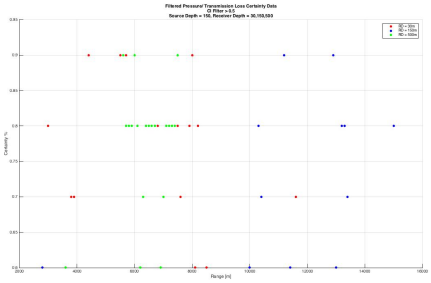

(b) Filtered TL

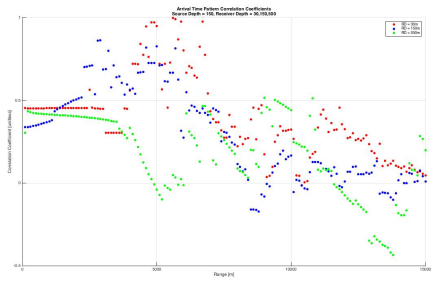

(c) Unfiltered Arrival Time

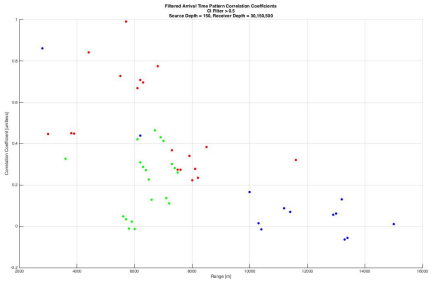

(d) Filtered Arrival Time

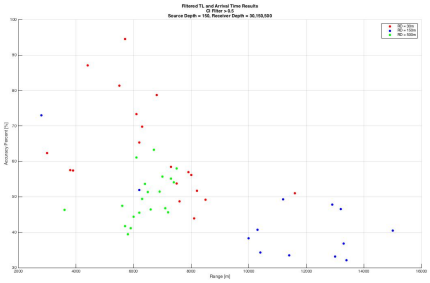

(e) Final Results

Figure A-13: Simulation #3 Results: 6k Range Data

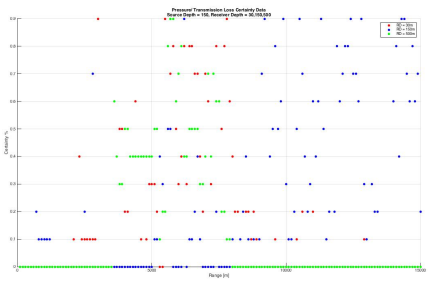

(a) Unfiltered TL

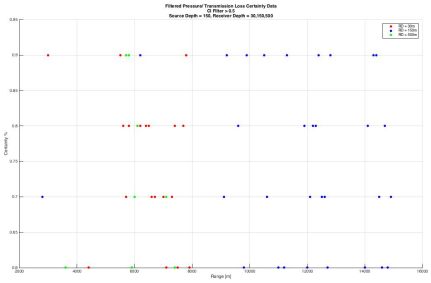

(b) Filtered TL

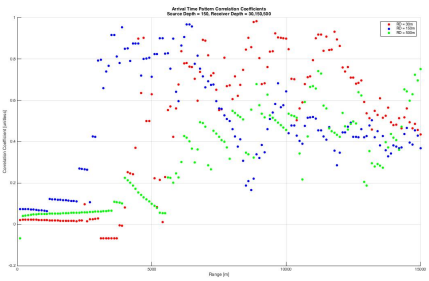

(c) Unfiltered Arrival Time

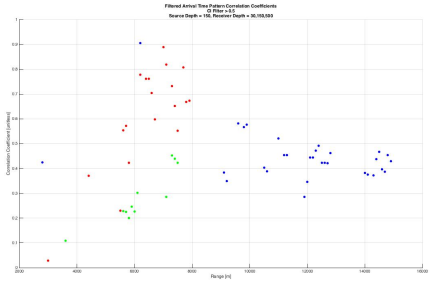

(d) Filtered Arrival Time

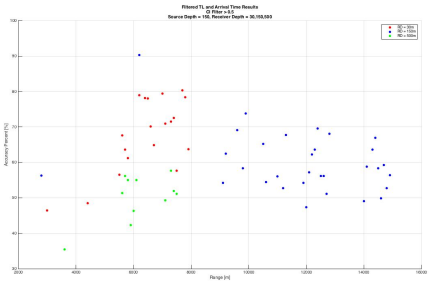

(e) Final Results

Figure A-14: Simulation #3 Results: 8k Range Data

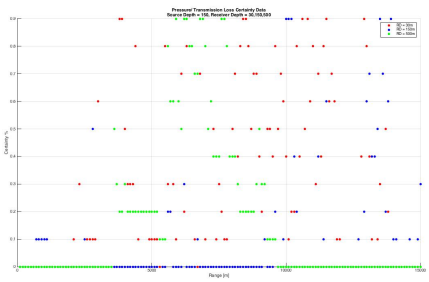

(a) Unfiltered TL

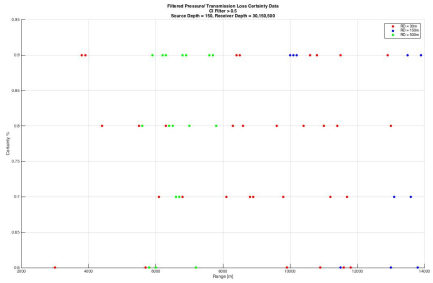

(b) Filtered TL

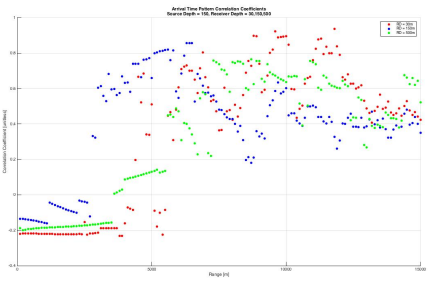

(c) Unfiltered Arrival Time

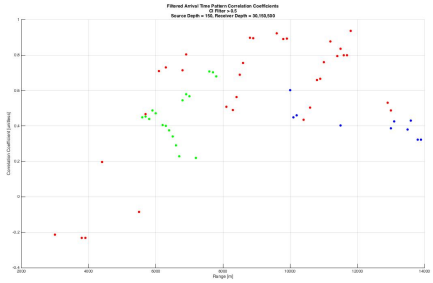

(d) Filtered Arrival Time

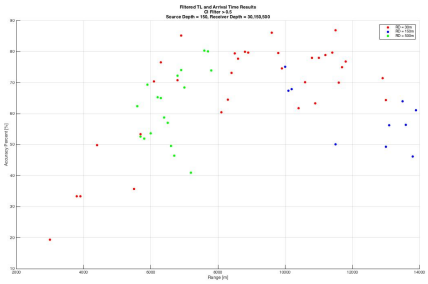

(e) Final Results

Figure A-15: Simulation #3 Results: 10k Range Data

A.4 Simulation #4 Results

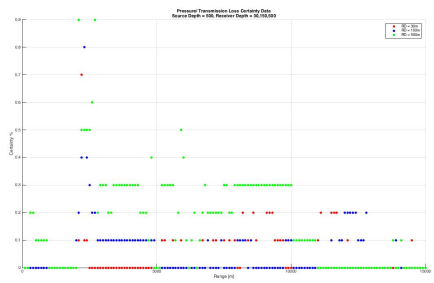

(a) Unfiltered TL

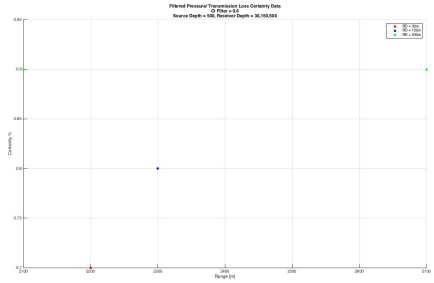

(b) Filtered TL

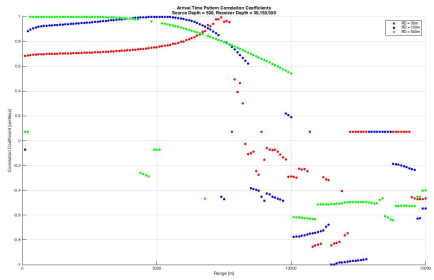

(c) Unfiltered Arrival Time

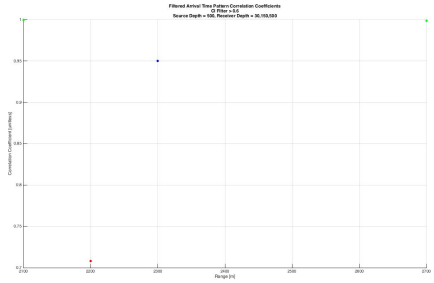

(d) Filtered Arrival Time

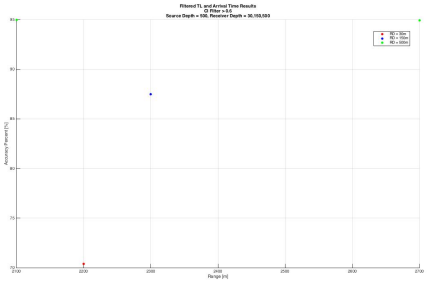

(e) Final Results

Figure A-16: Simulation #4 Results: 2k Range Data

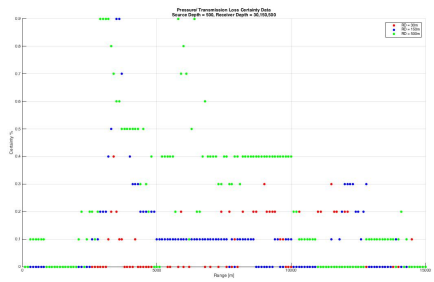

(a) Unfiltered TL

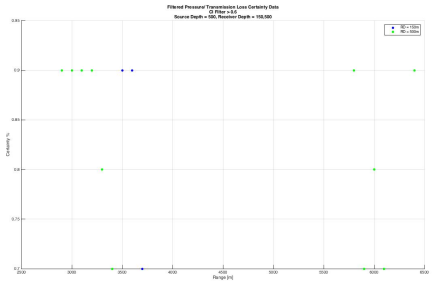

(b) Filtered TL

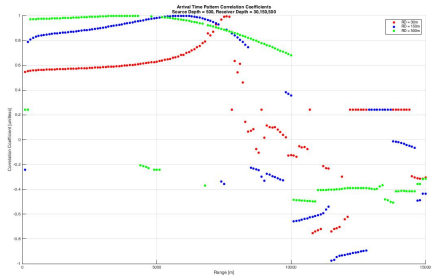

(c) Unfiltered Arrival Time

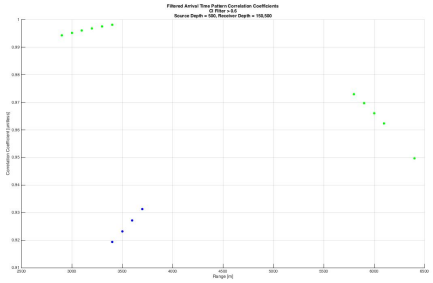

(d) Filtered Arrival Time

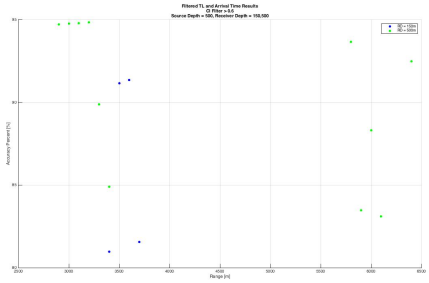

(e) Final Results

Figure A-17: Simulation #4 Results: 4k Range Data

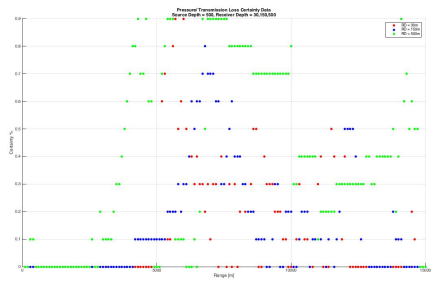

(a) Unfiltered TL

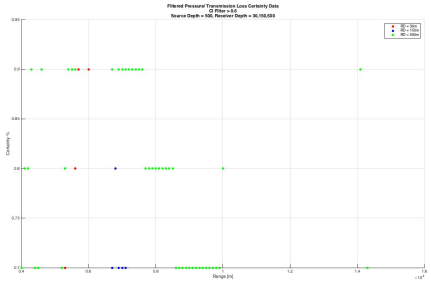

(b) Filtered TL

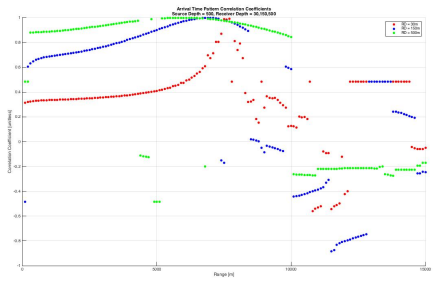

(c) Unfiltered Arrival Time

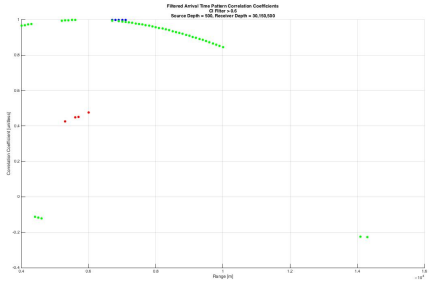

(d) Filtered Arrival Time

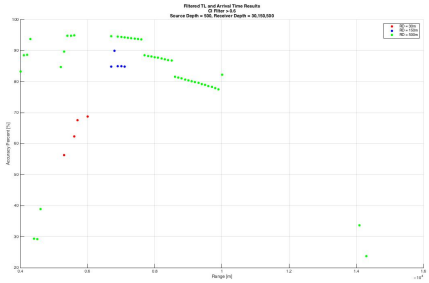

(e) Final Results

Figure A-18: Simulation #4 Results: 6k Range Data

(a) Unfiltered TL

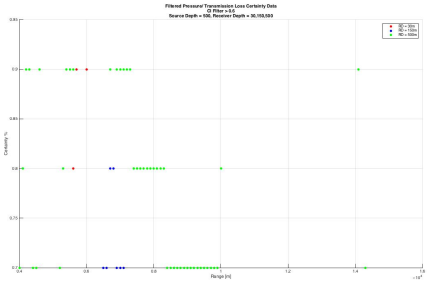

(b) Filtered TL

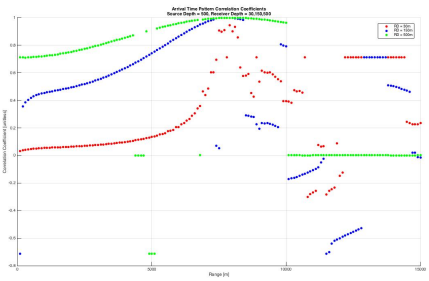

(c) Unfiltered Arrival Time

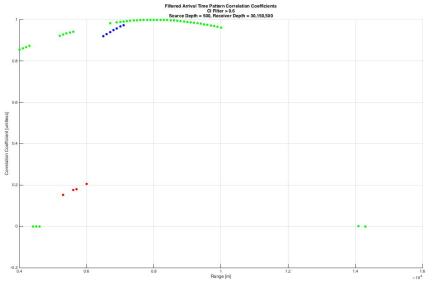

(d) Filtered Arrival Time

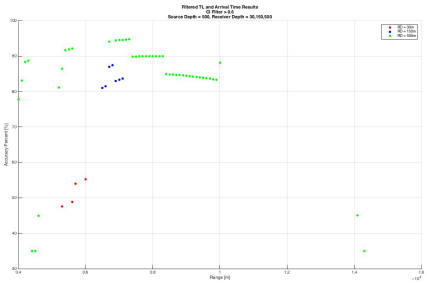

(e) Final Results

Figure A-19: Simulation #4 Results: 8k Range Data

(a) Unfiltered TL

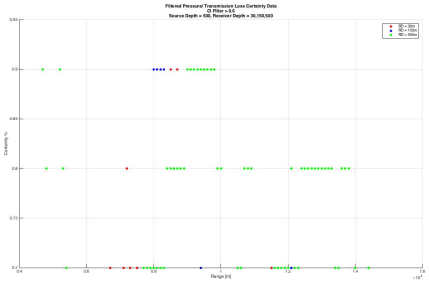

(b) Filtered TL

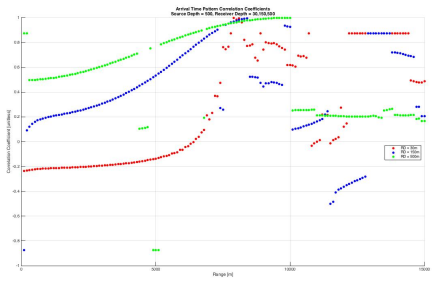

(c) Unfiltered Arrival Time

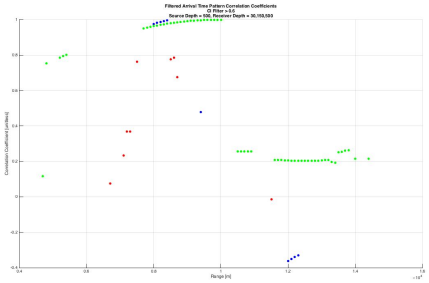

(d) Filtered Arrival Time

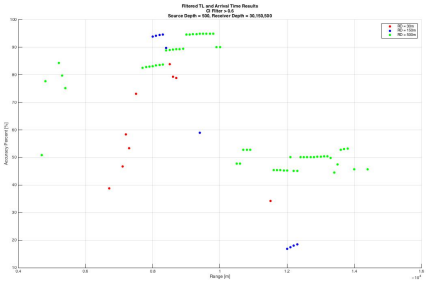

(e) Final Results

Figure A-20: Simulation #4 Results: 10k Range Data

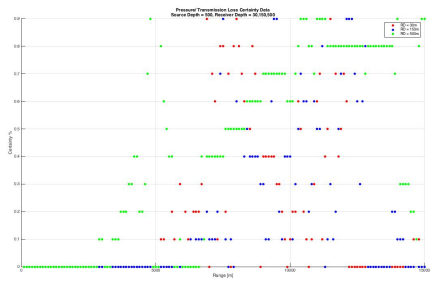

(a) Unfiltered TL

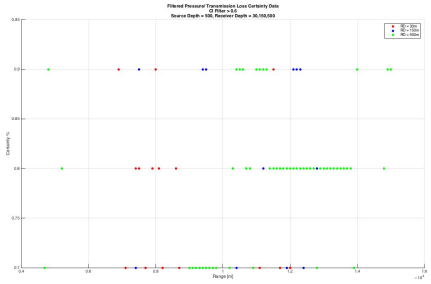

(b) Filtered TL

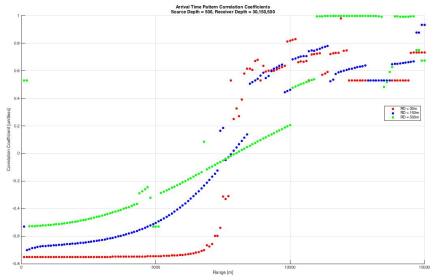

(c) Unfiltered Arrival Time

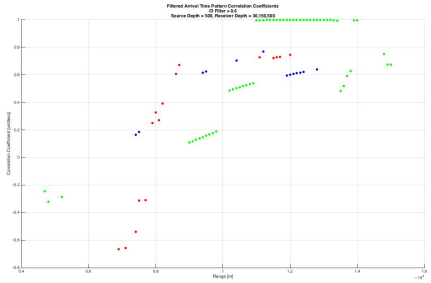

(d) Filtered Arrival Time

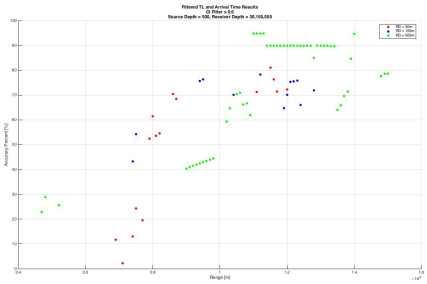

(e) Final Results

Figure A-21: Simulation #4 Results: 12k Range Data

Appendix B

Regional Data

B.1 ITP 84 Regional Data

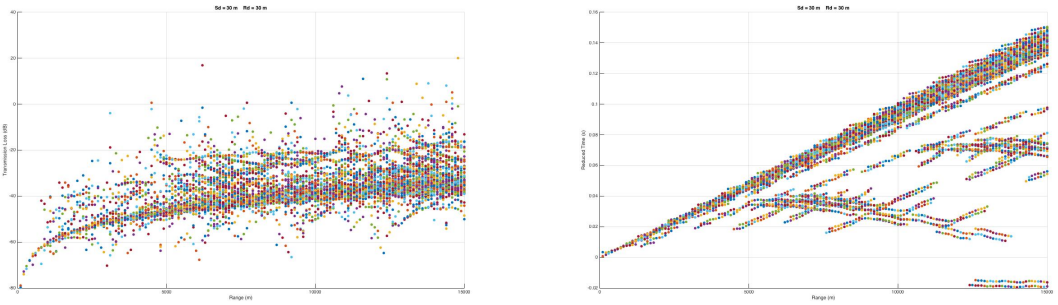

(a) TL Data **(b)** Arrival Time Data

Figure B-1: ITP84 Regional Data: Sd = 30m, Rd = 30m

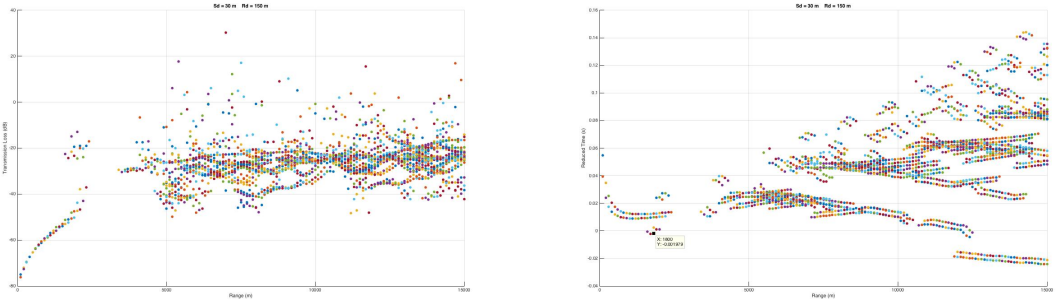

(a) TL Data **(b)** Arrival Time Data

Figure B-2: ITP84 Regional Data: Sd = 30m, Rd = 150m

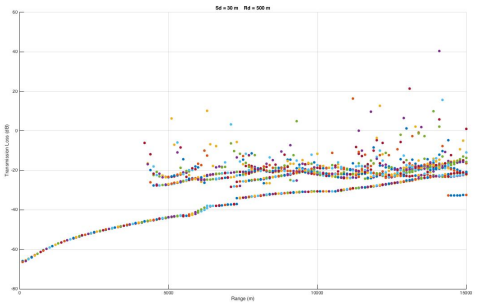

(a) TL Data

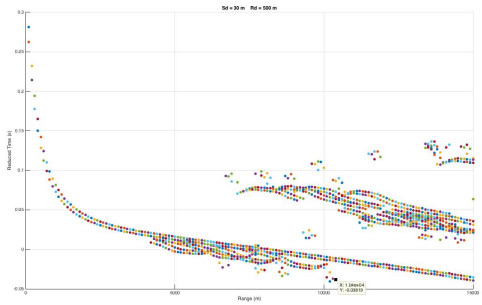

(b) Arrival Time Data

Figure B-3: ITP84 Regional Data: Sd = 30m, Rd = 500m

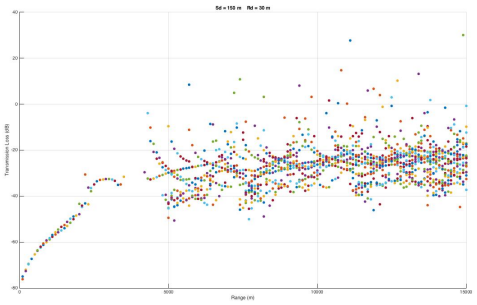

(a) TL Data

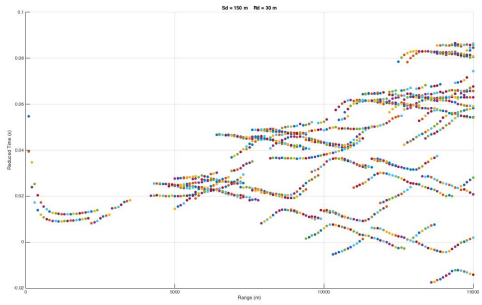

(b) Arrival Time Data

Figure B-4: ITP84 Regional Data: Sd = 150m, Rd = 30m

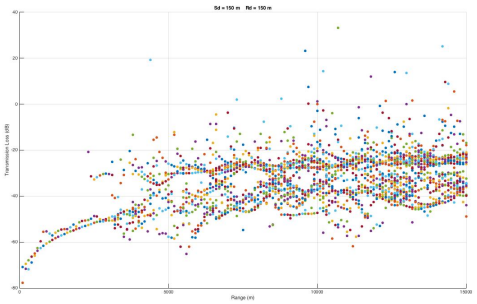

(a) TL Data

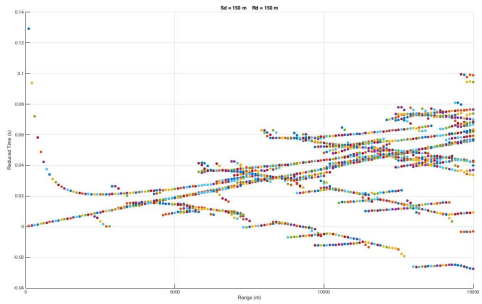

(b) Arrival Time Data

Figure B-5: ITP84 Regional Data: Sd = 150m, Rd = 150m

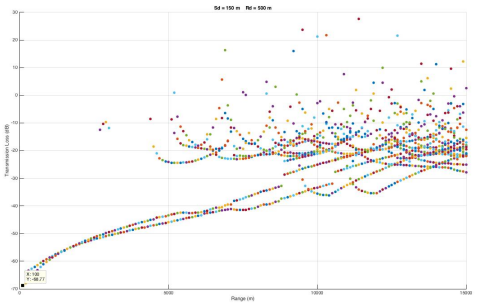

(a) TL Data

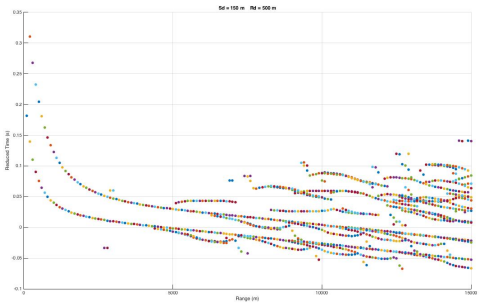

(b) Arrival Time Data

Figure B-6: ITP84 Regional Data: Sd = 150m, Rd = 500m

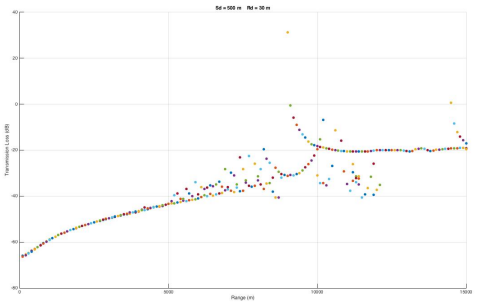

(a) TL Data

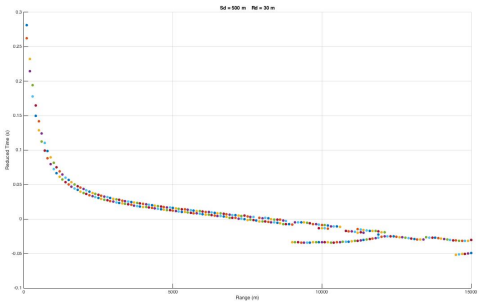

(b) Arrival Time Data

Figure B-7: ITP84 Regional Data: Sd = 500m, Rd = 30m

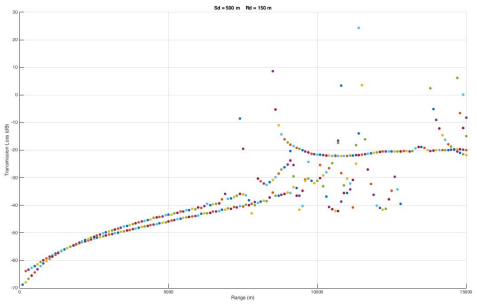

(a) TL Data

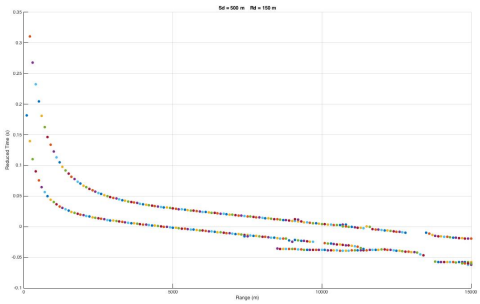

(b) Arrival Time Data

Figure B-8: ITP84 Regional Data: Sd = 500m, Rd = 150m

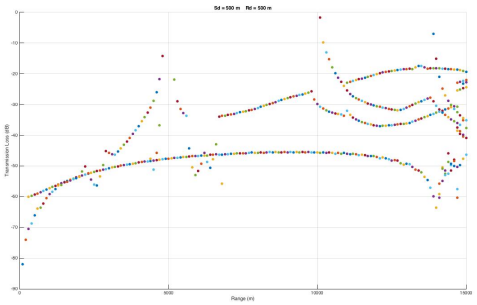

(a) TL Data

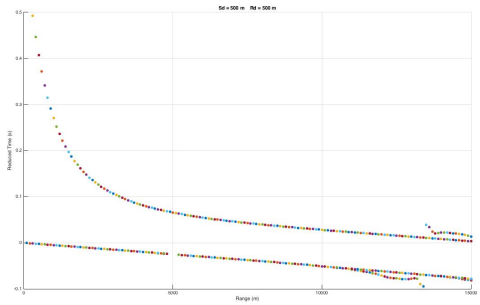

(b) Arrival Time Data

Figure B-9: ITP84 Regional Data: Sd = 500m, Rd = 500m

B.2 ITP 85 Regional Data

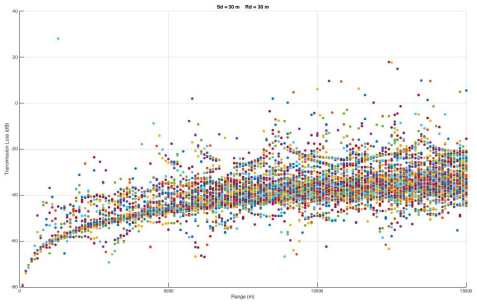

(a) TL Data

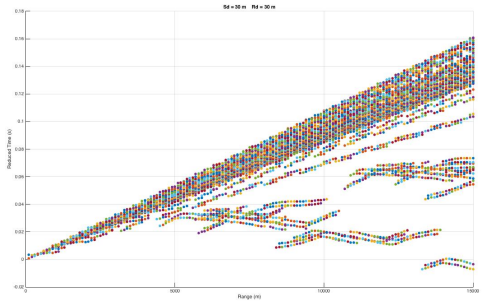

(b) Arrival Time Data

Figure B-10: ITP85 Regional Data: Sd = 30m, Rd = 30m

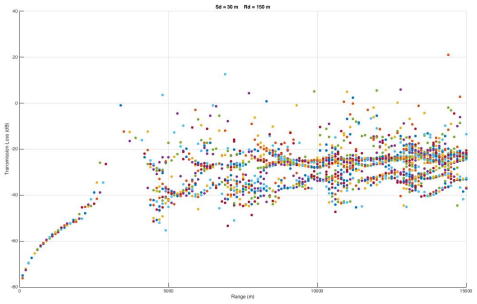

(a) TL Data

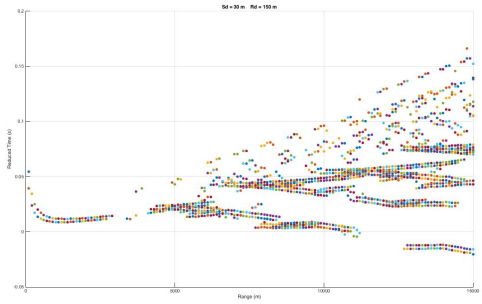

(b) Arrival Time Data

Figure B-11: ITP85 Regional Data: Sd = 30m, Rd = 150m

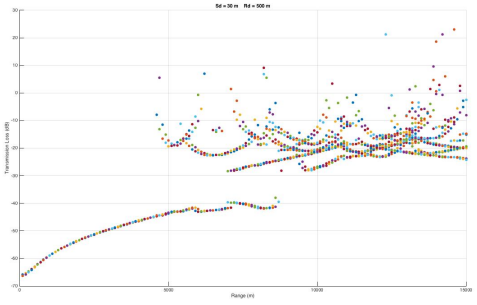

(a) TL Data

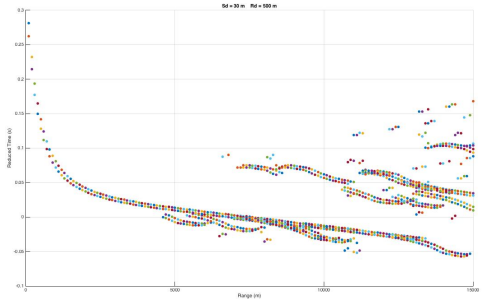

(b) Arrival Time Data

Figure B-12: ITP85 Regional Data: Sd = 30m, Rd = 500m

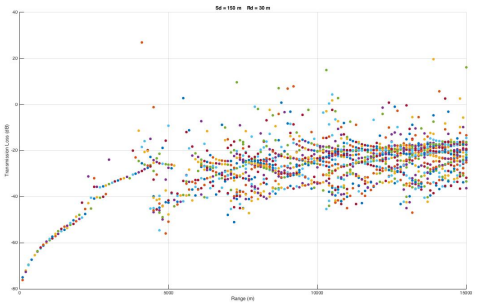

(a) TL Data

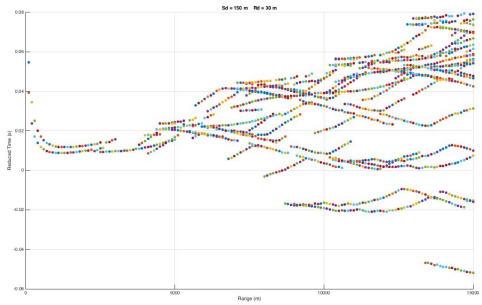

(b) Arrival Time Data

Figure B-13: ITP85 Regional Data: Sd = 150m, Rd = 30m

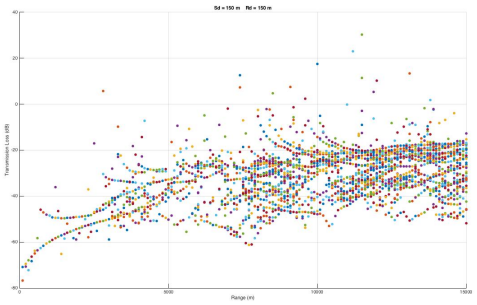

(a) TL Data

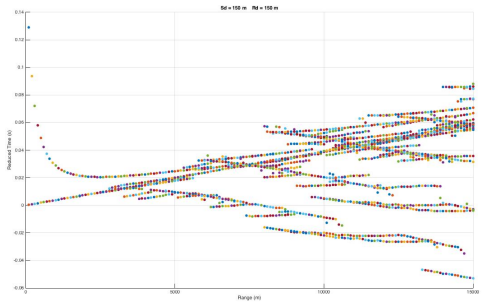

(b) Arrival Time Data

Figure B-14: ITP85 Regional Data: Sd = 150m, Rd = 150m

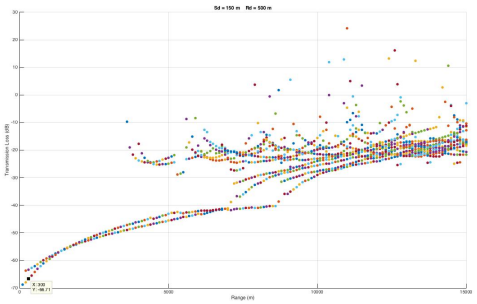

(a) TL Data

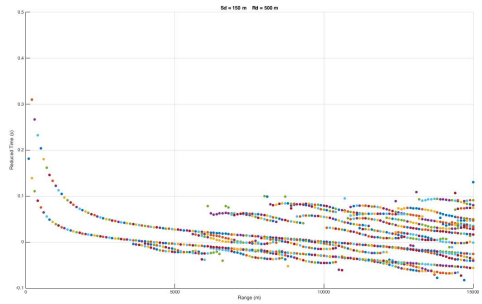

(b) Arrival Time Data

Figure B-15: ITP85 Regional Data: Sd = 150m, Rd = 500m

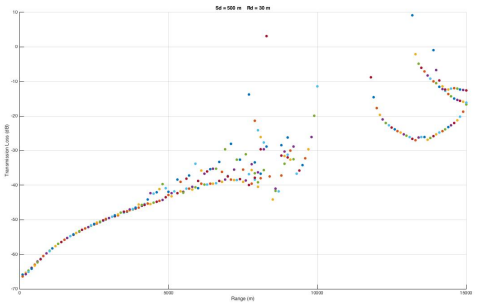

(a) TL Data

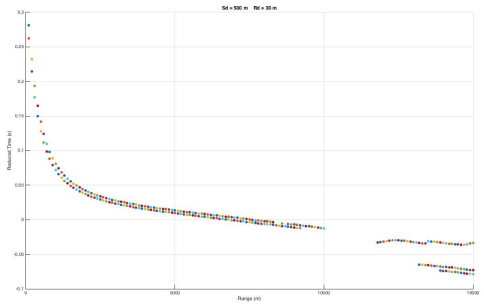

(b) Arrival Time Data

Figure B-16: ITP85 Regional Data: Sd = 500m, Rd = 30m

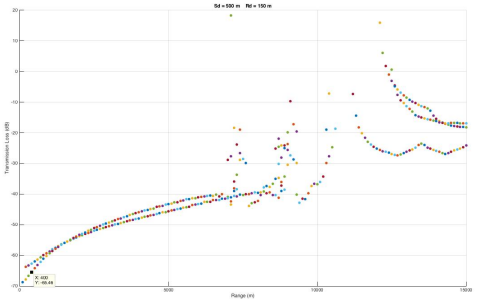

(a) TL Data

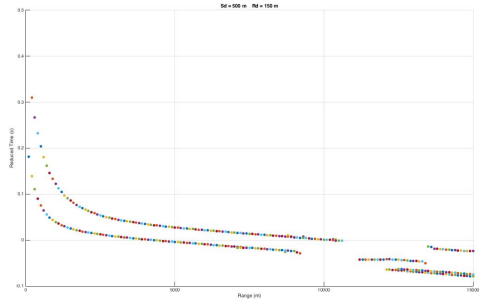

(b) Arrival Time Data

Figure B-17: ITP85 Regional Data: Sd = 500m, Rd = 150m

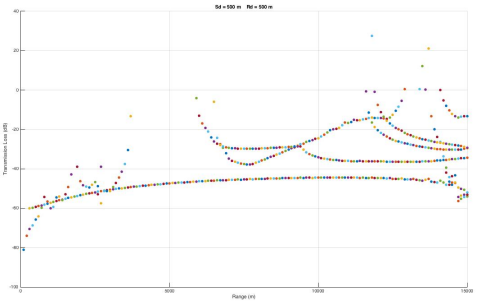

(a) TL Data

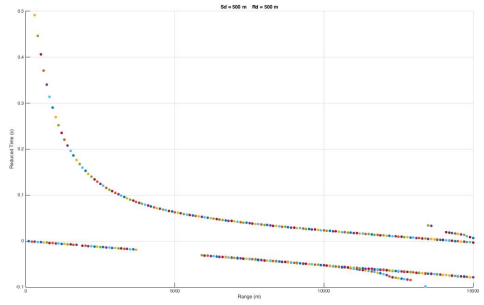

(b) Arrival Time Data

Figure B-18: ITP85 Regional Data: Sd = 500m, Rd = 500m

THIS PAGE INTENTIONALLY LEFT BLANK

Bibliography

[1] Christopher M. Bishop. *Pattern recognition and machine learning.* Information science and statistics. New York : Springer, c2006., 2006.

[2] Philip Budzik. *Arctic Oil and Natural Gas Potential.* U.S. Energy Information Administration Office of Integrated Analysis and Forecasting Oil and Gas Division, October 2009.

[3] Max Deffenbaugh. *A matched field processing approach to long range acoustic navigation.* c1994., 1994.

[4] Richard O. Duda, Peter E. Hart, and David G. Stork. *Pattern classification.* New York : Wiley, 2001., 2001.

[5] Ryan M. Eustice, L. Whitcomb, Louis, Hanumant Singh, and Matthew Grund. One-way travel-time inverted ultra-short baseline localization for low-cost autonomous underwater vehicles. *IEEE International Conference on Robotics and Automation (ICRA)*, May 29 - June 3 2017.

[6] Admiral Jonathan W. Greenert. *The United States Navy Arctic Roadmap for 2014 to 2030.* United States Navy, February 2014.

[7] Finn B. Jensen, William A. Kuperman, Michael B. Porter, and Henrik Schmidt. *Computational ocean acoustics.* Modern acoustics and signal processing. New York : Springer, c2011., 2011.

[8] The Ocean Acoustics Library. http://oalib.hlsresearch.com, Acoustics Toolbox.

[9] Xavier Lurton. *An introduction to underwater acoustics : principles and applications.* London ; New York : Springer ; Chichester, UK : Published in association with Praxis Pub., c2002., 2002.

[10] Douglas C. Montgomery, George C. Runger, and Norma Faris Hubele. *Engineering statistics.* [Hoboken, N.J.] : Wiley, c2011., 2011.

[11] Michael B. Porter. *The BELLHOP Manual and User's Guide: PRELIMINARY DRAFT.* Heat, Light, and Sound Research, Inc, 2011.

[12] Andrew Poulsen and Henrik Schmidt. Acoustic noise properties in the rapidly changing arctic ocean. *Proceedings of the 22nd International Congress on Acoustics*, September 2016.

[13] Ice-Tethered Profiler Program. Woods Hole Oceanographic Institution, (Toole et al., 2011; Krishfield et al., 2008), http://www.whoi.edu/itp.

[14] Orlando Camargo Rodriguez. *General description of the BELLHOP ray tracing program*. Signal Processing Laboratory, Universidade do Algarve, June 2008.

[15] Nicholas R. Rypkema, Erin M. Fischell, and Henrik Schmidt. Experimental results in synchronous-clock one-way-travel-time acoustic navigation for autonomous underwater vehicles. *Proceedings - IEEE International Conference on Robotics and Automation*, April 2007.

[16] Henrik Schmidt. *2.681 - Environmental Ocean Acoustics - Course Notes*. 2017.

[17] R.J. Urick. *Sound Propagation in the Sea*. Defense Advanced Research Projects Agency, Washington, DC, 1979.